



**Politecnico
di Torino**

Corso di Laurea Magistrale in Sustainable Nuclear Energy

Tesi di Laurea Magistrale

**Alternative weighting functions
for group collapsing of nuclear data
in Lead Fast Reactors
time-dependent analyses**

Relatori

prof. Sandra Dulla
dr. Nicolò Abrate

Candidato

Christian Vita

ANNO ACCADEMICO 2022-2023

Abstract

Generating accurate few-group constants for time-dependent analyses is a challenging task in fission reactor physics, especially for reactors with a fast spectrum. Recent efforts have focused on optimizing the selection of group structures using techniques like genetic algorithms[1]. Another approach to improving the quality of few-group constants involves using alternative weighting functions instead of the commonly used k -mode fundamental flux distribution, as several different eigenvalue formulations are possible in reactor physics. The most popular and widely used are known to be the multiplication and the time eigenvalues [2], since they retain a clear and physically important significance and yield meaningful information for the system design in steady and transient conditions. However, even if alternative eigenvalue formulation could be very interesting and useful depending on the kind of study that is carried out, their applications is still rather scarce in the literature. This work has been carried on with the NEMO research group at Politecnico di Torino and compares the performance of different eigenvalue formulations of the neutron transport equation (e.g., time or collision eigenproblems) when used in the collapsing process. The study evaluates the effectiveness of these alternative weighting spectra by conducting full-core transient calculations on a Lead Fast Reactor case with the FRENETIC nodal diffusion code. The results demonstrate that depending on the transient type and reactivity insertion, the few-group constants obtained using these alternative weighting spectra provide more accurate integral quantities (e.g., total power) compared to those obtained with the k -mode collapsed data.

Contents

1	Introduction	1
1.1	Introduction	1
1.1.1	Main physical quantities	2
1.1.2	Neutron Transport Equation (NTE)	4
1.1.3	Criticality problem	5
	References	7
2	The adoption of the FreeFEM++ language for the solution of the diffusion equation	9
2.1	FreeFEM++: Core Geometry	9
2.1.1	Preliminary calculation: Diffusion two group model	14
2.1.2	One hexagon calculation	24
	References	30
3	Eigenvalue Formulations	31
3.1	Theoretical introduction	31
3.1.1	γ - eigenvalue	32
3.1.2	Preliminary Studies	36
3.2	System geometry description	39
3.3	Energy grids	43
3.4	Considerations on neutron flux by using alternative eigenvalue	45
3.4.1	Preliminary considerations: k eigenvalue 33G Diffusion system	45
3.4.2	3D 33-G diffusion model: $k, \gamma, \alpha, \omega$ criticality evaluations	51
	References	65
4	Results	67
4.1	2D Transient analysis	71
4.2	Results of 2D transient analysis	74
5	Conclusions	81
	References	82

Chapter 1

Introduction

1.1 Introduction

The objective of this thesis is to investigate alternative weighting functions for collapsing the multi-group constants using the various eigenvalue formulation of the Neutron Transport Equation (NTE). Specifically the work focused on collapsing the group constants (e.g. diffusion coefficient, fission cross section etc...) from an intermediate number of groups (in this study, the reference case has 33 energy groups) into a few-group structure, in order to better represent the analysis of transients involving the full-core. The nuclear data are initially obtained from a full-core simulation using a Monte Carlo transport code. The nuclear data are then utilized as input in an in-house code developed in the work to solve various formulations of the criticality eigenvalue problem of the system and generate the weighting functions, which correspond to the fundamental mode of time neutron flux spectrum, required for the data collapsing procedure. The solver is implemented using the FreeFEM++ finite element language. The transients of the system under investigation are simulated using the FRENETIC code developed in the last ten years at Politecnico di Torino [1].

The subsequent sections of the thesis provide a brief overview of the theoretical principles underlying the adopted physical-mathematical model. The code development process within the FreeFEM++ environment will be discussed in detail, covering aspects such as the creation of the geometry, the mesh generation, and the definition of the mathematical system of equations, including equations and boundary conditions. Subsequently, a simple model consisting of a single homogeneous hexagon with 2 energy groups is initially examined to assess the solver's performance. More complex systems are then studied, and the discrepancies between the neutron distributions obtained using different forms of the eigenproblem will be analyzed. Following these investigations, the transients will be described and defined, both in a standalone 2D model focused on neutron dynamics only, and in a multiphysics 3D model where the neutron field is coupled with thermo-fluid dynamics.

In order to introduce the formulation of the considered eigenvalue formulations, a

theoretical introduction about the Neutron Transport Equation is reported.

1.1.1 Main physical quantities

In the following the reader will find a short list of the main physical quantities used in this work.

With t , it is indicated the time, $\vec{r} = (x, y, z)$ the spatial position, E the energy, $\vec{v} = (v_x, v_y, v_z)$ the velocity, $E_k = \frac{1}{2}m|\vec{v}^2|$ the kinetic energy, and $\vec{\Omega} = \frac{\vec{v}}{|\vec{v}|}$ the direction, defined as

$$\begin{cases} \vec{\Omega} = \Omega_x \vec{i} + \Omega_y \vec{j} + \Omega_z \vec{k} \\ \Omega_x^2 + \Omega_y^2 + \Omega_z^2 = 1. \end{cases} \quad (1.1)$$

Note that the spherical reference system is usually preferred, so defining as θ the latitude and as ϕ the longitude it is easy to specify

$$\begin{cases} \Omega_x = \sin(\theta) \cos(\phi) = \sqrt{1 - \mu^2} \cos(\phi) \\ \Omega_y = \sin(\theta) \sin(\phi) = \sqrt{1 - \mu^2} \sin(\phi) \\ \Omega_z = \cos(\theta) = \mu, \end{cases} \quad (1.2)$$

that is

$$\vec{\Omega} = \sqrt{1 - \mu^2} \cos(\phi) \vec{i} + \sqrt{1 - \mu^2} \sin(\phi) \vec{j} + \mu \vec{k}. \quad (1.3)$$

Now is possible to define the density function, which is a distribution function

$$n(\vec{r}, E, \vec{\Omega}, t). \quad (1.4)$$

This density function describes the number of neutron present inside an infinitesimal volume $d\vec{r}$, a energy range $(E; E + dE)$ and a flying direction inside the solid angle $d\Omega$. These variables constitute the so-called *phase space*. Moreover the neutron density also depends on the time.

In other words, the neutron density describes the number of neutrons, in the *phase space*, i.e. the number of particle per unit volume, velocity, energy and flying direction, moreover per unit time.

When neutrons move through space, they interact with matter. Neutrons can have different interactions with particles surrounding them: scattering, fission, capture are some of them. Each kind of interaction has a certain probability of occurrence. In general, we indicate with Σ_x the probability for unit of path that the event x occurs (i.e. the collision that generates the event x) and it is measured in cm^{-1} . Σ_x is also called *macroscopic cross section*. Each interaction is due to the collision of neutrons against other nuclei of the medium, as neutron vs neutron collisions are often neglected in nuclear engineering applications. The area of the target involved in the collision is called *microscopic cross section*; we generally indicate it with the symbol σ and it is measured in cm^2 or in barn ($1 \text{ barn} = 10^{-24} \text{ cm}^2$). Let us have now a wall of area A [cm^2], thickness s [cm], density of particles N [nuclei/cm^3] and a certain flux

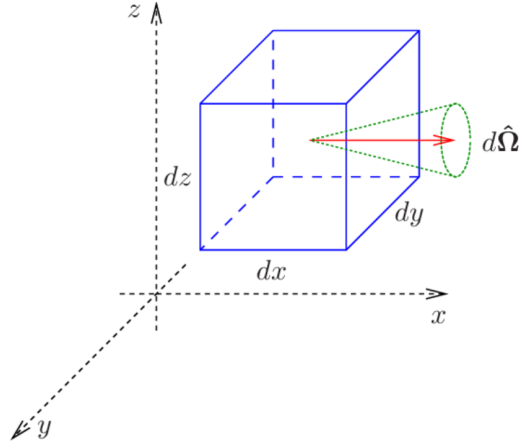


Figure 1.1: Graphic representation of the infinitesimal volume $d\vec{r}$, and $d\Omega$ solid angle.

of neutrons passing through it. The probability that the collision x occurs between neutrons and the wall particles is the fraction between the total volume of particles involved in the collision and the total volume of the wall. The first term can be evaluated multiplying the total number of particles in the wall, NAs , by the area of the particles involved in the collision, σ_x .

$$\frac{NAs\sigma_x}{As} = N\sigma_x = \Sigma_x, \quad (1.5)$$

Where Σ_x is called *macroscopic cross section*, knowing the cross section of each event is crucial to calculate the number of interactions of that type. For example, knowing the fission cross-section of a certain element, such as Uranium-235, allows us to evaluate how many fissions a certain neutron flux will generate. The number of interactions can be written as the total distance traveled by neutrons in a certain media multiplied by the probability for unit path (i.e. the macroscopic cross-section) of that kind of interaction. The total distance traveled by neutrons is the multiplication of the total number of neutrons by the distance traveled at their speed, v , by the time dt :

$$n(\vec{r}, E, \vec{\Omega}, t)d\vec{r}dEd\Omega vdt\Sigma_x. \quad (1.6)$$

Note that the quantity $n(\vec{r}, E, \vec{\Omega}, t)v$ is called *angular flux* or just *flux* and is indicated with $\phi(\vec{r}, E, \vec{\Omega}, t)$.

In order to know the total number of "x" interaction, for whatever energy and direction of the collided neutrons, has to be calculated in a certain region of the phase space the following quantity, which indicates the reactions of type per occurring:

$$\oint_{\Omega} \int_E \phi(\vec{r}, E, \vec{\Omega})\Sigma_x d\vec{r}dEd\Omega dt. \quad (1.7)$$

As said before, there are different kind of interactions, like *capture*, *fission*, *scattering*. Usually the capture and fission process are summed up to form the absorption cross section: $\Sigma_a(E, \vec{r}) = \Sigma_f(E, \vec{r}) + \Sigma_c(E, \vec{r})$. In general $\frac{1}{\Sigma_t}$ is also called "main free path", since it could be also considered a probability per unit length of colliding. In other words, if a "l" neutron fly length is considered, the probability that neutron goes on collision is equal to $p_{coll} = \Sigma_x l$. When $\phi(\vec{r}, E, \vec{\Omega}, t) d\vec{r} dE d\Omega dt$ is multiplied with a macroscopic crosssection, essentially the calculation considers all the neutrons inside the infinitesimal *phase space* ($d\vec{r} d\Omega dE$), times the probability the neutron collision. Notice that the traveled space by the neutron is given by $v dt$. Using this calculations for every interaction corss section, it is obtained the total number of neutrons that are *removed* from the observed *phase space* inside dt frame, to another energy range and/or direction and/or volume.

What if this interaction, instead, hallows neutrons entering the observed *phase space*, inside dt frame? In this case it has to be considered the the number of neutorns of a different phase space ($\phi(\vec{r}, E', \vec{\Omega}', t) d\vec{r} dE' d\Omega' dt$), their probability of collision ($\Sigma_x v dt$) and the probability that after the collision the same neutrons (in case of scattering) or new neutrons (in case of fission) are emitted inside the observed *phase space*. This last term depends on what kind of interaction is considered.

As concern the scattering the scattering probability density function f_s is defined: depends on the position of the neutron, on the energy before (E') and after (E) and on the direction before (Ω') and after (Ω) the collision. In particular, in an isotropic medium, probability does not depend on the incoming direction of the neutron (it is a rotational invariant), so it will depend only in the angle the two directions may form (i.e. we can consider just the scalar product of them): $f_s(\vec{r}, E' \rightarrow E, \vec{\Omega}' \rightarrow \vec{\Omega}) \implies f_s(\vec{r}, E' \rightarrow E, \vec{\Omega}' \cdot \vec{\Omega})$

Regarding fission, it is possible to define $\nu(\vec{r}, E')$, the number of neutrons emitted in \vec{r} by neutrons with energy E' (before the collision), and the *fission spectrum* $\chi(\vec{r}, E)$ which represents the probability density of being reissued within the energy interval ($E; E + dE$). . Moreover, fission can be considered isotropic, so the probability for a neutron of being reissued in a certain direction is equal for all direction (i.e. $\frac{1}{4\pi}$).

1.1.2 Neutron Transport Equation (NTE)

In the previous section, all the ingredients to build the NTE are given. Firstly an infinitesimal region of the *phase space* is considered in the dt frame. At this point all the source and sink themr are considered here below.

$$\begin{aligned}
 & [\text{neutron at time } (t + dt)] - [\text{neutron at time } (t)] = \\
 & \quad [\text{neutron moving in}] - [\text{neutron moving out}] \\
 & \quad - [\text{collided neutron}] + [\text{neutron scattered in from outside}] \\
 & \quad + [\text{source}]
 \end{aligned} \tag{1.8}$$

Using the described terms in the previous section, **Equation** (1.8) becomes:

$$\begin{aligned}
 & [n(\vec{r}, E, \vec{\Omega}, t + dt) - n(\vec{r}, E, \vec{\Omega}, t)] d\vec{r} dE d\Omega dt = -\nabla \cdot \vec{\Omega} \phi(\vec{r}, E, \vec{\Omega}, t) d\vec{r} dE d\Omega dt \\
 & - \Sigma_t(\vec{r}, E) \phi(\vec{r}, E, \vec{\Omega}, t) d\vec{r} dE d\Omega dt \\
 & + \oint d\Omega' \int dE' \Sigma_s(\vec{r}, E') \phi(\vec{r}, E', \vec{\Omega}', t) f_s(\vec{r}, E' \rightarrow E, \vec{\Omega}' \cdot \vec{\Omega}) d\vec{r} dE d\Omega dt \\
 & + S(\vec{r}, E, \vec{\Omega}, t) d\vec{r} dE d\Omega dt
 \end{aligned} \tag{1.9}$$

At this point the equation is divided with the differential *phase space* ($d\vec{r} dE d\Omega$) and then the difference between the neutron density at time ($t + dt$) and at time (t), since the time interval is infinitesimal, also this difference is a infinitesimal thus: $n(\vec{r}, E, \vec{\Omega}, t + dt) - n(\vec{r}, E, \vec{\Omega}, t) = dn(\vec{r}, E, \vec{\Omega}, t)$. Then equation **Equation** (1.9) is derived in time. **Equation** (1.9) becomes:

$$\begin{aligned}
 \frac{\partial n(\vec{r}, E, \vec{\Omega}, t)}{\partial t} & = -\nabla \cdot \vec{\Omega} \phi(\vec{r}, E, \vec{\Omega}, t) - \Sigma_t(\vec{r}, E) \phi(\vec{r}, E, \vec{\Omega}, t) \\
 & + \oint d\Omega' \int dE' \Sigma_s(\vec{r}, E') \phi(\vec{r}, E', \vec{\Omega}', t) f_s(\vec{r}, E' \rightarrow E, \vec{\Omega}' \cdot \vec{\Omega}) + S(\vec{r}, E, \vec{\Omega}, t)
 \end{aligned} \tag{1.10}$$

Since on the left hand side, the unknown variable is $n(\vec{r}, E, \vec{\Omega}, t)$, while on the right hand side is $\phi(\vec{r}, E, \vec{\Omega}, t)$; the first term is rewritten as: $n(\vec{r}, E, \vec{\Omega}, t) = \frac{1}{v} \phi(\vec{r}, E, \vec{\Omega}, t)$. Hence the previous equation became:

$$\begin{aligned}
 \frac{1}{v} \frac{\partial \phi(\vec{r}, E, \vec{\Omega}, t)}{\partial t} & = -\nabla \cdot \vec{\Omega} \phi(\vec{r}, E, \vec{\Omega}, t) - \Sigma_t(\vec{r}, E) \phi(\vec{r}, E, \vec{\Omega}, t) \\
 & + \oint d\Omega' \int dE' \Sigma_s(\vec{r}, E') \phi(\vec{r}, E', \vec{\Omega}', t) f_s(\vec{r}, E' \rightarrow E, \vec{\Omega}' \cdot \vec{\Omega}) + S(\vec{r}, E, \vec{\Omega}, t)
 \end{aligned} \tag{1.11}$$

Note that, for sake of simplicity, fission term has been neglected. Following the same procedure the NTE with the fission term.

$$\begin{aligned}
 \frac{1}{v} \frac{\partial \phi(\vec{r}, E, \vec{\Omega}, t)}{\partial t} & = -\nabla \cdot \vec{\Omega} \phi(\vec{r}, E, \vec{\Omega}, t) - \Sigma_t(\vec{r}, E) \phi(\vec{r}, E, \vec{\Omega}, t) \\
 & + \oint d\Omega' \int dE' \Sigma_s(\vec{r}, E') \phi(\vec{r}, E', \vec{\Omega}', t) f_s(\vec{r}, E' \rightarrow E, \vec{\Omega}' \cdot \vec{\Omega}) \\
 & + \oint d\Omega' \int dE' \Sigma_f(\vec{r}, E') \phi(\vec{r}, E', \vec{\Omega}', t) \frac{\chi(\vec{r}, E)}{4\pi} + S(\vec{r}, E, \vec{\Omega}, t)
 \end{aligned} \tag{1.12}$$

1.1.3 Criticality problem

First, the **Equation** (1.12) is written in operator form. Before the operators descriptions, it is important to point out, that, since the aim is to study the criticality of the system, the time dependence is not considered.

$$\hat{T} = \nabla \cdot \vec{\Omega} + \Sigma(\vec{r}, E) \quad (1.13)$$

$$\hat{\vartheta} = \oint d\Omega' \int dE' \Sigma_s(\vec{r}, E') f_s(\vec{r}, E' \rightarrow E, \vec{\Omega}' \cdot \vec{\Omega}) \quad (1.14)$$

$$\hat{F} = \oint d\Omega' \int dE' \Sigma_f(\vec{r}, E') \frac{\chi(\vec{r}, E)}{4\pi} \quad (1.15)$$

Then is possible to define the operator as:

$$\hat{L} = \hat{T} - \hat{\vartheta} \quad (1.16)$$

Finally the **Equation** (1.12) can be formulated with the operator form

$$\hat{T}\phi = \hat{F}\phi + \hat{\vartheta}\phi + \hat{S}\phi \quad (1.17)$$

Where the fission process is introduced. Now that the problem is set, it is possible to argue that, in principle, we are not sure that **Equation** (1.12) has a meaningful solution. To have a physical solution we need to verify that our system is *sub-critical* otherwise the presence of the external source will make it diverge. So we consider a system without a source and the corresponding equation is **Equation** (1.18). This equation is homogeneous. thus to find a non-zero solution, we introduce an *eigenvalue* k . Once k is inserted, a solution to this equation is always guaranteed and it is called an *eigenfunction*.

If $k = 1$ the system is called critical, which means the neutron population self-sustains. If k is more or less than one, this means that k has not a direct physical meaning but provides us important information: $k < 1$ means that fission process is not able to compensate the leakages, the neutron population is not self-sustaining itself and the system is called sub-critical; $k > 1$ means that the fission process is producing more neutrons than those that are lost, the system is called *super-critical*.

$$\hat{T}\phi = \frac{1}{k}\hat{F}\phi + \hat{\vartheta}\phi \quad (1.18)$$

References

- [1] D. Caron, R. Bonifetto, S. Dulla, V. Mascolino, P. Ravetto, L. Savoldi, D. Valerio, and R. Zanino. «Full-core coupled neutronic/thermal-hydraulic modelling of the EBR-II SHRT-45R transient». In: *International Journal of Energy Research* 42.1 (2018), pp. 134–150. DOI: <https://doi.org/10.1002/er.3571>. eprint: <https://onlinelibrary.wiley.com/doi/pdf/10.1002/er.3571>. URL: <https://onlinelibrary.wiley.com/doi/abs/10.1002/er.3571>.

Chapter 2

The adoption of the FreeFEM++ language for the solution of the diffusion equation

In this chapter, a comprehensive account will be provided regarding the development of the finite element solver, which is intended to address and resolve the criticality problem. The description commences with an elaboration on the methodology employed to generate the reactor core's geometry. Moreover, a meticulous examination of a singular hexagonal system comprising homogeneous material with two energy groups will also be undertaken. The primary aim of this analysis is to ascertain the verification of the developed FreeFEM++ solver. As a benchmark for this assessment, the analytical solutions of k_∞ (infinite multiplication factor) and k_{eff} (effective multiplication factor) are employed.

2.1 FreeFEM++: Core Geometry

Firstly a short description of FreeFEM++ software is given: *FreeFEM is a partial differential equation solver for non-linear multi-physics systems in 1D, 2D, 3D and 3D border domains (surface and curve). Problems involving partial differential equations from several branches of physics, such as fluid-structure interactions, require interpolations of data on several meshes and their manipulation within one program. FreeFEM includes a fast interpolation algorithm and a language for the manipulation of data on multiple meshes. FreeFEM is written in C++ and its language is a C++ idiom.* [1].

As a first step to build the solver, it is necessary to build the geometry of a generic hexagonal-assembly core reactor. The geometry definition in FreeFEM++ is based on the usage of the *border* command. In order to build a hexagonal-core-configuration,

the most important parameter are essentially three:

- **Hexagon Pitch:** it is the distance between the two parallel side of the same hexagon
- **Number of sextant's rows:** The sextant is the minimum symmetric portion of an generic hexagonal geometry. This concept is extremely important for hexagonal-shaped-core, since it is possible to study only one sixth of the system, provided that the material arrangement is symmetric as well, saving computational effort and CPU time.
- **Number of hexagonal element for each row:** Since, in principal, the core geometry can be quite irregular, this parameter is very important in order to generate a program as much general as possible.

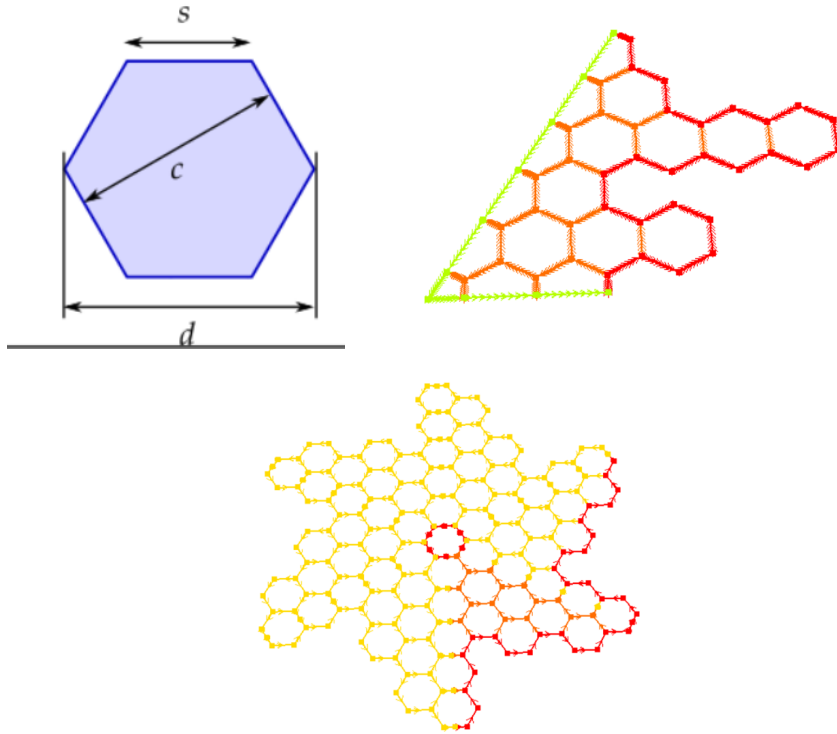


Figure 2.1: (top-left): the "c" parameter represents the hexagon's pitch. (top-right): an example of generic sextant geometry. (bottom): generic core geometry

As concern the singular hexagon geometry, only the first parameter is needed, of course. The result is reported in figure 2.2

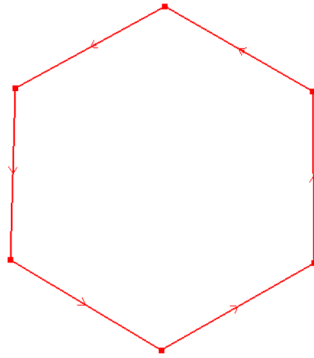


Figure 2.2: One Hexagon geometry, built with *FreeFEM*.

After the construction of the geometry, the mesh definition is needed: FreeFEM++ is able to construct its own mesh structure, starting from the nodes of the geometry's borders. For example, in figure 2.2 the element is "linked" by six nodes (corners and arrows), and an example of the automatically generated mesh is reported in the following figure.

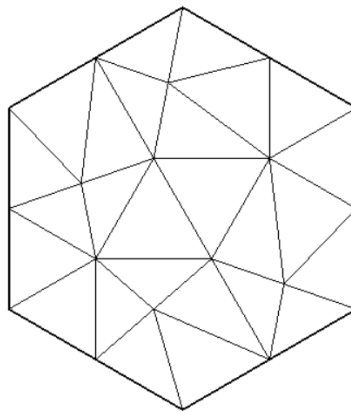


Figure 2.3: One Hexagon mesh, automatically built with *FreeFEM*.

Unfortunately there is not a direct command to impose the construction of a structured mesh, however -for simple geometry- it is possible to adopt this scheme: generate the geometry only with 6 nodes (one for each "corner"), in doing so, the hexagon mesh will be formed automatically by 6 equilateral triangles, perfectly distributed in the element. After that, use a special command ("**trunc**") to truncate the mesh. Here below an example is reported.

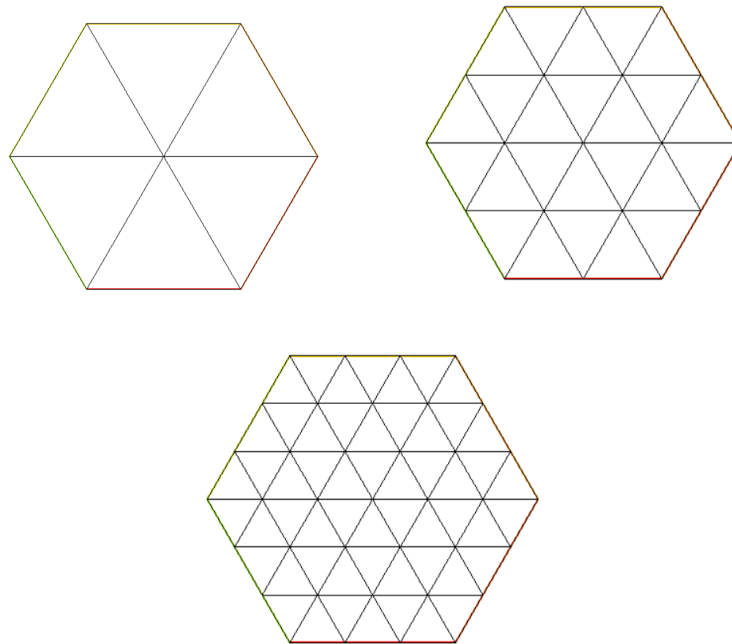


Figure 2.4: (top-left): simple structured mesh with only one element per border. (top-right): structured mesh with two element per border.(bottom):structured mesh with three element per border

This geometry, even if extremely simple, could be still useful to study simpler case in order to understand if the elementary, basic program is consistent or not. This aspect will be shown later.

As concern more complicated geometry, the procedure is definitely much more complicated. As mentioned earlier, it is typically more common to focus on studying a subsection of the complete core geometry, specifically one-sixth of it, which is commonly referred to as a "sextant." Constructing such a geometry presents a challenge due to the requirement that the edges of the hexagons comprising the sextant must not intersect or overlap.

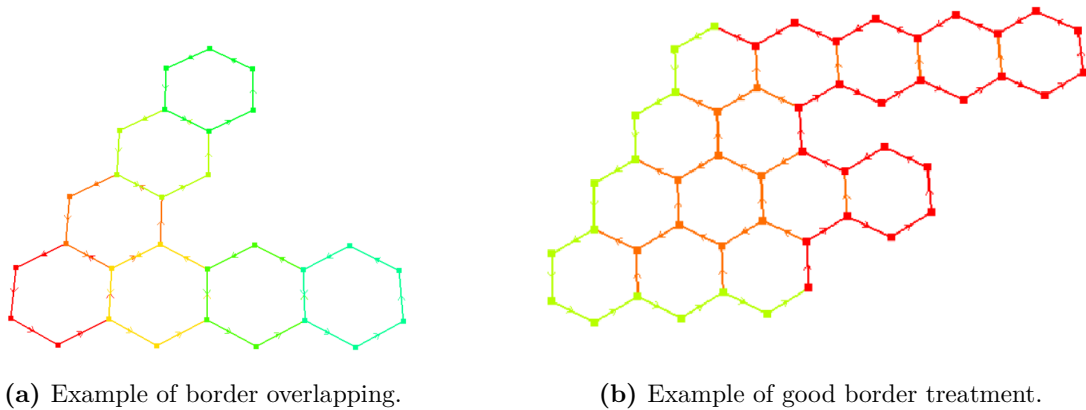


Figure 2.5: Examples of wrong geometry treatment 2.5a, and good one 2.5b.

Looking at **Figure 2.5a**, focusing on the different color of the border, is easy to understand that the border are in contact to each others. This fact causes the impossibility to create a mesh, because of some conflicts in FreeFEM++’s algorithm, while in **Figure 2.5b** the borders are not overlapped, as can be seen. This last one is the right strategy to allow FreeFEM++ to generate a mesh.

To create this type of geometry without falling into the problem just described, the procedure is not trivial. The adopted method is quite complicated but reliable: it consists on assembly of the right element-type piece by piece, knowing *ex ante* their distribution and so the number of borders surrounding the considered element. Due to this step by step assembly method, this method has been baptised as *IKEA method* and it can be schematized as follows:

1. Insertion of the fundamental input data (previously listed) .
2. knowing the distribution of the hexagonal elements, their centers can be identified.
3. Since the number of hexagons for any rows is known, it is possible to select the right border arrangement type among the ones listed in **Figure 2.6**
4. At this point, a vector containing all the points’ coordinates of the geometry has been created. The command **”border”** can be used to generate the structure.

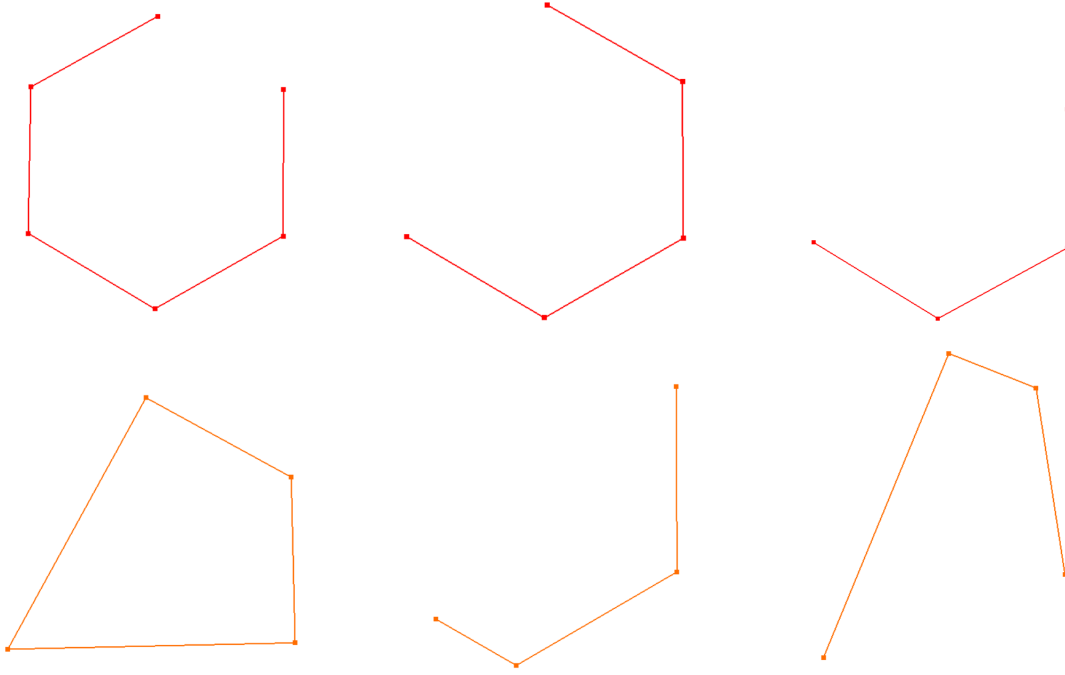


Figure 2.6: All the different kinds of border arrangement used to build the sextant.

Till now, it has been described the scheme used to create the geometry of a generic hexagonal-core. The next step is to carry on a simple case of criticality problem (**Section 1.1.3**). So in the next section the concept of multi group theory and the mathematical model used to handle NTE will be briefly introduced.

2.1.1 Preliminary calculation: Diffusion two group model

Theoretical introduction: Diffusion Theory and Multi group method

The common feature to all deterministic solution methods is usually that approximations are needed to deal with the continuous-energy dependence of flux and cross sections. The energy spectrum is divided into discrete groups, which are indexed in descending order, starting from the highest group ($g = 1$) with upper energy boundary E_0 . The angular group flux in group g is defined as:

$$\phi_g(\vec{r}, \vec{\Omega}) = \int_{E_g}^{E_{g-1}} \phi(\vec{r}, \vec{\Omega}, E) dE. \quad (2.1)$$

Reaction cross sections are averaged over the same energy intervals in such a way that the reaction rates are preserved. For this reason a generic cross section ($\Sigma_i(\vec{r}, E)$) is be defined as:

$$\Sigma_{i,g} = \frac{\oint \int_{E_{g-1}}^{E_g} \Sigma_i(\vec{r}, E) \phi(\vec{r}, \vec{\Omega}, E) dE d\Omega}{\oint \int_{E_{g-1}}^{E_g} \phi(\vec{r}, \vec{\Omega}, E) dE d\Omega}. \quad (2.2)$$

In other words, the flux is used as weighting function for the evaluation of $\Sigma_{i,g}$. The same discussion is still valid for any other quantity of the NTE.

The energy-dependence is not the only problem in solving the transport equation. Another problem lies in the angular dependence. The integration over the angular variable yields the neutron continuity equation (**Equation** (1.12)), which is independent of $\vec{\Omega}$. The problem with this equation, however, is that there is another function to be solved, namely the current density $\vec{J}(\vec{r}, E, t)$ that is the product of the *angular flux* and the $\vec{\Omega}$ direction. The connection of the two unknown functions necessarily demands the reinstatement of the angular dependence.

$$\vec{J}(\vec{r}, E, \vec{\Omega}, t) = \vec{\Omega}\phi(\vec{r}, E, \vec{\Omega}, t) \quad (2.3)$$

The exact treatment of the angular variable is simply not possible and approximation methods and additional assumptions are needed to attain a solution. There are practically four main categories of deterministic solution methods [2]:

1. The Method of characteristics.
2. The collision probability method.
3. The discrete ordinates method (also known as S_n).
4. The method of spherical harmonics (also known as P_n).

Instead, the following paragraph describes the use of *Diffusion model*, which is one of the simplest means to approach neutron transport problems. The diffusion theory is basically equivalent to the first-order spherical harmonics method (P_1), and also of the second order discrete ordinates method (S_2); but it can also be derived directly, as will be done in the following.

Diffusion processes are encountered in various fields of physics and they are related to the collective movement of a large number of particles through a permeable medium. The phenomenon is stochastic at the microscopic level, as each particle undergoes an individual random walk process while colliding with its surroundings. A typical example is the mixing of gases or liquids initially separated from each other. The common feature to all diffusion processes is that the motion takes place without a net external force, from a higher to a lower concentration. The diffusion model can also be used for describing the flow of neutrons through the reactor core. Neutron diffusion theory is an approximation to the general transport theory, and as was stated in the previous chapter, it is one of the simplest means to solve neutron transport problems. A good starting point for the derivation of diffusion theory is the neutron continuity **Equation** (1.12), which is integrated over the energy variable to remove the continuous energy-dependence. The mathematical used procedure is the same of the already explained formulations of **Equation** (2.1) and **Equation** (2.2). So for most of the terms of **Equation** (1.12) it is sufficient to substitute $\phi(\vec{r}, E, \vec{\Omega}, t)$ with the *scalar flux* (or *total flux*: $\Phi_g(\vec{r}, t)$). The same is done also for the total cross section that embed all the collision phenomena leading the neutron to escape from the system. Thus,

$\Sigma_t(\vec{r}, E) \implies \Sigma_{t,g}(\vec{r})$. As concern the neutron current density: $J(\vec{r}, E, t) \implies J_g(\vec{r}, t)$. The integration of the time-derivate term yields:

$$\int_{E_g}^{E_{g-1}} \frac{1}{v} \frac{\partial \phi(r, \vec{E}, t)}{\partial t} = \frac{\partial}{\partial t} \int_{E_g}^{E_{g-1}} \frac{1}{v} \phi(r, \vec{E}, t) dE = \frac{1}{v_g} \frac{\partial \Phi_g}{\partial t}. \quad (2.4)$$

Where:

$$\frac{1}{v_g} = \frac{\int_{E_g}^{E_{g-1}} \frac{1}{v} \phi(\vec{r}, E) dE}{\int_{E_g}^{E_{g-1}} \phi(\vec{r}, E) dE} = \frac{\int_{E_g}^{E_{g-1}} n(\vec{r}, E) dE}{\int_{E_g}^{E_{g-1}} \phi(\vec{r}, E) dE} \quad (2.5)$$

The integration of the source terms is a bit more complicated. The group-wise form of the fission source is written as:

$$\int_{E_g}^{E_{g-1}} \left[\int_0^\infty \chi(E) \nu \Sigma_f(\vec{r}, E') \phi(\vec{r}, E', t) dE' \right] dE = \chi_g \sum_{g'=1}^G [\nu \Sigma_{f,g'}(\vec{r}) \Phi_{g'}(\vec{r}, t)] \quad (2.6)$$

As concern the scattering term, it is a bit more complicated. For the sake of simplicity it could be directly defined a cross section quantity for the scattering term as: $\Sigma_s(\vec{r}, E' \rightarrow E)$ and discretaising in energy it becomes:

$$\Sigma_{s,g \rightarrow g'} = \frac{\int_{E_g}^{E_{g-1}} \int_{E_g}^{E_{g-1}} \Sigma_s(\vec{r}, E' \rightarrow E) \phi(\vec{r}, E') dE dE'}{\int_{E_g}^{E_{g-1}} \phi(\vec{r}, E') dE'} \quad (2.7)$$

The collection of the above results yields for the group-wise continuity equation:

$$\begin{aligned} \frac{1}{v_g} \frac{\partial \Phi(\vec{r}, t)}{\partial t} + \nabla \cdot \vec{J}(\vec{r}, t) + \Sigma_{t,g}(\vec{r}) \Phi_g(\vec{r}, t) \\ = \\ \sum_{g'=1}^G [\Sigma_{s,g' \rightarrow g}(\vec{r}) \Phi_{g'}(\vec{r}, t)] + \chi_g \sum_{g'=1}^G [\Sigma_{f,g'}(\vec{r}) \Phi_{g'}(\vec{r}, t)] \end{aligned} \quad (2.8)$$

At this point the actual diffusion theorem can be used. The *Fick's Law* suggests that the neutron current density is proportional to the flux gradient, hence:

$$\vec{J}(\vec{r}, t) = -D_g(\vec{r}) \nabla \Phi_g(\vec{r}, t), \quad (2.9)$$

where $D_g(\vec{r})$ is known as the *diffusion coefficient*. It can be demonstrated in different ways that the diffusion coefficient has the form of:

$$D_g(\vec{r}) = \frac{1}{3 \Sigma_{tr,g}(\vec{r})} \quad (2.10)$$

where $\Sigma_{tr,g}(\vec{r})$ is the *transport-corrected total cross section*, or simply the *transport cross section*, given by:

$$\Sigma_{tr,g}(\vec{r}) = \Sigma_{t,g}(\vec{r}) - \bar{\mu}_0 \Sigma_{s,g}(\vec{r}) \quad (2.11)$$

Parameter $\bar{\mu}_0$ is the cosine of the average scattering angle, while the parameter $\Sigma_{s,g}(\vec{r})$ is the same of $\Sigma_{s,g \rightarrow g}(\vec{r})$, so the **internal-group scattering**.

Now, combining **Equation** (2.8) and **Equation** (2.9) the continuity equation becomes:

$$\begin{aligned} \frac{1}{v_g} \frac{\partial \Phi(\vec{r}, t)}{\partial t} + \nabla \cdot D_g(\vec{r}) \nabla \Phi_g(\vec{r}, t) + \Sigma_{t,g}(\vec{r}) \Phi_g(\vec{r}, t) = \\ \sum_{g'=1}^G [\Sigma_{s,g' \rightarrow g}(\vec{r}) \Phi_{g'}(\vec{r}, t)] + \chi_g \sum_{g'=1}^G [\Sigma_{f,g'}(\vec{r}) \Phi_{g'}(\vec{r}, t)] \end{aligned} \quad (2.12)$$

Once **Equation** (2.12) has been found, it can be adapted to any number of groups (the total number is indicated with the letter G). In reactor physics, the *two group diffusion model* is very popular to design and analyse LWRs. It consists in dividing the energy spectrum into only two energy groups. Group 1, or the *fast group* consists of neutrons with energy above $0.625eV$. Neutrons below this energy belong to group 2, or the *thermal group*. The group boundary is chosen in such a way that the energy peak formed by fully thermalised neutrons is completely enclosed within the thermal group, as can be seen in **Figure 2.7**

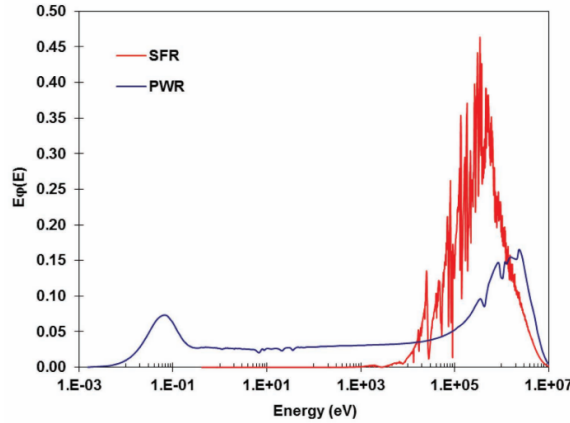


Figure 2.7: Examples of the Energy spectrum of a thermal reactor (**PWR**) and a fast reactor (**SFR**), [3]. The thermal peak of energy does not overcome the $0.625eV$. As concern the SFR's *spectrum*, it has no peak in the thermal region, due to the fact that the SFR is a fast reactor where neutrons are not *thermalized* by a *moderator*.

The steady-state equations in the criticality eigenvalue form can be written as:

$$\begin{cases} -D_1 \nabla^2 \Phi_1(\vec{r}) + \Sigma_{r,1} \Phi_1(\vec{r}) = \frac{1}{k_{eff}} [\nu \Sigma_{f,1} \Phi(\vec{r}) + \nu \Sigma_{f,2} \Phi_2(\vec{r})] \\ -D_2 \nabla^2 \Phi_2(\vec{r}) + \Sigma_{a,2} \Phi_2(\vec{r}) = \Sigma_{s,1 \rightarrow 2} \Phi(\vec{r}) \end{cases} \quad (2.13)$$

Some considerations can be made,

- Being **Equation** (2.13) refers to critical condition of the reactor, so no time dependence is present.
- χ_1 and χ_2 are still present in the equation system: it is assumed that, consistently with the fission features, the two-group fission spectrum is simply $\chi_1 = 1$ and $\chi_2 = 0$ (since the minimum energy of fission neutron is of the order of 100 eV, and the energy grid distinguishes only neutrons with $E < 0.625$ eV and $E > 0.625$ eV).
- The fast removal. cross section $\Sigma_{r,1}$ gives the rate at which neutrons are removed from the fast group either by absorption or down-scattering to group 2: $\Sigma_{r,1} = \Sigma_{a,1} + \Sigma_{s,1 \rightarrow 2}$
- The removal cross section in group 2 is practically reduced to $\Sigma_{a,2}$, due to the lack of up-scattering
- Laplacian operator derives from the assumption that a homogeneous medium is considered, thus: $\nabla \cdot D\nabla\Phi(\vec{r}) \implies D\nabla^2\phi(\vec{r})$

In order to predict if the reactor configuration allows to reach the criticality of the system, as previously anticipated in **Section 1.1.3**, the *eigenvalue* must be equal as to 1. However usually, before doing the calculation using **Equation** (2.13), an **infinite system** is considered. By considering an infinite system is possible to evaluate the so called k_∞ : this parameter is very important since allows to know if the reactor could be critical independently from its geometry.

In case of an infinite system, the solution of two group model can involve only constant solution in a steady state case. In fact, if ϕ_1 and ϕ_2 were not constant, neutrons would move from position with high flux to position with lower flux and the system would not be steady. For this reason the **Equation** (2.13) becomes:

$$\begin{cases} \Sigma_{r,1}\Phi_1(\vec{r}) = \frac{1}{k_{eff}} [\nu\Sigma_{f,1}\Phi(\vec{r}) + \nu\Sigma_{f,2}\Phi_2(\vec{r})] \\ \Sigma_{a,2}\Phi_2(\vec{r}) = \Sigma_{s,1 \rightarrow 2}\Phi(\vec{r}) \end{cases} \quad (2.14)$$

In order to have a solution, the determinant of the matrix of the system should be zero.

$$\begin{vmatrix} \Sigma_{r,1} - \frac{1}{k}\nu\Sigma_{f,1} & -\frac{1}{k}\nu\Sigma_{f,2} \\ -\Sigma_{s,1 \rightarrow 2} & \Sigma_{a,2} \end{vmatrix} = (\Sigma_{r,1} - \frac{1}{k}\nu\Sigma_{f,1})(\Sigma_{a,2}) - (-\frac{1}{k}\nu\Sigma_{f,2})(-\Sigma_{s,1 \rightarrow 2}) = 0 \quad (2.15)$$

From the characteristic expression, the expression of k_∞ is obtained:

$$k_\infty = \frac{\nu\Sigma_{f,1}}{\Sigma_{r,1}} + \frac{\nu\Sigma_{f,2}\Sigma_{s,1 \rightarrow 2}}{\Sigma_{a,2}\Sigma_{r,1}} \quad (2.16)$$

k_∞ is a number, to attach to a material for an infinite medium. k_∞ characterizes your system from the material point of view and in no way your geometry since in an infinite system is impossible to define a geometry. If k_∞ is larger than one, then it is possible to realize steady state critical reactor in a finite geometry using these materials. If k_∞ is lower than one, then no way to obtain critical steady state in a finite geometry because in finite geometry ulterior losses are introduced, due to leakages.

If it is greater than 1, the reactor core could reach the criticality condition. In order to know if the system actually reaches the criticality condition, the geometrical aspect must be considered too. Hence the study of the finite system is carried on.

In this case, the fluxes are no more constrained to be constant by the infinite medium hypothesis, and **Equation** (2.15) becomes:

$$\begin{pmatrix} \nabla^2 & 0 \\ 0 & \nabla^2 \end{pmatrix} \begin{pmatrix} \phi_1 \\ \phi_2 \end{pmatrix} + \begin{pmatrix} -\frac{1}{L_1^2} + \frac{\nu\Sigma_{f,1}}{kD_1} & -\frac{\nu\Sigma_{f,2}}{kD_1} \\ \frac{\Sigma_{s,1\rightarrow 2}}{D_2} & -\frac{1}{L_2^2} \end{pmatrix} \begin{pmatrix} \phi_1 \\ \phi_2 \end{pmatrix} = 0 \quad (2.17)$$

L_1^2 and L_2^2 are the *diffusion areas* and are defined as:

$$L_1^2 = \frac{D_1}{\Sigma_{r,1}} = \frac{D_1}{\Sigma_{a,1} + \Sigma_{s,1\rightarrow 2}} \quad (2.18)$$

$$L_2^2 = \frac{D_2}{\Sigma_{r,2}} = \frac{D_2}{\Sigma_{a,2}} \quad (2.19)$$

This equation can be written in compact form as:

$$\nabla^2 \hat{I}\vec{\phi} + \hat{A}\vec{\phi} = 0 \quad (2.20)$$

What we want to do is to find the eigenvectors of \hat{A} to represent the unknown flux vector. To obtain them we need to find first the eigenvalues of \hat{A} , i.e solving the following linear system:

$$(\hat{A} - \omega\hat{I})\vec{\Psi} = 0. \quad (2.21)$$

To solve this equation we need to impose the determinant of the matrix $\hat{A} - \omega\hat{I}$ is equal to zero

$$|\hat{A} - \omega\hat{I}| = 0. \quad (2.22)$$

After some manipulation we get an algebraic equation in ω to be solved for the two eigenvalues:

$$\omega^2 + \omega \left(\frac{1}{L_2^2} + \frac{1}{L_2^2} - \frac{\nu\Sigma_{f1}}{kD_1} \right) + \frac{1}{L_2^2} \frac{1}{L_2^2} - \frac{\nu\Sigma_{f1}}{kD_1 L_1^2} - \frac{\nu\Sigma_{f1}}{kD_1} \frac{\Sigma_{1\rightarrow 2}}{D_2} = 0, \quad (2.23)$$

whose solution is:

$$\omega_{1,2} \frac{1}{2} \left(\frac{\nu \Sigma_{f1}}{k D_1} - \frac{1}{L_2^2} - \frac{1}{L_1^2} \right) \pm \sqrt{\left(\frac{-\nu \Sigma_{f1}}{k D_1} + \frac{1}{L_2^2} + \frac{1}{L_1^2} \right)^2 - 4 \left(\frac{1}{L_1^2} \frac{1}{L_2^2} - \frac{\nu \Sigma_{f1}}{k D_1 L_1^2} - \frac{\nu \Sigma_{f2} \Sigma_{1 \rightarrow 2}}{k D_1 D_2} \right)} \quad (2.24)$$

it should be noted that both ω_1 and ω_2 depend on the eigenvalue k . Are the eigenvalues of matrix \hat{A} real? To ensure this condition, the quantity under the square root has to be positive. This term is made of two quantities. One is defined as a square quantity, so it is always positive; for the second one a constrain must be imposed. In fact in order to have real eigenvalues, the following term has to be positive.

$$\frac{1}{L_1^2} \frac{1}{L_2^2} - \frac{\nu \Sigma_{f1}}{k D_1 L_1^2} - \frac{\nu \Sigma_{f2} \Sigma_{1 \rightarrow 2}}{k D_1 D_2} > 0 \quad (2.25)$$

We isolate the value of k and get the following condition

$$k < \frac{\nu \Sigma_{f1}}{\Sigma_1} + \frac{\nu \Sigma_{f2} \Sigma_{1 \rightarrow 2}}{\Sigma_2 \Sigma_1} = k_\infty \quad (2.26)$$

The condition for having real ω 's eigenvalues is that the k of the finite system has to be smaller then the value k_∞ of the infinite medium. From a physical point of view this is guaranteed, because in a finite geometry there will be also the contribution of leakages to reduce the value of the multiplication factor k . Later in this section a posteriori mathematical proof will be given. So the two values of the ω 's are real, one positive and one negative. We define them as:

$$\omega_1 = \mu^2 \quad (2.27)$$

$$\omega_2 = -\xi^2 \quad (2.28)$$

Once the eigenvalues are defined, we can obtain the eigenvectors of the matrix \hat{A} , substituting in **Equation** (2.21) the previously found eigenvalues. Since the determinant of the matrix is zero (we enforced that to find eigenvalues), of course we have a degree of freedom inside the eigenvectors. So we set the first component $\Psi^{(1)} = 1$ and find the second one as:

$$\Psi^{(2)} = \frac{\frac{\Sigma_{1 \rightarrow 2}}{D_2}}{\frac{1}{L_2^2 + \omega}} \quad (2.29)$$

Inserting the two values of ω_1 and ω_2 we get the actual second components, respectively:

$$\Psi_1^{(1)} = \frac{\frac{\Sigma_{1 \rightarrow 2}}{D_2}}{\frac{1}{L_2^2} - \mu^2} \quad (2.30)$$

$$\Psi_1^{(2)} = \frac{\frac{\Sigma_{1 \rightarrow 2}}{D_2}}{\frac{1}{L_2^2} - \xi^2} \quad (2.31)$$

We have obtained what we were seeking: now we're able to express the fluxes in the base of the eigenvectors of matrix \hat{A} . We need to introduce some functions of space to fully describe the fluxes' dependence from space since the eigenvectors are not depending on space.

$$\begin{pmatrix} \phi(\vec{r}) \\ \phi(\vec{r}) \end{pmatrix} = f_1(\vec{r}) \begin{pmatrix} 1 \\ \Psi_1^{(2)} \end{pmatrix} + f_2(\vec{r}) \begin{pmatrix} 1 \\ \Psi_2^{(2)} \end{pmatrix} = f_1(\vec{r})\Psi_1^{(2)} + f_2(\vec{r})\Psi_2^{(2)} \quad (2.32)$$

And we obtain the definition of the fluxes in terms of the eigenvectors of the matrix \hat{A}

$$\phi_1 = f_1 + f_2 \quad (2.33)$$

$$\phi_2 = \Psi_1^{(2)} f_1 + \Psi_2^{(2)} f_2 \quad (2.34)$$

Thus,

$$\begin{pmatrix} \nabla^2 & 0 \\ 0 & \nabla^2 \end{pmatrix} [f_1 \vec{\Psi}_1 + f_2 \vec{\Psi}_2] + \hat{A}[f_1 \vec{\Psi}_1 + f_2 \vec{\Psi}_2] = 0 \quad (2.35)$$

Developing the products

$$\nabla^2 f_1 \vec{\Psi}_1 + \nabla^2 f_2 \vec{\Psi}_2 \underbrace{f_1 \hat{A} \vec{\Psi}_1}_{\omega_1 \vec{\Psi}_1} + f_1 \underbrace{\hat{A} \vec{\Psi}_2}_{\omega_2 \vec{\Psi}_2} = 0 \quad (2.36)$$

Then exploiting the fact that $\vec{\Psi}_1$ and $\vec{\Psi}_2$ are linearly independent we obtain two separates equations:

$$\nabla^2 f_1 + \omega_1 f_1 = 0 \quad (2.37)$$

$$\nabla^2 f_2 + \omega_2 f_2 = 0 \quad (2.38)$$

Using the definition of the ω 's we get:

$$\nabla^2 f_1 + \mu^2 f_1 = 0 \quad (2.39)$$

$$\nabla^2 f_2 - \xi^2 f_2 = 0 \quad (2.40)$$

Which are two separates and independent diffusion equations. The first equation is describing a multiplicative diffusive medium, the second one an absorbing diffusive medium. The linear combination of the two describes the starting problem. We began from a problem in which the two unknowns were present in both equations, and using this technique we can solve two separate equations, one for each unknown, then reconstruct the fluxes and get the solution of our starting coupled problem.

To solve equations **Equation** (2.39) we assume our geometry to be the 1D plane slab. The equations in this geometry are formulated as:

$$\frac{d^2 f_1(x)}{dx^2} + \mu^2 f_1 = 0 \quad (2.41)$$

$$\frac{d^2 f_2(x)}{dx^2} - \xi^2 f_2 = 0 \quad (2.42)$$

There is no doubt in the signs of the equations so the general solutions are:

$$f_1(x) = A_1 \cos(\mu x) + C_1 \sin(\mu x) \quad (2.43)$$

$$f_1(x) = A_2 \cosh(\xi x) + C_2 \sinh(\xi x) \quad (2.44)$$

For symmetry reasons $C_1 = C_2 = 0$, and so:

$$f_1(x) = A_1 \cos(\mu x) \quad (2.45)$$

$$f_1(x) = A_2 \cosh(\xi x) \quad (2.46)$$

the boundary conditions are:

$$\phi_1 \left(\pm \frac{H}{2} \right) = 0 \quad (2.47)$$

$$\phi_2 \left(\pm \frac{H}{2} \right) = 0 \quad (2.48)$$

But do these boundary conditions make sense physically? No, because there is no reason to assume that the extrapolated length of the systems are equal for both fluxes. This would mean both fluxes vanish at the same extrapolated distance. The answer is no. The extrapolated distance is dependent from the cross section and the diffusion coefficient which are different for the two groups. We can think that this slab “changes” size depending on the group you’re observing. Then we look at the values of these extrapolated distances and we discover they are very similar. They are not the same but they are similar for nuclear reactor theory. We can then say that this is not a physical boundary condition but it’s not a bad approximation. Reconstructing the fluxes using the the previous definition:

$$\phi_1 = A_1 \cos(\mu x) + A_2 \cosh(\mu x) \quad (2.49)$$

$$\phi_2 = A_1 \Psi_1^{(1)} \cos(\mu x) + A_2 \Psi_2^{(2)} \cosh(\mu x) \quad (2.50)$$

We can impose now one of the BC for each flux since imposing the symmetry we already determined two of the unknowns coefficients. We get a system to solve for A_1 and A_2

$$\begin{cases} A_1 \cos(\mu \frac{H}{2}) + A_2 \cosh(\mu \frac{H}{2}) = 0 \\ A_1 \Psi_1^{(1)} \cos(\mu \frac{H}{2}) + A_2 \Psi_2^{(2)} \cosh(\mu \frac{H}{2}) = 0 \end{cases} \quad (2.51)$$

Imposing the determinant of the matrix of coefficients of this linear system to be zero we get

$$\cos(\mu \frac{H}{2}) \cosh(\mu \frac{H}{2}) (\Psi_2^{(2)} - \Psi_1^{(1)}) = 0 \quad (2.52)$$

The only possibility to satisfy this equation is to set

$$\cos\left(\mu\frac{H}{2}\right) = 0 \quad (2.53)$$

Which can be satisfied by choosing the argument of the cosine equal to any odd-multiple number of $\frac{\pi}{2}$

$$\mu\frac{H}{2} = (2n - 1)\frac{\pi}{2} \quad (2.54)$$

which gives us

$$\mu = \mu_n(k) = (2n - 1)\frac{\pi}{H} \quad (2.55)$$

The result is that there is not only a solution of this problem, but there are infinite. In steady state we choose the first one with $n = 1$ that is called fundamental solution to describe our system with a always positive quantity. In fact higher order eigenvalues can produce oscillating solutions. They can be useful in transient conditions. Having obtained this result leads us to set A_2 to zero, in fact to obtain the following equality we need $A_2 = 0$

$$\underbrace{A_1\cos\left(\mu\frac{H}{2}\right)}_{=0} + A_2\cosh\left(\mu\frac{H}{2}\right) = 0 \quad (2.56)$$

All the constants are defined $A_2 = C_1 = C_2 = 0$ and A_1 can assume any value and can be set once the power of our system is defined. The two fluxes are

$$\phi_1 = A_1\cos(\mu_n x) \quad (2.57)$$

$$\phi_2 = A_2\Psi_1^{(2)}\cos(\mu_n x) \quad (2.58)$$

Setting $n = 1$ we get the fundamental solution which is the only meaningful solution in steady state. We define the *geometrical buckling* as:

$$\mu(k) = \frac{\pi}{H} = B \quad (2.59)$$

But using the definitioun of μ_1 we have derived previously

$$\mu_1^2 = \frac{1}{2}\left(\frac{\nu\Sigma_{f1}}{kD_1} - \frac{1}{L_2^2} - \frac{1}{L_1^2}\right) + \frac{1}{2}\sqrt{\left(\frac{-\nu\Sigma_{f1}}{kD_1} + \frac{1}{L_2^2} + \frac{1}{L_1^2}\right) - 4\left(\frac{1}{L_1^2} \frac{1}{L_2^2} - \frac{\nu\Sigma_{f1}}{kD_1 L_1^2} - \frac{\nu\Sigma_{f2} \Sigma_{1 \rightarrow 2}}{kD_1 D_2}\right)} \quad (2.60)$$

We can equate this expression to the one of the curvature buckling which is a known quantity to obtain the value of the effective multiplication factor k_{eff}

$$k_{eff} = \frac{1}{\Sigma_{r,1}} \left[\overbrace{\frac{\nu \Sigma_{f,1}}{1 - L_1^2 B_g^2}}^{\text{fast neutron chain}} + \overbrace{\frac{\nu \Sigma_{f,2} \Sigma_{s,1 \rightarrow 2}}{\Sigma_{a,2} (1 - L_1^2 B_g^2) (1 - L_2^2 B_g^2)}}^{\text{thermal neutrons chain}} \right] \quad (2.61)$$

Where:

- B_g : is defined as *geometrical buckling* and its definition changes depending on the core geometry.
- $\frac{1}{1+L_1^2 B_g^2}$: prbability to not leak out from the system for fast neutrons.
- $\frac{1}{1+L_2^2 B_g^2}$: prbability to not leak out from the system for thermal neutrons.

2.1.2 One hexagon calculation

In **Section 2.1**, it has been explained the scheme used to create the geometry's system directly on FreeFEM and also how to create a *automatically-generated* mesh; now the further step is to define the eigenvalue problem. As a first attempt, a very easy case both from the geometrical view point and for the NTE treatment: the considered geometry is simply one hexagon with the center in the coordinates $\vec{r} = (x_c, y_c) = (0,0)$. As regards the NTE treatment, as anticipated, a *two-group diffusion model* (see **Equation (2.17)**). Thanks to these simplifying assumption, it is possible to compare the numerical result obtained with FreeFEM++, with the analytical result, described with equations **Equation (2.16)** and **Equation (2.61)**. The steps followed for this study are:

1. The analytical results for both k_∞ and k_{eff} have been found by defining a Matlab script.
2. Definition of the problem and the calculation of k_{eff} using FreeFEM++ with a coarse mesh.
3. Comparison of the analytical result with the numerical one.

As said, firstly the k_∞ analytical result is calculated by using the **Equation (2.16)**, then the analytical k_{eff} . These analytical results are reported here below:

	Result	Reference
k_∞	1.0687	Equation (2.16)
$k_{eff,a}$	0.1531	Equation (2.61)

It is important to highlight the fact that: $k_\infty > k_{eff,a}$ and so, even if the geometry-independent *multiplicative eigenvalue* is bigger than one, once the geometric aspect is

introduced, the eigenvalue becomes almost ten times smaller. It means that, considering only the material present in the studied system- in this case only enriched uranium dioxide- the core **could** be critical. The fact that once the geometrical aspect is introduced the value gets such a reduction, should not be surprising, since the considered geometry is quite small (the system's area is: $6l^2p = 168.823 \text{ cm}^2$ and so the neutron leakages increases a lot.

As regards the $k_{eff,a}$ calculation, here below is reported the **Equation** (2.61):

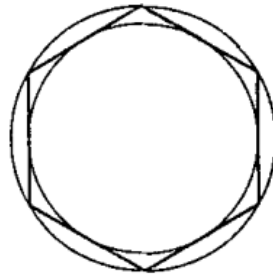
$$k_{eff} = \frac{1}{\Sigma_{r,1}} \left[\overbrace{\frac{\nu \Sigma_{f,1}}{1 - L_1^2 B_g^2}}^{\text{fast neutron chain}} + \overbrace{\frac{\nu \Sigma_{f,2} \Sigma_{s,1 \rightarrow 2}}{\Sigma_{a,2} (1 - L_1^2 B_g^2) (1 - L_2^2 B_g^2)}}^{\text{thermal neutrons chain}} \right]$$

All the terms that constitutes the above formula are known, except for the *geometrical buckling* parameter (B_g^2). In fact, this parameter is directly related to the geometry of the system. Unfortunately, very few scientific articles has been found useful in order to better define B_g^2 for a hexagonal-assembly geometry. According to [4], the hexagon's B_g^2 can be evaluated with a semi-empirical formulation.

From the experimental results shown in [5], it has been suggested that the buckling of a regular polygon is inversely proportional to the square of the radius R_C of the corresponding circumscribed circle:

$$B_g^2 \sim \left(\frac{a_n}{R_c} \right)^2, \quad (2.62)$$

where a_n is a constant that depends on the type of regular polygon under consideration. For example, for a square, a_n is equal to π ($B_{g,square}^2 = 2(\frac{\pi}{L})^2$, where L is the square's side); for a circle, instead, $B_{g,circle}^2 = (\frac{2.405}{R})^2$. In order to carry on this study, three circles are considered: the inscribed one, the circumscribed one and the one with same area of the considered polygon(**Figure 2.8**).



**Regular
hexagon**

Figure 2.8: Hexagonal polygon with circumscribed and inscribed circles [5].

For an hexagon the results of this study are:

Number of sides, N	$\frac{R_I}{R_c} = \cos(\frac{\pi}{N})$	Volume Fraction, $\frac{A_n}{(\pi R_c^2)}$	Geometric Constants
6 (hexagon)	0.8660	0.8270	$2.644 < a_n < 2.777$

Thanks to these information, it is possible to calculate the geometrical buckling for the studied geometry. Moreover, still in the same article ([4]), different calculations have been reported, in which the selected a_n value is 2.675. Using this value, for the considered geometry, the geometrical buckling is equal to:

$$B_g^2 = \left(\frac{a_n}{R_C}\right)^2 = (2.675p/2)^2 = 0.2709$$

Thus, the final analytical $k_{eff,a}$ is equal to: $k_{eff} = 0.1531$. The consistency of this calculation can be proved by checking **Figure 2.9** in which is reported the table of results of the article.

Examples of MRBEM Calculation Results

Geometry	Radius of Circumcircle, R_c (cm)	Eigenvalue Estimate, λ_e	Number of Iterations, n	Calculated Eigenvalue, k_{eff}	Geometric Buckling, B_g^2 (cm ⁻¹)	Geometric Constant, $a_n \sim R_c \cdot B_g$	CPU Time ^a (s)
Regular triangle	5.0	0.020	5	0.02106	7.0213E-1 ^b	4.190	13.52
	10.0	0.078	5	0.08085	1.7553E-1	4.190	13.61
	20.0	0.27	5	0.27838	4.3883E-2	4.190	13.69
	50.0	0.87	5	0.88125	7.0213E-3	4.190	13.76
	100.0	1.27	5	1.27602	1.7553E-3	4.190	13.78
Square	5.0	0.036	5	0.03705	3.9487E-1	3.142	13.47
	10.0	0.13	5	0.13797	9.8718E-2	3.142	13.54
	20.0	0.42	5	0.43253	2.4680E-2	3.142	13.65
	50.0	1.06	5	1.07537	3.9487E-3	3.142	13.86
	100.0	1.36	5	1.36523	9.8718E-4	3.142	13.82
Regular pentagon	5.0	0.044	5	0.04568	3.1838E-1	2.821	13.43
	10.0	0.16	5	0.16742	7.9594E-2	2.821	13.57
	20.0	0.49	5	0.50170	1.9899E-2	2.821	13.82
	50.0	1.13	4	1.13776	3.1838E-3	2.821	9.93
	100.0	1.39	4	1.38941	7.9595E-4	2.821	9.86
Regular hexagon	5.0	0.049	5	0.05062	2.8632E-1	2.675	13.38
	10.0	0.18	4	0.18387	7.1580E-2	2.675	9.59
	20.0	0.53	5	0.53773	1.7895E-2	2.675	13.77
	50.0	1.16	5	1.16612	2.8632E-3	2.675	13.99
	100.0	1.40	4	1.39980	7.1581E-4	2.675	9.91
Regular octagon	5.0	0.055	4	0.05565	2.5955E-1	2.547	9.56
	10.0	0.20	4	0.20030	6.4887E-2	2.547	9.61
	20.0	0.57	5	0.57207	1.6221E-2	2.547	13.83
	50.0	1.19	5	1.19091	2.5954E-3	2.547	13.95
	100.0	1.41	5	1.40858	6.4899E-4	2.548	13.98

Figure 2.9: Results of the semi-empirical adopted formulation for B_g^2 calculation used in [4].

It is important to remember that the hexagon's **pitch** is equal to 17.1, and so, the circumscribed circle must have an radius equal to: $\frac{pitch}{2} = \frac{p}{2} = 8.55 \text{ cm}$, hence between $R_C = 5 \text{ cm}$ and $R_C = 10 \text{ cm}$. For this reason it is expected that the evaluated $k_{eff,a}$ must be between the two corresponding values and so:

$$\underbrace{0.05062}_{\text{considering } R_C = 5} \leq \underbrace{0.1531}_{\text{considering } R_C = 8.55} \leq \underbrace{0.18387}_{\text{considering } R_C = 10}$$

Till now, only the analytical results have been addressed. These results are very important, in particular:

- k_∞ : If > 1 , the system **could** be *critical*

- $k_{eff,a}$: is the effective analytical value of k . It will be used to check the validity of the elemental model.

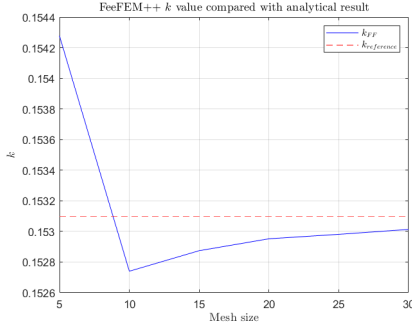
After defining the already described problem, on **FreeFEM** the calculation can be made. In **Table 2.1** and **Table 2.2** results are reported. It has been reported the $k_{eff,num}$ results and their distance from the analytical value expressed in pcm (ϵ), and finally the needed computational time.

<i>number of element</i>	$k_{eff,num}$	ϵ (<i>pcm</i>)	CPUt
5	0.154277	117.700	1.18
10	0.15274	36.000	1.196
15	0.152874	22.600	1.761
20	0.152952	14.800	2.27
25	0.152981	11.900	3.902
30	0.153013	8.700	6.367

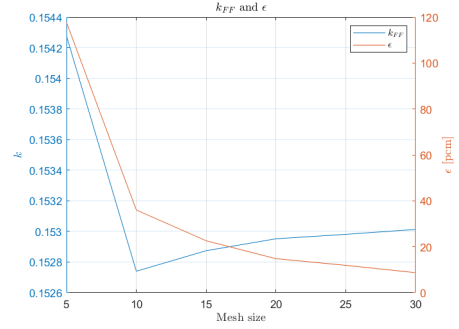
Table 2.1: Results for the one hexagon two-group diffusion model. $w_{eff,num}$, ϵ [*pcm*], CPU time values are reported by considering a fixed first order polynomial Galerkin minimisation error method and improving the mesh refinement.

P_n	$k_{eff,num}$	ϵ (<i>pcm</i>)	CPUt
1	0.154277	117.700	2.116
2	0.153378	27.800	1.482
3	0.153198	9.800	2.713
4	0.153189	8.900	7.194

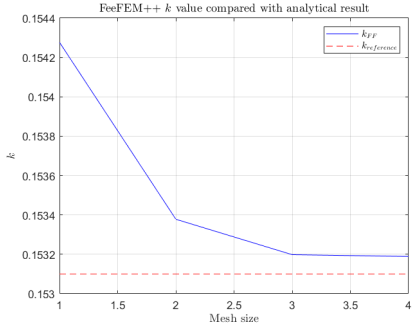
Table 2.2: Results for the one hexagon two-groups diffusion model. $k_{eff,num}$, ϵ [*pcm*], CPU time values are reported by considering a fixed mesh parameter $n = 5$ (number of element per border), and increasing the polynomial order



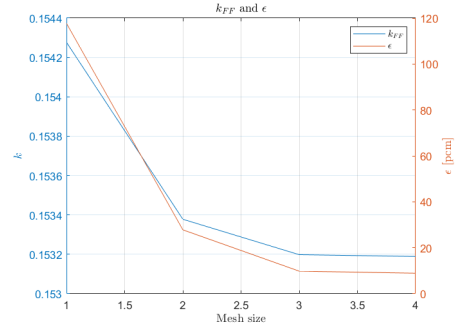
(a) $k_{eff,num}$ versus mesh refinement parameter. The analytical value is also reported.



(b) ϵ behaviour by increasing the mesh refinement error.



(c) $k_{eff,num}$ versus polynomial order. The analytical value is also reported.



(d) ϵ error behaviour by increasing polynomial order.

As it can be deduced from the reported results, two strategies have been adopted in order to highlight which one is more efficient in term of *computational time*. The first one is improving the results by increasing the *mesh refinement parameter*, while for the second is increasing the order of the polynomial used in the *Galerkin error minimisation method*. It is important to notice that in **FreeFEM**, the maximum usable polynomial order is equal to four. For the first study, the polynomial order has been fixed at one, while for the second calculation scheme the mesh refinement parameter has been fixed to 5, that means five elements per geometry's border are used (practically, since the hexagonal geometry is made of six borders, 30 elements are used to discretize the geometry). Referring to the second case, by using the maximum available polynomial order, the minimum error reached is equal to 58.098 *pcm*. Of course, in order to correctly compare the two resolution approach, it is possible to use as reference the error (ϵ), and comparing the CPU times. In **Figure 2.10** has been reported the comparison.

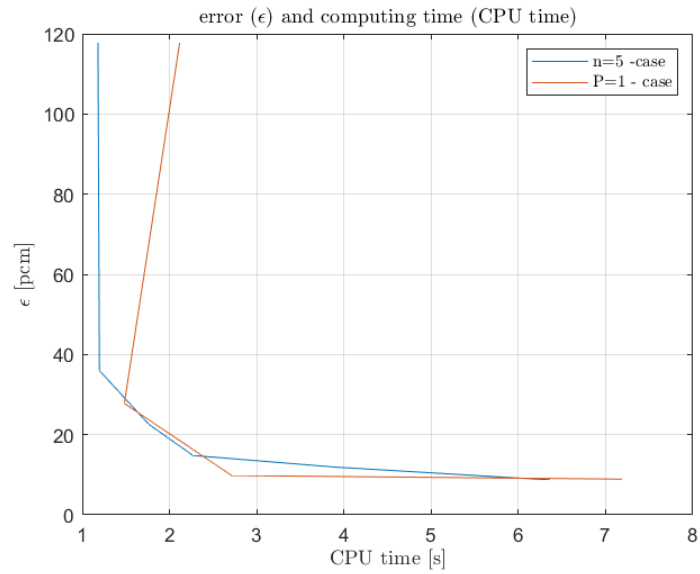


Figure 2.10: Comparison between the CPU times needed to the first resolution method (*orange*), and the second one (*blue*).

It is not trivial to say *a priori* which one of the method is more efficient in term of computational times. What can be seen quite easily from **Figure 2.10** is that when low refinement is used (both for test function-polynomial order and number of mesh element per border), it is worth to set a polynomial order to the first order and increase the mesh refinement parameter.

References

- [1] FreeFEM. *FreeFem++ Introduction*. [Online; accessed 27-December-2022]. 2022. URL: <https://doc.freefem.org/introduction/>.
- [2] Tanay Mazumdar and S.B. Degweker. «Solution of neutron transport equation by Method of Characteristics». In: *Annals of Nuclear Energy* 77 (2015), pp. 522–535. ISSN: 0306-4549. DOI: <https://doi.org/10.1016/j.anucene.2014.12.029>. URL: <https://www.sciencedirect.com/science/article/pii/S030645491400677X>.
- [3] Won Yang. «Fast reactor physics and computational methods». In: *Nuclear Engineering and Technology* 44 (Mar. 2012). DOI: 10.5516/NET.01.2012.504.
- [4] Masafumi Itagaki, Yoshinori Miyoshi, and Hideyuki Hirose. «A Geometric Buckling Expression for Regular Polygons: II. Analyses Based on the Multiple Reciprocity Boundary Element Method». In: *Nuclear Technology* 103.3 (1993), pp. 392–402. DOI: 10.13182/NT93-A34859.
- [5] Yoshinori Miyoshi, Masafumi Itagaki, Masanori Akai, Hideyuki Hirose, and Masao Hashimoto. «A Geometric Buckling Expression for Regular Polygons: I. Measurements in Low-Enriched UO₂-H₂O Lattices». In: *Nuclear Technology* 103.3 (1993), pp. 380–391. DOI: 10.13182/NT93-A34858.

Chapter 3

Eigenvalue Formulations

3.1 Theoretical introduction

A central issue in Nuclear Reactor Engineering is understanding whether the neutron population throughout the core is stable in time, decreases or increases with it, during the operations of the reactor life. By definition, a critical nuclear reactor is able to self-sustain a controlled fission chain reaction, i.e. the phenomenon in which neutrons generated by fission reactions.

If the aforementioned equilibrium is verified, the neutron population in the reactor is independent of time, and the unique neutron source term is represented by fissions. In other words, the *criticality* condition is reached when the total amount of neutron that is generated by fission reactions is equal to the amount of neutrons that disappear from the system, due to absorption or leakage out of the outer surface.

Mathematically, the criticality problem is approached as an eigenvalue problem, an expression which reads:

$$\hat{A}\phi = \lambda\phi \quad (3.1)$$

where \hat{A} is a matrix $\in \mathbb{R}^{m \times n}$, λ is a scalar, real or complex, and ϕ is the *non-trivial solution* vector such that the expression in **Equation** (3.1) is verified. The eigenvectors having in common the same eigenvalue form an *eigenspace*.

In **Section 1.1.3** is explained the oldest and most popular formulation known as the *multiplication eigenvalue* k . Here is reported the already explained formulation of k :

$$\hat{L}\phi + \hat{R}\phi = \hat{S}\phi + \frac{1}{k}\hat{F}\phi$$

In the following sections, the *alternative eigenvalue formulation* are described, which are:

- Collision eigenvalue: γ
- Time eigenvalue considering precursors elements: ω

- Time eigenvalue not considering precursors elements: α
- Density eigenvalue: δ
- Capture eigenvalue: θ

3.1.1 γ - eigenvalue

The γ -eigenvalue is called the *collion eigenvalue*, and may be seen as a "direct eigenvalue of the integro-differential neutron transport equation". As its denomination suggests, γ is inserted to modify of both the scattering-in and the fission terms of the neutrons balance. In operator notation the transport equation become:

$$(\widehat{L} + \widehat{R})\phi = \frac{1}{\gamma}(\widehat{S} + \widehat{F})\phi \quad (3.2)$$

Likewise the k eigenvalue, the set of eigenvalue for which **Equation** (3.2) is verified, is referred to as the γ -eigenvalue spectrum whereas the corresponding eigenfunctions ϕ are denoted as γ -modes. As already explained for the k_0 , the γ_0 is called the *fundamental eigenvalue* and is the term within the *eigenvalue-spectrum* with the largest real part, and also the fundamental eigenvalue solution is characterised by a uniform sign of its associated *eigenfunction* solution. The physical meaning of the γ_0 is: "the ratio between the number of neutrons produced by the scattering-in and the fission source term, and the number of those lost due to collisions and leakage through the system boundaries". Concerning the critical condition, a system is declared critical if $\gamma_0 = 1$, as subcritical if $\gamma_0 < 1$ and finally supercritical if $\gamma_0 > 1$.

It is important to remark the fact that in Neutron Diffusion equation model the Removal operator is defined as:

$$\widehat{R} = \begin{bmatrix} \Sigma_{r,1} & 0 & \dots & 0 \\ 0 & \Sigma_{r,2} & & \\ \vdots & & \ddots & 0 \\ 0 & \dots & 0 & \Sigma_{r,G} \end{bmatrix} \quad (3.3)$$

Where $\Sigma_{r,i}$ is the removal cross section of the i -th energy group. While in Neutron Transport equation model the removal operator is defined as:

$$\widehat{R} = \begin{bmatrix} \Sigma_{t,1} & 0 & \dots & 0 \\ 0 & \Sigma_{t,2} & & \\ \vdots & & \ddots & 0 \\ 0 & \dots & 0 & \Sigma_{t,G} \end{bmatrix} \quad (3.4)$$

Where $\Sigma_{t,g}$ is the total cross section of the g -th energy group. The total cross section includes all neutron-nucleus interaction phenomena and the relation with the removal cross section is:

$$\Sigma_{r, g} = \Sigma_{t, g} - \Sigma_{g \rightarrow g}. \quad (3.5)$$

When diffusion model is adopted, the Removal operator is typically defined following **Equation** (3.3), since, in principle the inside-group scattering term is present in both sides of the equation. Thus for consistency, when removal operator is defined as **Equation** (3.3), the inside-group scattering is not present inside the scattering matrix. However, when γ eigenvalue formulation is adopted, the described approach is not full consistent, since on the right hand side both fission and scattering operator are scaled by a factor $\frac{1}{\gamma}$, including also the inside-group scattering that in principle should be present in both sides of the equation. For this reason the already described approach is not fully consistent, since in both sides the inside-group scattering term is not present. However, for simplicity, in this work **Equation** (3.3) definition is used for all the eigenvalue formulations.

The ω and α -eigenvalue

The second eigenvalue formulation proposed in the history of reactor physics is the so-called time eigenvalue, which is also the most employed one after the multiplication eigenvalue. This formulation has recently attracted more attention due to its strong relationship with the time evolution of an off-critical system, which could be of interest in order to obtain better few-group constant for dynamic calculations. The time eigenvalue is also the only natural spectral formulation of the transport equation, being associated with its Laplace transform. For this reason the associated eigenfunctions are often referred to as the natural modes.

There are two formulations of the time eigenvalue: the most general one (ω -eigenvalue) was proposed by Henry, and it takes in to account the presence of the delayed neutrons, while the second formulation (α -eigenvalue) does not consider the presence of the precursors, thus the concentrations of the elements born as fission fragments; they can be stable or unstable and decay into other radionuclides through the emission of various radiations, including neutrons. First the ω -eigenvalue is introduced, whose definition is:

$$\widehat{L}\phi + \widehat{R} + \omega\widehat{T} = \widehat{S}\phi + \widehat{F}_p\phi + \sum_{i=0}^R \frac{\lambda_i}{\omega + \lambda_i} \widehat{F}\phi \quad (3.6)$$

The reported formulation is the non linear version, in order to keep the linear shape of the problem the **Equation** (3.6) is divided in to two equations:

$$\begin{cases} \frac{\omega}{v}\phi + \widehat{L}\phi + (\widehat{C} + \widehat{F}_T + \widehat{S}_T)\phi = \widehat{S}\phi + \widehat{F}\phi + \sum_{r=1}^R \lambda_r \epsilon_r \\ \omega \epsilon_r = \widehat{F}_{d,r}\phi - \lambda_r \epsilon_r \end{cases} \quad (3.7)$$

While when the delayed neutron contribution, are neglected, the α eigenvalue, i.e. the *prompt time eigenvalue*, would be obtained,

$$\widehat{L}\phi + (\widehat{R} + \alpha\widehat{T})\phi = \widehat{S}\phi + \widehat{F}\phi \quad (3.8)$$

The hypothesis at the basis of these formulations is that the neutron flux (and the precursor concentrations as well, in the case of ω) is separable in time and described by an exponential decay,

$$\phi(\vec{r}, E, \vec{\Omega}, t) = \tilde{\phi}(\vec{r}, E, \vec{\Omega})e^{\alpha t} \quad (3.9)$$

Thanks to this assumption, the time-derived term in the transport equation became:

$$\frac{\partial}{\partial t}\phi(\vec{r}, E, \vec{\Omega}, t) = \frac{\partial}{\partial t}\tilde{\phi}(\vec{r}, E, \vec{\Omega})e^{\alpha t} = \alpha\tilde{\phi}(\vec{r}, E, \vec{\Omega})e^{\alpha t} = \alpha\phi(\vec{r}, E, \vec{\Omega}, t) \quad (3.10)$$

This equation allows highlighting the physical meaning of the time eigenvalues, which are the time frequencies characterising the free evolution of the system. The most peculiar feature of this spectral form is that its spectrum is featured by a continuous and a discrete parts, located on the left and on the right, respectively, of the so-called Corngold limit, defined as $\min(v(E)\Sigma_t(E))$. Another well-known aspect characterising the time spectrum when the delayed neutrons are considered is the presence of clusters of discrete eigenvalues, which are usually known as *delayed frequencies*. As shown by Henry [1], these discrete eigenvalues tend to accumulate at the right of $-\lambda_i$, i.e the opposite of the decay constant of the i -th neutorn precursors family. As concern the *fundamental* eigenvalue, [2] shown only one eigenstate, associated with $\omega + \lambda_1 > 0$, has a uniform sign, in fact, the other eigenvalues that constitutes the spectrum in the clast region of the spectrum, are featured by fluxes with uniform sign but not for the precursors concentration C_i in this case the associated model are featerued by $\omega + \lambda_i < 0$ (notice that if among the "R" families of precursors, the one that results with negative C corressponds to the family whose decay constant, *lambda* satisfies the inequity over mentioned).

By combining **Equation** (3.10) with **Equation** (3.8) the result is (For sake of simplicity, only the α formulation is rephrased in operator formalism):

$$\left(\widehat{T} + \frac{\alpha}{v}\right)\phi = (\widehat{S} + \widehat{F})\phi \quad (3.11)$$

It may be seen a kind of increment of the total macroscopic cross-section Σ_t by a factor of $\frac{\alpha}{v}$, referred to as *fictitious capture* or *time-absorption* term.

As concern the *criticality* condition, these eigenvalues differ from the other formulations in fact, if the reactor is critical, no time variation is needed to change the reactivity of the system, so the operator " \widehat{T} " vanishes but since, thanks to the assumption of treating the time variable as an independent variable, $\widehat{T} = \frac{\alpha}{v}$, it is possible to conclude that in case of *critical* condition α_0 or ω_0 are equal to zero. Moreover if these formulations are negative, the system neutron population will decay over time following an exponential behaviour and, as a consequence, the system will be subcritical; on the contrary, the positive sign will make neutron population diverge over time (supercritical system).

δ -eigenvalue

The so-called effective density factor expresses a modification of the nuclides densities through which criticality may be achieved. Specifically, the δ -eigenvalue problem in operator formalism reads:

$$\widehat{L}\phi = \frac{1}{\delta}(\widehat{S} + \widehat{F} - \widehat{R})\phi \quad (3.12)$$

δ -eigenvalue has influence on both the removal term and on the source terms of the neutron balance, constituted by the scattering-in and the fission contribution. This eigenvalue lends itself to two different physical interpretations: first, it can be seen as a tuning parameter acting on the competition between neutron production and removal terms, whose density is varied by the same amount (i.e δ itself). Alternatively the second interpretation makes it appropriate to dub δ , as the "streaming eigenvalue" that changes the relationship between angular flux (ϕ) and current ($\vec{\Omega}\phi$). In this case δ turns out to be a scaling parameter that affects the size of the system. In this way, if the system geometry is rescaled, and rescaled by a Λ factor, δ is also simply rescaled by a Λ factor but the interesting thing is that the energy spectrum of the neutron flux does not change. This feature appears to be a considerable advantage with respect to the other spectral formulations previously discussed, which introduce some distortions in the energy spectrum.

The *criticality* condition is given by $\delta_0 = 1$, it means that no elements concentration variations are needed (according to the first interpretation) or, again, no geometry variation are needed (second interpretation). If the system is supercritical, in order to reduce the neutrons population, the system domain can be rescaled in order to increase the leakage term, \widehat{L} , by a factor δ and so $\delta_0 > 1$ and *vice versa*, so if reactor is in a subcritical condition, $\delta_0 < 1$.

θ -eigenvalue

This eigenvalue is known as the *capture eigenvalue*, and its formulation is inspired by the fact that k and γ act on specific reaction channels, an eigenvalue acting on neutron capture can be introduced as well:

$$(\widehat{L} + \widehat{F}_0 + \widehat{S}_0 - \widehat{F} - \widehat{S})\phi = \frac{1}{\theta}\widehat{C}\phi. \quad (3.13)$$

the physical interpretation is quite straightforward: it expresses the number of neutrons that must be captured in order to maintain the criticality of the system. Since in this case the eigenvalue acts on a loss term, the criticality conditions are reversed: when the system is critical $\theta_0 = 1$, while, if subcritical, the system needs to decrease the term of captures and since on the right hand side of the equation $\frac{1}{\theta}\widehat{C}$, $\theta_0 > 1$, if instead the system is in a supercritical condition, for the same consideration, $\theta_0 < 1$. In the case of subcritical system, if the capture term has to be strongly reduced, θ_0 can also assume negative values. In such a case, the criticality could be reached only substituting, the removal with a a production term. In case of negative value, it seems

quite unphysical, but actually, if the number of neutrons cannot be adjusted, the only way to compensate for this lack of particles is to introduce them by means of a negative capture. Despite this fact may sound misleading, this property may be very useful for the design of a reactor, because, in this specific situation, the designer could be immediately aware that it is necessary to increase the multiplication properties of the system. The same situation with k or γ , is more difficult to interpretate, since they would not provide a one-way suggestion, for example the lack of neutrons could be due to an excessive leakage-out term or a too low quantity of fission material to respect with absorption one. Therefore, due to its tight connection with the capture reactions, this eigenvalue could be useful for the design of specific components of a reactor, e.g., control rods and breeding blankets.

3.1.2 Preliminary Studies

The different eigenvalue formulations are characterised by their own eigenvalue *spectrum*, and for each eigenvalue that solves the problem is associated with an eigenvector or eigenfunction that is the problem's solution. Each eigenvalue formulations can give a different value of the solution, which of course changes with space (\vec{r}), energy (E), direction ($\vec{\Omega}$) and time. Some simplifications occurs by using the diffusion model (**Equation** (2.17)): the direction discretisation is not needed and so solutions are "direction-independent"; moreover since the problem that is solved with the eigenvalue formulation is an approach to *criticality*, the problem is time-independent too. The final problem is discretized only in space and energy field. As concerns the space domain subdivision, in FreeFEM++, the problem is treated in space by using the *finite elements* logic provided that a mesh is defined. At the end, thanks to all the previous considerations, the *neutron diffusion equation* must be subdivided in energy groups only. The final problem sets an equation for each group of energy. The final system is a set of fully-coupled differential equations and the general formulation of the g -th equation is:

$$\nabla \cdot D_g \nabla \phi_g + \Sigma_{r,g} \phi_g = \sum_{g'}^G \Sigma_{g' \rightarrow g} \phi_{g'} + \chi_g \sum_{g'}^G \Sigma_{f,g'} \phi_{g'} \quad (3.14)$$

The space dependence is not reported in previous formulation, while \mathbf{G} is the total number of considered energy groups, \mathbf{g} is the reference energy group considered in **Equation** (3.14) and \mathbf{g}' is a general group different from \mathbf{g} ($\mathbf{g}' \neq \mathbf{g}$). The equations system with \mathbf{G} groups become:

$$\left\{ \begin{array}{l}
 -\nabla \cdot D_1 \nabla \phi_1 + \Sigma_{r,1} \phi_1 = \chi_1 \sum_{g'}^G \Sigma_{f,g'} \phi_{g'} \\
 -\nabla \cdot D_2 \nabla \phi_2 + \Sigma_{r,2} \phi_2 = \Sigma_{1 \rightarrow 2} \phi_1 + \chi_2 \sum_{g'}^G \Sigma_{f,g'} \phi_{g'} \\
 -\nabla \cdot D_3 \nabla \phi_3 + \Sigma_{r,3} \phi_3 = \Sigma_{1 \rightarrow 3} \phi_1 + \Sigma_{2 \rightarrow 3} \phi_2 + \chi_3 \sum_{g'}^G \Sigma_{f,g'} \phi_{g'} \\
 \vdots \\
 -\nabla \cdot D_g \nabla \phi_g + \Sigma_{r,g} \phi_g = \sum_{g'}^G \Sigma_{g' \rightarrow g} \phi_{g'} + \chi_g \sum_{g'}^G \Sigma_{f,g'} \phi_{g'} \\
 \vdots \\
 -\nabla \cdot D_G \nabla \phi_G + \Sigma_{r,G} \phi_G = \sum_{g'}^G \Sigma_{g' \rightarrow G} \phi_{g'} + \chi_G \sum_{g'}^G \Sigma_{f,g'} \phi_{g'}
 \end{array} \right. \quad (3.15)$$

It is important to notice that the scattering term of the first three equations has been made explicit. It has been done with the aim to highlight an important aspect: the scattering process is a phenomenon where neutrons collide with other particles and due to this interaction the lost energy and so no *up-scattering is considered*. For this reasons, for example, in the first equation of this system ($g = 1$) the scattering term is not present: Since the first energy group contains the most energetic neutrons, they physically can not receive scattered neutrons from other groups. While in equation $g = 2$, only one term is present ($\Sigma_{1 \rightarrow 2}$) since only the neutron of the first group after colliding and losing a certain amount of energy could be scattered into the second energy groups. The scattering cross section after the energy discretisation is called *energy transfer matrix* and it can be written like:

$$\Sigma_{g' \rightarrow g} = \begin{bmatrix} \Sigma_{1 \rightarrow 1} & \cdots & \Sigma_{G \rightarrow 1} \\ \vdots & \ddots & \vdots \\ \Sigma_{1 \rightarrow G} & \cdots & \Sigma_{G \rightarrow G} \end{bmatrix}$$

Since in the diffusion equation on the left hand side the removal term (Σ_r) which is defined as:

$$\Sigma_r = \Sigma_a + \Sigma_f + \Sigma_{g' \rightarrow g}$$

the diagonal term of the previously defined matrix can be deleted *ex ante*, thus, the scattering matrix became:

$$\Sigma_{g' \rightarrow g} = \begin{bmatrix} 0 & \Sigma_{2 \rightarrow 1} & \cdots & \Sigma_{3 \rightarrow 1} \\ \Sigma_{1 \rightarrow 2} & 0 & \cdots & \Sigma_{3 \rightarrow 2} \\ \vdots & \ddots & \ddots & \vdots \\ \Sigma_{1 \rightarrow G} & \cdots & \Sigma_{(G-1) \rightarrow G} & 0 \end{bmatrix}$$

Coming back to **Equation** (3.15), as can be seen it is a system of linear differential equation and so in order have a "well posed" system, boundary conditions are needed. Since it is assumed a *vacuum boundary condition kind*, the incoming current must be equal to zero. The general expression to impose an incoming current at the boundary of the system equal to zero is:

$$\vec{J}(\vec{r}_s, \vec{\Omega}_{in}, E) = 0 \quad (3.16)$$

Where with \vec{r}_s is indicated the position of the position vector at the boundary region, while with Ω_{in} it is meant the direction vector for which $\Omega_{in} \cdot \vec{n} < 0$.

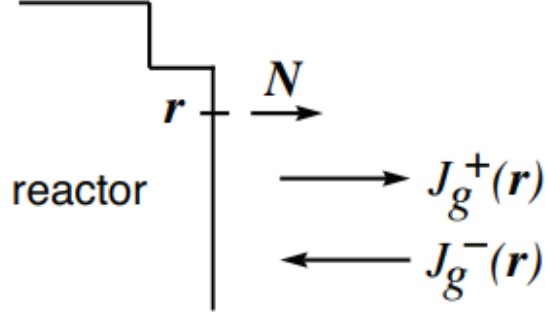


Figure 3.1: outgoing current and incoming current simplified visualization.

Looking at **Equation** (3.14), the current term is not explicit in the formulation so it has to be reconstruct. The outgoing and incoming current, respectively, \vec{J}^+ and \vec{J}^- can be obtained from the neutron current and flux distribution provided the angular flux is represented by a limited P_1 expansion:

$$J_g^+ = \frac{1}{4}\phi_g + \frac{1}{2}\vec{J}_g \cdot \vec{n} = \frac{1}{4}\phi_g + \frac{1}{2}D_g\nabla\phi_g \cdot \vec{n} \quad (3.17)$$

$$J_g^- = \frac{1}{4}\phi_g - \frac{1}{2}\vec{J}_g \cdot \vec{n} = \frac{1}{4}\phi_g - \frac{1}{2}D_g\nabla\phi_g \cdot \vec{n} \quad (3.18)$$

Since only the incoming current at the boundary must be imposed equal to zero **Equation** (3.18) gives the following information:

$$\frac{1}{4}\phi_g - \frac{1}{2}\nabla\phi_g \cdot \vec{n} = 0 \implies \nabla D_g\phi_g \cdot \vec{n} = \frac{1}{2}\phi_g$$

and so the equaitons' system is well posed:

$$\left\{ \begin{array}{l}
 -\nabla \cdot D_1 \nabla \phi_1 + \Sigma_{r,1} \phi_1 = \chi_1 \sum_{g'}^G \Sigma_{f,g'} \phi_{g'} \\
 -\nabla \cdot D_2 \nabla \phi_2 + \Sigma_{r,2} \phi_2 = \Sigma_{1 \rightarrow 2} \phi_1 + \chi_2 \sum_{g'}^G \Sigma_{f,g'} \phi_{g'} \\
 -\nabla \cdot D_3 \nabla \phi_3 + \Sigma_{r,3} \phi_3 = \Sigma_{1 \rightarrow 3} \phi_1 + \Sigma_{2 \rightarrow 3} \phi_2 + \chi_3 \sum_{g'}^G \Sigma_{f,g'} \phi_{g'} \\
 \vdots \\
 -\nabla \cdot D_g \nabla \phi_g + \Sigma_{r,g} \phi_g = \sum_{g'}^G \Sigma_{g' \rightarrow g} \phi_{g'} + \chi_g \sum_{g'}^G \Sigma_{f,g'} \phi_{g'} \\
 \vdots \\
 -\nabla \cdot D_G \nabla \phi_G + \Sigma_{r,G} \phi_G = \sum_{g'}^G \Sigma_{g' \rightarrow G} \phi_{g'} + \chi_G \sum_{g'}^G \Sigma_{f,g'} \phi_{g'} \\
 \\
 D_g \nabla \phi_1 \cdot \vec{n} = \frac{1}{2} \phi_1 \\
 D_g \nabla \phi_2 \cdot \vec{n} = \frac{1}{2} \phi_2 \\
 D_g \nabla \phi_3 \cdot \vec{n} = \frac{1}{2} \phi_3 \\
 \vdots \\
 D_g \nabla \phi_g \cdot \vec{n} = \frac{1}{2} \phi_g \\
 \vdots \\
 D_g \nabla \phi_G \cdot \vec{n} = \frac{1}{2} \phi_G
 \end{array} \right. \quad (3.19)$$

All the previous considerations had the aim to set the theoretical framework; in the following a detailed description of the problem's geometry is reported

3.2 System geometry description

As already explained above, the thesis work was developed in a research context that has the objective of studying generation-IV fast reactors specifically, the so-called "LFRs" ("Lead Fast Reactors") among The European Demonstrator Project for the Advanced Lead Fast Reactor (ALFRED) is a significant endeavor in Europe, centered on the creation of fourth-generation Lead Fast Reactors (Gen-IV). The goals of Gen-IV include sustainability, reducing the amount of radioactive waste in the long term, reducing the risk of nuclear proliferation, enhancing safety measures, and cutting costs. ALFRED, a 300 MW thermal pool-type prototype, intends to demonstrate the technical proficiency of LFR technology and examine the potential for LFR Small Modular Reactors (SMRs).

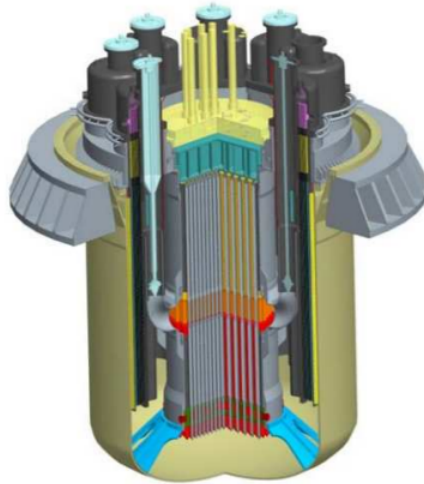


Figure 3.2: ALFRED 3D sketch

Here below a smaller version of ALFRED's core is reported **Figure 3.3**

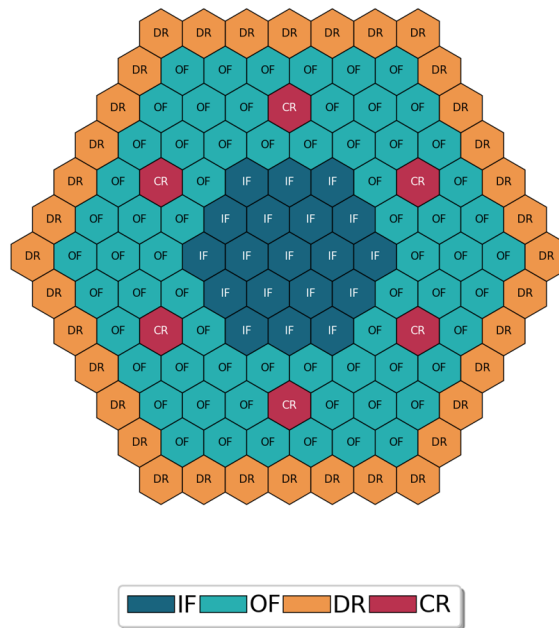


Figure 3.3: A smaller and simplified version of ALFRED core. Only four different elements are considered: IF,OF,CR,DR; respectively: inner fuel, outer fuel, control rod, reflector

Actually this is a simplified version of the actual ALFRED's core. In fact as can be seen in **Figure 3.3** only four kind of materials are present. Here are reported a legend of the element and a short description regarding fuel element [3].

- **IF**: inner fuel ($Pu/(Pu + U)$ [wt.%) = 21.70)
- **OF**: outer fuel ($Pu/(Pu + U)$ [wt.%) = 27.80)
- **DR**: reflector
- **CR**: control rod

To build this geometry with FreeFEM++ it has been used the same code that the author has developed for the previous example. Few information are needed referred to a single sextant of the core: once the sextant is construct, the mentioned code, rotate the calculated points six times by 30°

Number of rows:	7
Number of hexagons for each row:	$row_i = N_{rows} - i$
Pitch [cm] :	17.1

The result is reported here below :

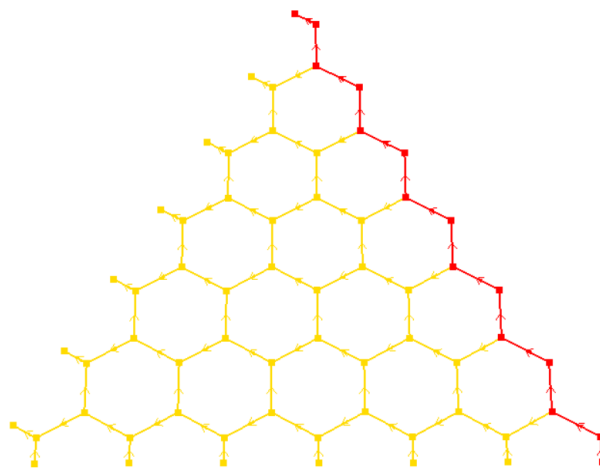


Figure 3.4: FreeFEM++ sextant preliminary geometry to be rotated by 30° for six times

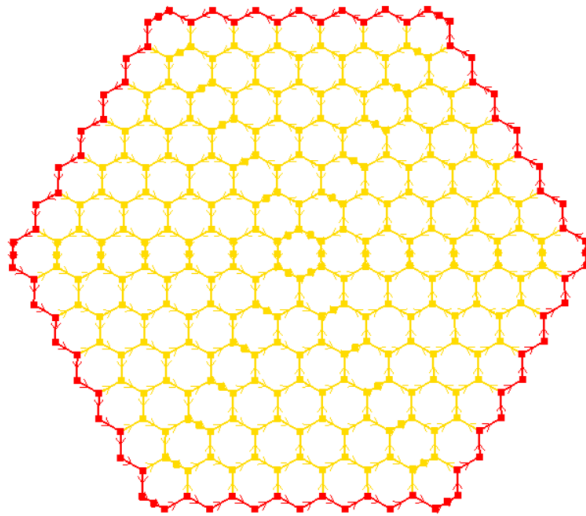


Figure 3.5: *FreeFEM+* ALFRED full core geometry obtained by the rotation of the sextant geometry for six times

Some edges have different colors than others: the red ones are the outer edges of the outermost hexagons and therefore correspond to the edges of the system on which the boundary conditions will be imposed.

Looking closely at the geometry, it can be seen that it has a one-sixth symmetry with respect to a single sextant, allowing us to consider only one sextant of the geometry, showed in **Figure 3.6**

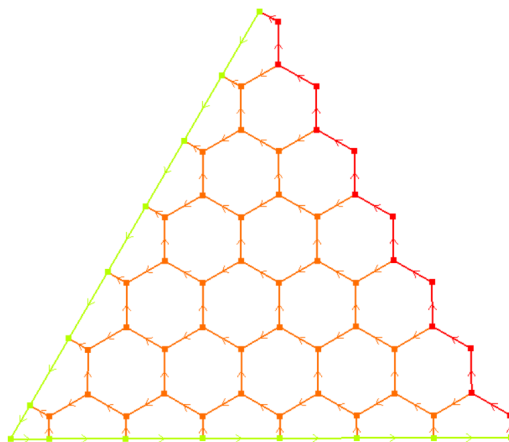


Figure 3.6: *FreeFEM++* ALFRED single sextant with two different kind of boundary, on the red edges the *vacuum BC* will be imposed while on the green one the *Specular reflective BC*

In this case two kinds of boundary conditions were be applied: on the red edges the already discussed *vacuum BC*, while as concern the green edges a *reflective boundary condition* is imposed. The latest one is a symmetric condition in which the incoming and outgoing angular fluxes at the interface are equal, i.e.:

$$\phi(\vec{r}_b, E, \vec{\Omega}) = \phi(\vec{r}_b, E, \vec{\Omega}'), \quad (3.20)$$

for $\vec{n} \cdot \vec{\Omega} = -\vec{n} \cdot \vec{\Omega}'$. In order to achieve such a condition, regions I and II must be identical. If the geometry of the problem allows its use, it results in significant reduction in model size, and therefore in computation time.

3.3 Energy grids

To address the criticality study for the different formulations of the eigenvalue problem, as just discussed, it is necessary to consider different energy group grids, so as to discretize the energy field of the neutron transport or neutron diffusion equations. In the framework of this work three different energy grids are defined.

Table 3.1: 33 Energy groups using ECCO-33 grid.

Group	Upper boundary [MeV]	Lower Boundary [MeV]
1	2.000000E+01	1.000000E+01
2	1.000000E+01	6.065307E+00
3	6.065307E+00	3.678794E+00
4	3.678794E+00	2.231302E+00
5	2.231302E+00	1.353353E+00
6	1.353353E+00	8.208500E-01
7	8.208500E-01	4.978707E-01
8	4.978707E-01	3.019738E-01
9	3.019738E-01	1.831564E-01
10	1.831564E-01	1.110900E-01
11	1.110900E-01	6.737947E-02
12	6.737947E-02	4.086771E-02
13	4.086771E-02	2.478752E-02
14	2.478752E-02	1.503439E-02
15	1.503439E-02	9.118820E-03
16	9.118820E-03	5.530844E-03
17	5.530844E-03	3.354626E-03
18	3.354626E-03	2.034684E-03
19	2.034684E-03	1.234098E-03
20	1.234098E-03	7.485183E-04
21	7.485183E-04	4.539993E-04
22	4.539993E-04	3.043248E-04
23	3.043248E-04	1.486254E-04
24	1.486254E-04	9.166088E-05
25	9.166088E-05	6.790405E-05
26	6.790405E-05	4.016900E-05
27	4.016900E-05	2.260329E-05
28	2.260329E-05	1.370959E-05
29	1.370959E-05	8.315287E-06
30	8.315287E-06	4.000000E-06
31	4.000000E-06	5.400000E-07
32	5.400000E-07	1.000000E-07
33	1.000000E-07	1.000000E-11

Table 3.2: Group boundaries in MeV adopted for the few-group calculations.

9G	$2.231 \cdot 10^0$	$4.979 \cdot 10^{-1}$	$1.111 \cdot 10^{-1}$	$2.479 \cdot 10^{-2}$	$5.531 \cdot 10^{-3}$	$2.035 \cdot 10^{-3}$	$7.485 \cdot 10^{-4}$	$5.4 \cdot 10^{-7}$
6G	$2.231 \cdot 10^0$	$4.979 \cdot 10^{-1}$		$2.479 \cdot 10^{-2}$	$5.531 \cdot 10^{-3}$		$7.485 \cdot 10^{-4}$	$5.4 \cdot 10^{-7}$
3G		$4.979 \cdot 10^{-1}$					$7.485 \cdot 10^{-4}$	

It is important to remember that the final object of the work requires to collapse the nuclear data from a finer model, which therefore considers a sufficiently high number of energy groups, to a coarser model with a smaller number of energy groups. For this reason, after having done control simulations to test the code, using for example a model with only three energy groups or six, it is possible to move on to the more

complex model from which the neutron spectrum will be extracted and used to collapse the nuclear data from higher to lower energy grids.

3.4 Considerations on neutron flux by using alternative eigenvalue

In this section some preliminary considerations have been made. Moreover it has been solved the criticality problem by adopting alternative eigenvalue formulations.

3.4.1 Preliminary considerations: k eigenvalue 33G Diffusion system

Here are reported the data obtained solving the eigenvalue problem by using a diffusion 33G model:

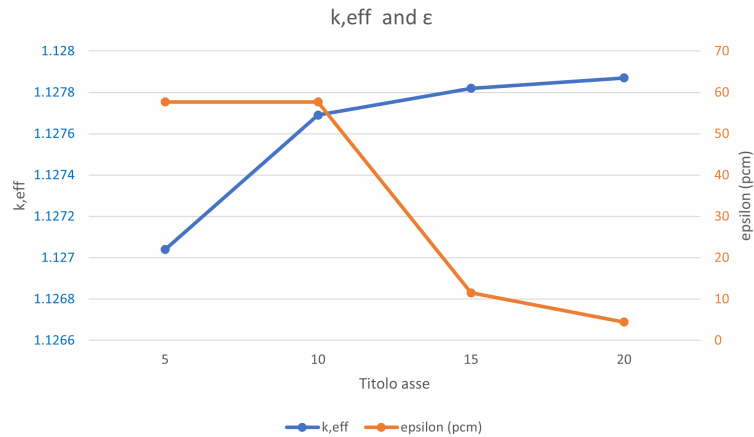


Figure 3.7: Results of the simulation for sextant geometry and 33G model. The **blue** curve indicates the evolution of k_{eff} with respect to the number of element per border, while the **orange** one, refers to ϵ the relative error between calculated value, expressed in *pcm*. NOTE that all the simulation have been carried out fixing as test function's order $P1$ (polynomial of first order).

Here the total flux distribution has been plotted:

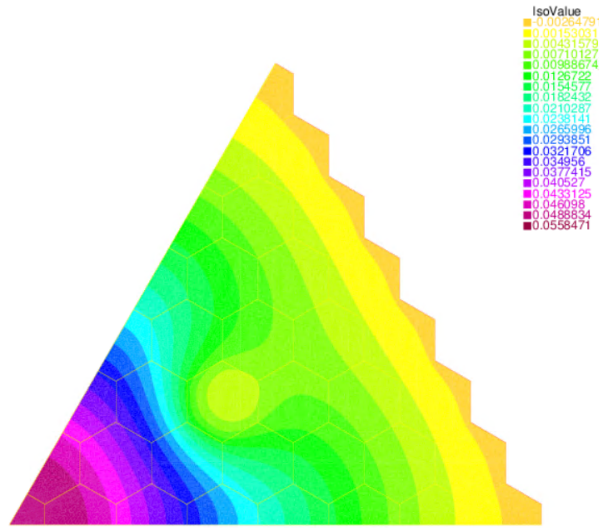


Figure 3.8: Total flux (integrated over energy groups) distribution over the sextant domain

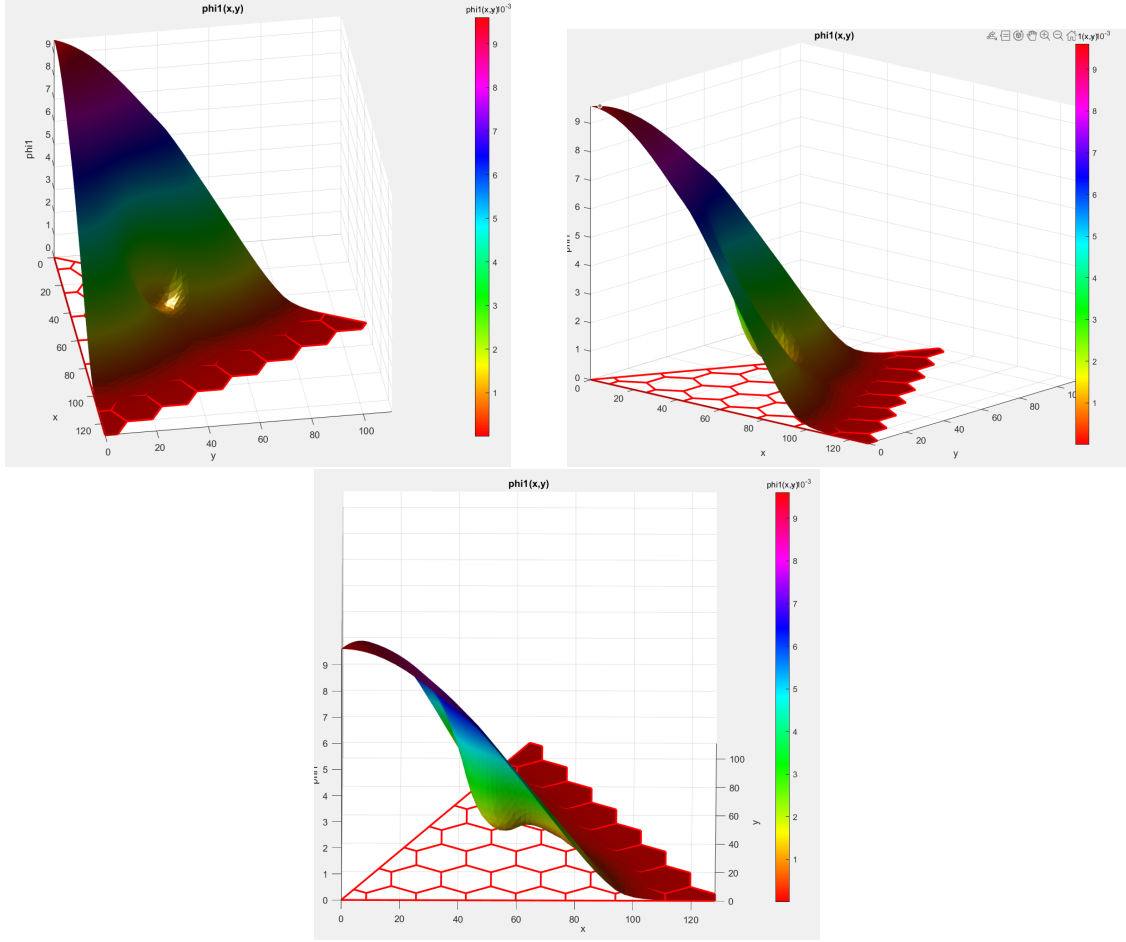


Figure 3.9: 3D plots of the total neutron flux (integrating over all energy groups) over a sextant of the system. The three plots are of the same simulation result with different angulation. The red grid in $z = 0$ plane, is the system borders. In the central region of the sextant, the flux sharply decreases, this region corresponds to the region where the *control rod* is inserted. This result

In **Figure 3.9** some 3D graphs of the neutronic flux over a sextant of the system. The three plots come from the same simulation result with different angulations. The red grid in $z = 0$ plane is the system borders. In the central region of the sextant, the flux sharply decreases. This flux dip corresponds to the region where the *control rod* is inserted. These graphs allow a better visualisation of the results. It is important to highlight a aspect that may be misleading: as previously described, the reactor core is featured in the second-last "ring of hexagons" by a neutron reflector (see **Figure 3.3**); however its presence does not seems to have any particular effect on the neutron flux. This is due to the fact that the reflection is better for thermal neutrons, and since the neutron spectrum of this core is fast (or *hard*), the number of fast neutrons are much larger than the one of thermal neutrons. Hence, the it is difficult to observe the real effect on the energy integrated flux ($\phi_{tot}(x, y) = \sum_g^G \phi_g(x, y)$). To better appreciate the

reflection effect **Figure 3.11** considers only a partial amount of energy fluxes within the more thermal groups.

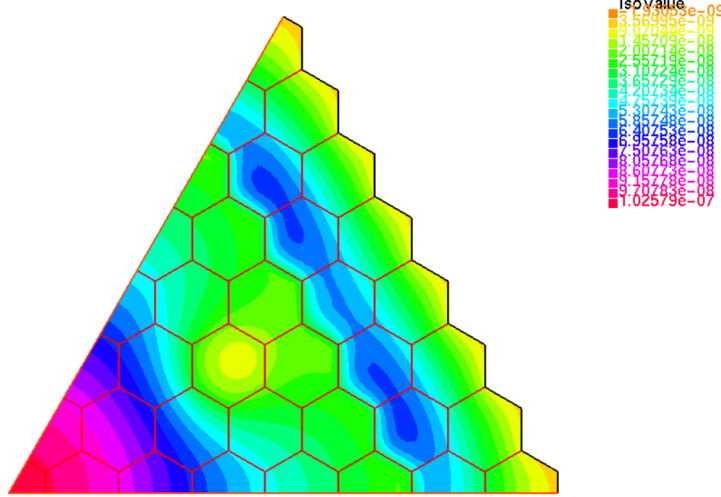


Figure 3.10: Thermal fraction of the neutron flux distribution over sextant' domain

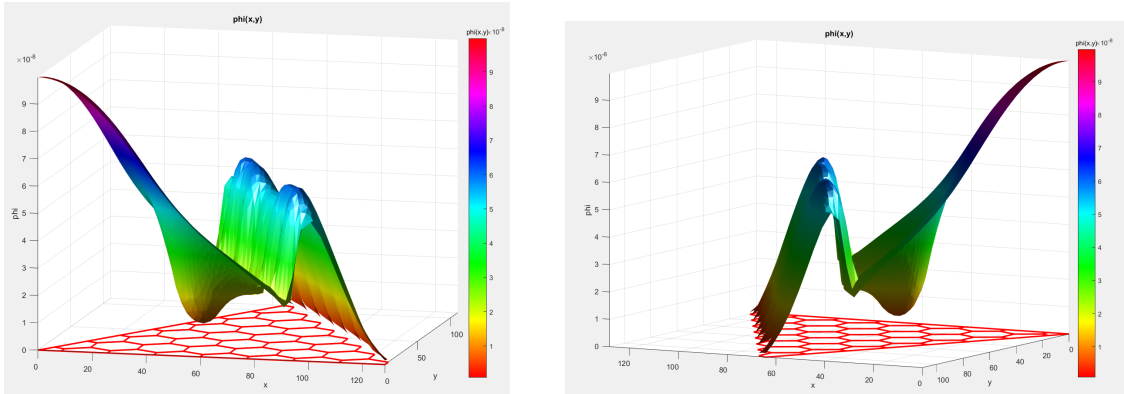


Figure 3.11: 3D plots of the neutronic profile over a sextant of the system. The two plots are of the same simulation result with different angulation. The red grid in $z = 0$ plane, is the system borders. In the central region of the sextant, the flux sharply decreases, that region corresponds to the region where the *control rod* is inserted. While in the near-border region, the picks are due to the reflection effect of the more external material.

These results obtained so far refer to a 2D framework. The neutronic module of the FRENETIC code permits model 2D and 3D geometries too. However, coupled neutronics/thermal-hydraulics simulations can be computed only using a 3D geometry, i.e considering also the axial dimension of the core. This is due to the fact that, in order to know the actual power generate by the core, and consequently, the fuel and coolant temperature, the axial advection should be properly modelled. The thermal-hydraulic module calculates the temperature distribution with a one-dimensional model along

the axial length of each fuel assembly (FA). The heat transfer between neighboring FAs is considered in a weak radial coupling manner, i.e with a "1D+2D" approach. In **Figure 3.12** the same reactor core of **Figure 3.3** is portayed focusing on its axial features. The implementation of a 3D model would require a heavier implementation on FreeFEM++ code. However, taking advantage of the fact that the assemblies are homogeneous axially, the equations can be modified introducing an axial buckling factor B_z ([4]). Let us consider the diffusion neutron equation in its general form:

$$-\nabla \cdot D_g \nabla \phi_g + \Sigma_{r,g} \phi_g = \chi_g \sum_{g=1}^G \phi_{g'} \nu_g \Sigma_{f,g'} + \sum_{\substack{g=1 \\ g \neq g'}}^G \Sigma_{g \rightarrow g'} \phi_g \quad (3.21)$$

Form now on, the focus will be only on the left hand side and assuming axially homogeneous FAs $D_g(\vec{r}) \rightarrow D_g(x, y)$, so:

$$\begin{bmatrix} \frac{\partial}{\partial x} & \frac{\partial}{\partial y} & \frac{\partial}{\partial z} \end{bmatrix} D_g(x, y) \begin{bmatrix} \frac{\partial \phi}{\partial x} \\ \frac{\partial \phi}{\partial y} \\ \frac{\partial \phi}{\partial z} \end{bmatrix}$$

Equation (3.21) becomes:

$$-\frac{\partial}{\partial x} D_g(x, y) \frac{\partial \phi}{\partial x} - \frac{\partial}{\partial y} D_g(x, y) \frac{\partial \phi}{\partial y} - D_g(x, y) \frac{\partial^2 \phi}{\partial z^2} + \Sigma_{r,g}(x, y) \phi_g = \dots \quad (3.22)$$

At this point it is possible to make the hypothesis of flux spatial separability:

$$\phi_g(\vec{r}) = \phi_g(x, y, z) = \phi_g(x, y) \cos(B_z z). \quad (3.23)$$

Substituting **Equation (3.23)** in to **Equation (3.22)** yields

$$\begin{aligned} & -\cos(B_z z) \nabla_{x,y} D_g(x, y) \cdot \nabla \phi_g(x, y) + B_z^2 D_g(x, y) \phi_g \cos(B_z z) + \Sigma_{r,g} \phi_g(x, y) \cos(B_z z) \\ & = \\ & \chi_g \sum_{g=1}^G \phi_{g'}(x, y) \nu_g \Sigma_{f,g'}(x, y) \cos(B_z z) + \sum_{\substack{g=1 \\ g \neq g'}}^G \Sigma_{g \rightarrow g'}(x, y) \phi_g(x, y) \cos(B_z z) \end{aligned} \quad (3.24)$$

Since the term " $\cos(B_z z)$ " multiplies all the members in both sides of the equation, it can be divided from both sides assuming that $\cos(B_z z) \neq 0$ that is true (except for $z = \frac{H}{2}$ and $z = -\frac{H}{2}$). The value of B_z^2 can be founded by solving:

$$\begin{cases} \frac{d^2 f(z)}{dz^2} = -B_z^2 f(z) \\ \phi(x, y, z = \frac{H}{2}) = 0 \\ \phi(x, y, z = -\frac{H}{2}) = 0 \end{cases} \quad (3.25)$$

The fact that at $z = \frac{H}{2}$ and $z = -\frac{H}{2}$ the flux is equal to zero, implies that along axial direction neutron flux has a cosinusoidal profile.

$$\begin{cases} \cos(B_z \frac{H}{2}) = 0 \\ -\cos(B_z \frac{H}{2}) = 0 \end{cases} \implies B_{z_n} \frac{H}{2} = \frac{(2n+1)\pi}{2} \quad (3.26)$$

Where $n = 0, 1, 2, 3, \dots$ so, $n \in \mathbb{N}$. Taking $n = 0 \implies B_z \frac{H}{2} = \frac{\pi}{2} \implies B_z^2 = (\frac{\pi}{H})^2$.

This assumption helps to significantly reduce the complexity of the model. The neutron profile over the sextant is always similar to the one in **Figure 3.8**, but k changes, as can be seen in **Figure 3.13**:

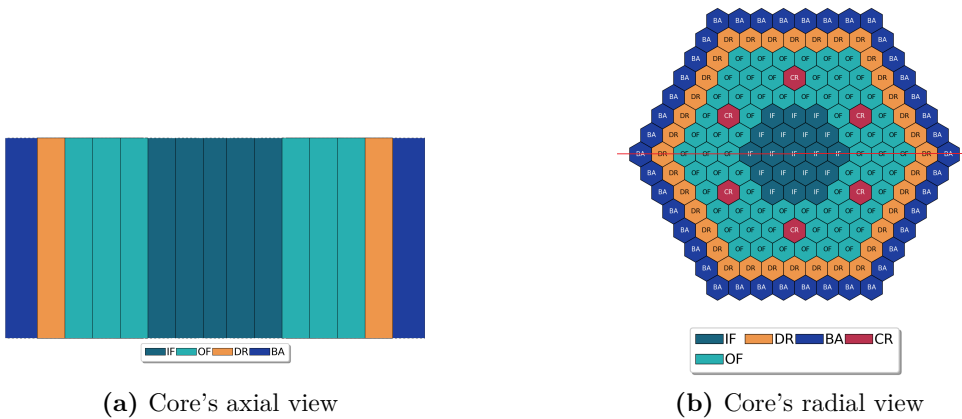


Figure 3.12: ALFRED's core design views. **Figure 3.12a** reports the axial view of the cut symbolized by the red line appearing in **Figure 3.12b**.

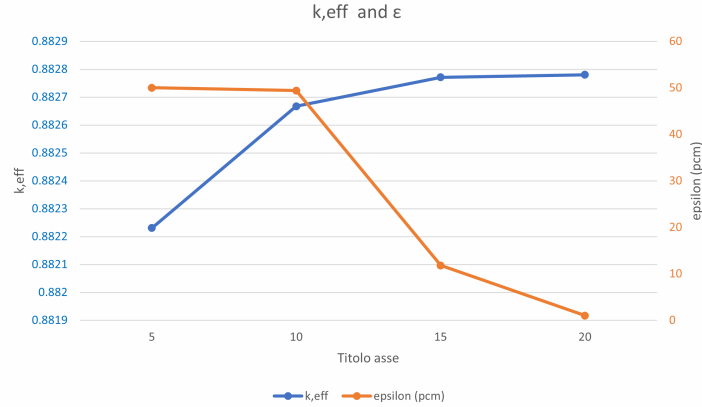


Figure 3.13: Results of the simulation for sextant geometry and 33G model with the additional term that takes in consideration the axial leakages. The **blue** curve indicates the evolution of k_{eff} with respect to the number of element per border, while the **orange** one, refers to ϵ the relative error between calculated value, expressed in *pcm*. NOTE that all the simulation have been carried out fixing as test function's order *P1* (polynomial of first order).

Thanks to this study, it is possible to say that in order to have a good accuracy of the result, concerning this system, $nn = 5$ is a fine enough mesh parameter.

3.4.2 3D 33-G diffusion model: k , γ , α , ω criticality evaluations

As already anticipated, once the model is ready on FreeFEM++, the first step to follow in order to run the transient simulation in FRENETIC with the collapsed data, is to obtain the various energy the spectra from FreeFEM++. It is important to remind the fact that during the transient reactor's conditions that will be simulated, is expected a temperature change inside the system, and is extremely important to take in consideration the crosssection feedback effect with respect to temperature changes. In order to do that, FRENETIC needs a library of group constants, for some set of temperatures. Of course, for each temperature configurations, the spectra would change, since cross sections change. In order to have all the set of data it is necessary to first evaluate the neutron spectrum with 33-groups, for each core spatial configuration and at each temperature, Then the nuclear data can be collapsed with spectra. The spectrum definition is the following:

$$\psi_g = \int_{V_i} d\vec{r} \phi_g. \quad g=1,\dots,G \quad i=1,\dots,N \quad (3.27)$$

Where ψ_g is the energy spectrum of the g -th energy group, and is obtained integrating the neutron flux ϕ_g over the spatial domain, V_i . Note that ϕ_g is summed over all the regions of the same type. In order to make a transient simulation, FRENETIC needs at least three set of data referred to different temperature. Once loaded these

library of data, FRENETIC handle the time evolution of the system, by interpolating the loaded nuclear data.

Nuclear data are function not only of the fuel temperature but also of the coolant one: thermal equilibrium during the evolution of the transient before to be reached, so the fuel and coolant temperatures have different values and, so, it is necessary to combine all the possible and **realistic** configuration of the system's temperatures. Here is reported a table with the chosen temperatures.

T_{fuel} [K]	$T_{coolant}$ [K]
673	673
1073	673
1073	1073
1437	673
1473	1073
1473	1473

Table 3.3: Total meaningful temperatures combinations

Notice that the actual total number of possible configurations are 9 (three temperatures are considered for both fuel and coolant medium), but only six are reported in the previous table since the discarded ones have no physical meaning, as the coolant temperature can not be higher then the fuel one.

Moreover, in order to simulate a larger number of transient events, new reactor's element configuration could be considered, for example, the easier case but still with an important validity for transient studies, is the case of the presence or not of the control rods. Again, in order to pass the correct data in FRENETIC software, it is necessary to calculate the spectra of the new configurations too, for each temperature. Finally, the total amount of simulation to carry on in FreeFEM++ for the evaluation of neutrons spectrum for each temperature and core configurations, are 12.

This whole process has to be done for each eigenvalue formulations that has been considered.

The selected eigenvalue formulations that has been studied are four:

1. k : multiplication eigenvalue.
2. γ : collision eigenvalue.
3. α : time eigenvalue (without precursors).
4. ω : time eigenvalue (with precursors).

Therefore the excluded eigenvalues formulations are:

1. θ : capture eigenvalue.
2. δ : density eigenvalue.

The reason why these last formulations have not been studied has to be investigated by focusing on their mathematical formulation and also remark the fact that the built FreeFEM++ solver uses a diffusive model.

Focusing on δ formulation, as can be seen in the formulation reported in **Equation** (3.12), the density eigenvalue has the characteristics to not modify, in principal at least, the nuclear data, but only the geometrical features. In fact **Equation** (3.12) can be rewritten as:

$$\delta \widehat{L}\phi = (\widehat{S} + \widehat{F} - \widehat{R})\phi,$$

δ multiplies the *leakage* operator, which is defined in the transport formulation as the streaming term:

$$Leakage = \nabla \cdot \vec{J} = \nabla \cdot (\vec{\Omega}\phi)$$

It is therefore easy to see that no nuclear data is present inside the "L" operator. The streaming term just reported follows the transport definition, but as previously said, the solver that has been created in FreeFEM+ uses a diffusive model. In diffusion, the streaming term become,

$$Leakage = -\nabla(D\nabla\phi) \underset{\substack{\uparrow \\ \text{homogeneous medium}}}{=} -D\nabla^2\phi$$

The crucial point is that the diffusion coefficient "D" is defined as:

$$D = \frac{1}{3\Sigma_t},$$

where Σ_t is the total cross-section. Hence, using the diffusion model, the fact that the δ eigenvalue material-independent is lost. For this reason, the obtained results are difficult to interpreted, since the eigenvalue would scale not only the geometrical aspect, but also the material proprieties.

Concerning θ eigenvalue, in order to better explain why the diffusion model could be not suitable for this eigenvalue formulation, it is worth to study more deeply why diffusion model works correctly for k , γ , α and ω formulations.

In the following table the eigenvalues formulation are recalled.

Table 3.4: Formulations of eigenvalue formulations considered in this study

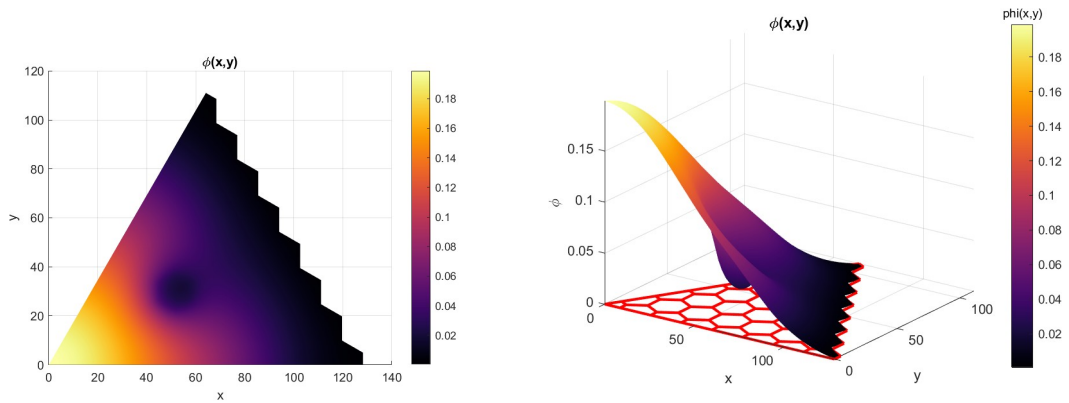
Eigenvalue	Formulation
k	$(\widehat{L} + \widehat{R} - \widehat{S})\phi = \frac{1}{k}\widehat{F}\phi$
γ	$(\widehat{L} + \widehat{R})\phi = \frac{1}{\gamma}(\widehat{S} + \widehat{F})\phi$
α	$\widehat{L}\phi + (\widehat{R} + \alpha\widehat{T})\phi = \widehat{S}\phi + \widehat{F}\phi$
ω	$\widehat{L}\phi + \widehat{R} + \omega\widehat{T} = \widehat{S}\phi + \widehat{F}_p\phi + \sum_{i=0}^R \frac{\lambda_i}{\omega + \lambda_i} \widehat{F}\phi$

Looking as reference **Table 3.4:**

- k acts on \widehat{F} that is defined as $\nu\Sigma_f$. The eigenvalue can be seen as a scaling factor acting on the fission propriety of the material, but it can be seen alternatively as a scale factor acting only on ν , that is not "embedded" in D .
- γ acts on $\nu\Sigma_f$, but also on Σ_s . Strictly speaking, this would mean that Σ_t and therefore D should also change, but, similarly to k , it is plausible to assume that Σ_s is multiplied by a "virtual" ν_s which is always equal to 1 (the scattering emits a neutron) and that eventually is re-scaled by gamma itself. This means that, if gamma were 1, $\frac{\nu}{\gamma}$ neutrons would be emitted by fission, and $\frac{\nu_s}{\gamma}$ neutrons would be emitted by scattering.
- both concerning α and ω by looking at **Equation** (3.10) (same for ω), in these case the eigenvalues are not properly a scaling factor.

Going back to θ , it is not reasonable to assume a virtual ν_c , i.e. a number of neutrons removed from capture, so that theta does not modify Σ_c . This cannot be assumed because the interactions are always neutron-nucleus, therefore it is the single neutron that is captured. In other words: if it is assumed ν_c , then it should be assumed also a ν_f^* , i.e. the number of neutrons absorbed by fission, and a ν_s^* , i.e. the number of neutrons interacting by scattering. But these definitions don't make much sense. Therefore in order to also consider the θ and δ formulations, it is necessary to untie the streaming term from the nuclear material data; for example instead using a diffusion model to handle the direction discretization, the P_N or the S_N models could be used, at the price of a bigger number of equations to be handle.

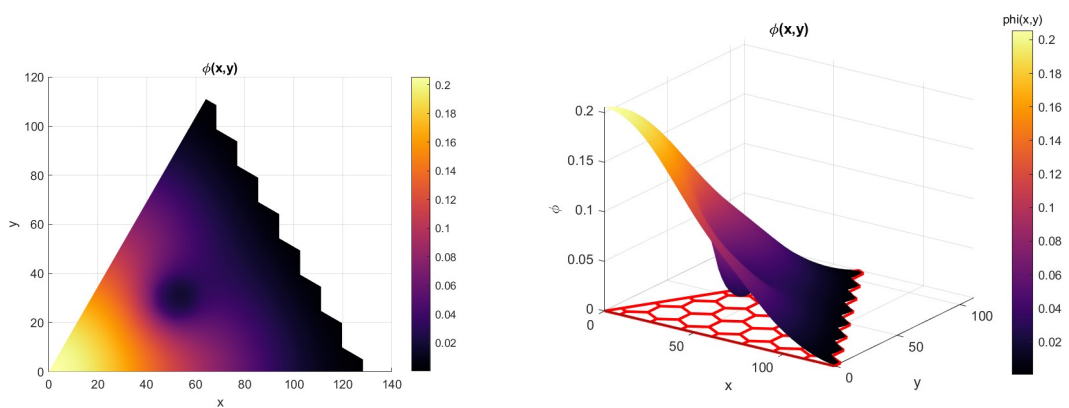
For sake of simplicity, in the following are reported the plot of the results for the selected eigenvalue formulation only at the temperature combination $T_f = 673$ K and $T_c = 673$ K.



(a) 2D plot of k eigenvalue formulation results for a 33G diffusion 3D model.

(b) 3D plot of k eigenvalue formulation results for a 33G diffusion 3D model.

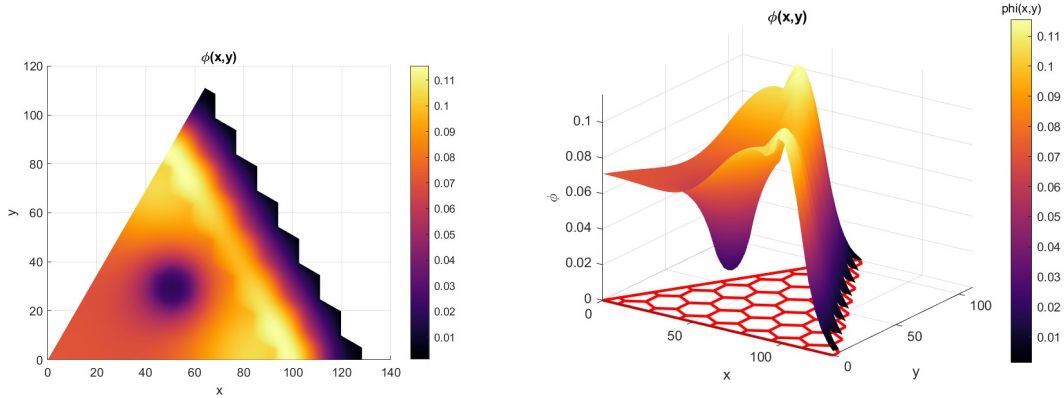
Figure 3.14: k eigenvalue formulation total neutron flux $T_f = 673$ K and $T_f = 673$ K.



(a) 2D plot of γ eigenvalue formulation results for a 33G diffusion 3D model.

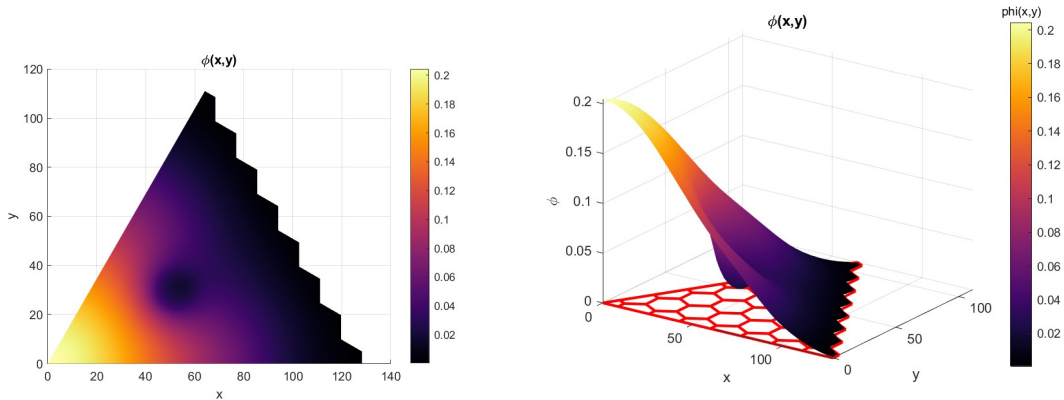
(b) 3D plot of γ eigenvalue formulation results for a 33G diffusion 3D model.

Figure 3.15: γ eigenvalue formulation total neutron flux $T_f = 673$ K and $T_f = 673$ K.



(a) 2D plot of α eigenvalue formulation results for a 33G diffusion 3D model. (b) 3D plot of α eigenvalue formulation results for a 33G diffusion 3D model.

Figure 3.16: α eigenvalue formulation total neutron flux $T_f = 673$ K and $T_f = 673$ K.

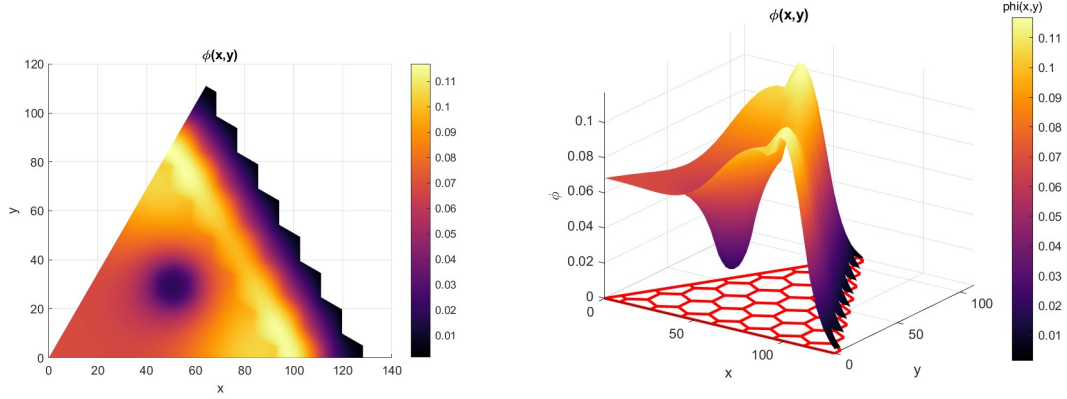


(a) 2D plot of ω eigenvalue formulation results for a 33G diffusion 3D model. (b) 3D plot of ω eigenvalue formulation results for a 33G diffusion 3D model.

Figure 3.17: ω eigenvalue formulation total neutron flux $T_f = 673$ K and $T_f = 673$ K.

As can be easily observed from the previous graphs, at least as regards the flow profile on the sextant, the different formulations of the eigenvalues practically generate very similar spatial results, except for the eigenvalue α . This behaviour is hardly understandable also due to the fact that, usually, α and ω have same neutron flux shape. This result, needs a more detailed study.

By observing also the higher order eigenfunction obtained solving the problem by adopting ω formulation, it has been observed that one of the results shown the following behaviour:



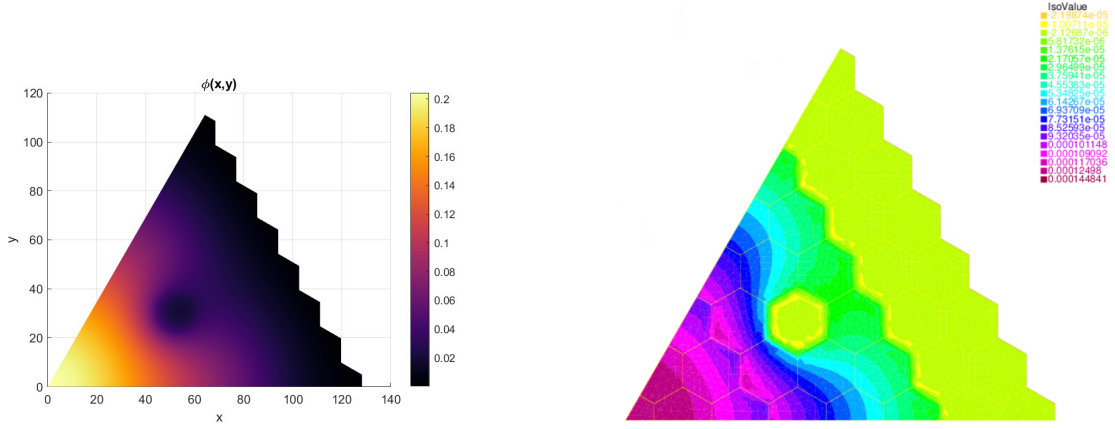
(a) 2D plot of ω eigenvalue formulation results for a 33G diffusion 3D model.

(b) 3D plot of ω eigenvalue formulation results for a 33G diffusion 3D model.

Figure 3.18: ω eigenvalue formulation total neutron flux $T_f = 673$ K and $T_f = 673$ K.

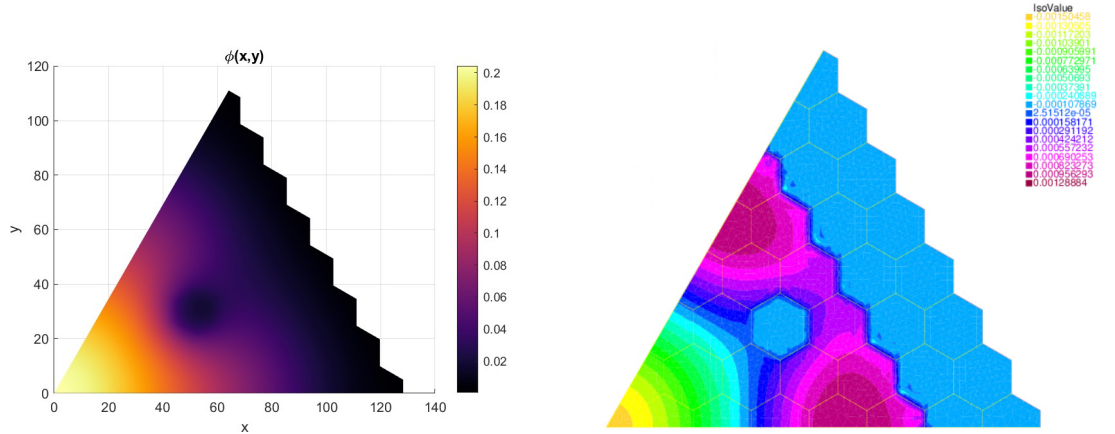
The flux shape over the sextant in **Figure 3.18** is -heuristically- equal to **Figure 3.16**. This behaviour can be explained with a deeper study of ω and α eigenvalue spectra.

As well explained in [5] α and ω spectra have quite peculiar features. For example, one of the most important characteristic of this spectral form is that its spectrum is featured by a continuous and a discrete parts, located on the left and on the right, respectively, of the so-called *Corngold limit*, defined as $\min(v(E)\Sigma_t(E))$. Another well-known aspect characterising the time spectrum when the delayed neutrons are considered is the presence of clusters of discrete eigenvalues, which are usually known as *delayed frequencies*. As proved by [1] these discrete eigenvalues tend to accumulate at the right of $-\lambda_i$, i.e on the right side of the precursor decay family, $\forall i = 1, \dots, R$. The phenomenon of the eigenpair clustering, tightly related to the nature of the in-hour equation is explained by the presence of eigenstates featured by very similar fluxes but different precursors spatial concentrations: the fundamental eigenstate provides a homogeneous sign of the all the eigenfunctions of the equation system. In other words the neutron flux solution has a certain distribution with same sign all over the domain, but also the distribution of the precursors concentrations. In support of what has been said, the **Figure 3.19** shows the distributions on the sextant of the concentrations of the precursors generated by the fission reactions within the considered materials and the associated eigenfunction. As can be easily seen, the neutron distribution of the two eigenstate are heuristically, the same, while the precursors distribution are strongly different. In the first case (the fundamental one) the distribution is physically consistent with the neutron flux, and the numerical value has the same sign (typical behaviour of the fundamental solution), while in the second case, the precursor concentration has a weird distribution and the numerical value has a non-uniform sign.



(a) 2D plot of ω eigenvalue formulation results for a 33G diffusion 3D model. Fundamental solution (ω_0)

(b) 2D plot of precursors concentration distribution.



(c) 2D plot of ω eigenvalue formulation results for a 33G diffusion 3D model. This solution is a higher order harmonic, belonging to the cluster of solution close to one of the λ_f values.

(d) 2D plot of precursors concentration distribution.

Figure 3.19: Comparison of the precursor concentration distribution between fundamental harmonic solution and higher order one.

Referring to the in-hour equation(**Equation (3.28)**), this mean that the second solution belongs to one of the highlighted point in **Figure 3.20**, generated by GeoGebra, using precursor family data.

$$\rho(\omega) = \frac{l\omega}{l\omega + 1} + \frac{1}{l\omega + 1} \sum_{f=1}^F \frac{\omega\beta_f}{\omega + \lambda_f} \quad (3.28)$$

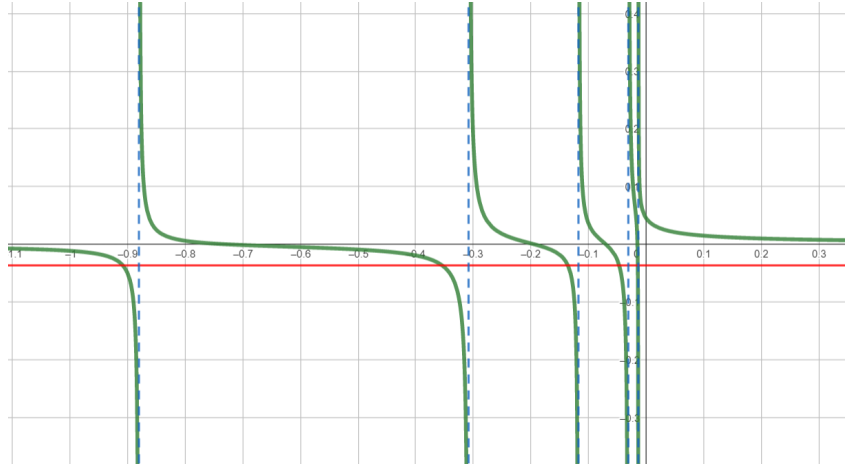


Figure 3.20: In-hour equation plot. The green line is the shape of the **Equation** (3.28), the blue dashed line corresponds to the λ_i values, while the red line is the value of reactivity, that is $\rho_0 \simeq -0.0379$ (since the corresponding to $k_{eff} = 0.96344$ and $\rho_0 = \frac{k_{eff}-1}{k_{eff}}$).

The clustering and the similarity between the fluxes are a critical issue for any eigenvalue algorithm aiming at retrieving only the most significant eigenvalue. However, as found in [2], among all the eigenstates, only the one characterised by $\omega + \lambda_1$ (where λ_1 is the higher decay frequency, and so the lower decay time among the all precursors family) has a uniform sign fluxes and precursors concentration. This feature is extremely important to provide a shift to enable the convergence of the numerical solver. Actually the interesting eigenstates are $R + 1$, where the additional one is the *prompt eigenstate*, where delayed neutrons are not affecting the system. In other words, the ω model collapses into α model. This last aspect explain why by solving the ω eigenvalue problem, one of the higher-order solutions, one has the same "weird behavior" of α model: it corresponds to the prompt eigenstate of ω spectrum. In some sense this is also a kind of verification for ϕ_0^α (fundamental solution of α eigenvalue problem). However the "weird" ϕ_0^α behavior has been already noticed by [6] and [7]. In order to better clarify this behavior, some of the concepts in [6] and [7] are reported here.

In [6] the study has been carried out for a small PHWR (Pressurized Heavy Water Reactor, see **Figure 3.21**)

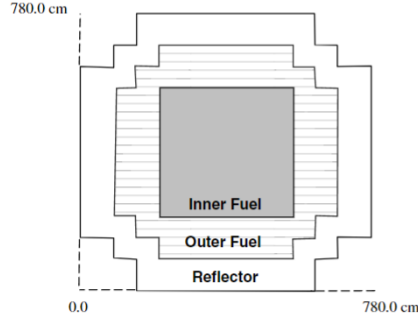


Figure 3.21: PHWR Core geometry used in [6].

The study has shown and compared the different results of the *criticality problem* for k and α eigenvalue model. First a slightly *super-critical* system, with a fundamental eigenvalue $k_0 = 1.0035$ and $\alpha_0 = 4.06182 \text{ (s}^{-1}\text{)}$; for both models the result is reported in **Figure 3.22**:

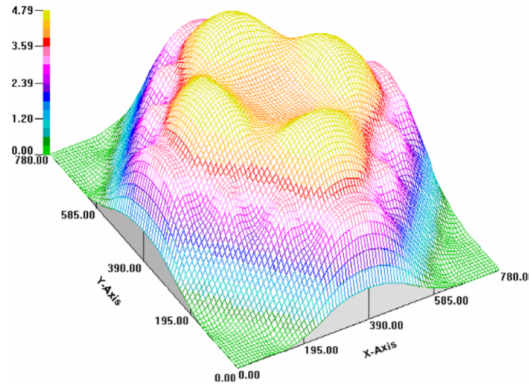


Figure 3.22: Thermal flux for both k and α models in [6]. The double humped shape arises because inner zone has fuel of lower reactivity than that of outer zone.

Afterwards, the same core system it has been studied(**Figure 3.21**), but with a stronger *sub-criticality* level and with a reflector (important remark: the system studied in this work is a fast spectrum, reflected strongly sub-critical system). Even [7] has analyzed such a system in the MUSE experiments, in which very short neutron pulses are delivered in the middle of the core of a small fast experimental reactor. The idea was to measure prompt α_0 and to estimate the sub-criticality using the formula $\alpha_0 = \frac{(k_{eff}-1)}{l}$. However, this formula was not found to be valid. Another issue in highly sub-critical system is that the α_0 is largely negative. Hence, the effective removal cross-section ($\Sigma_r^{eff} = \left(\Sigma_r + \frac{\alpha}{v}\right)$) may become negative. The strongly sub-critical system studied in [6], has an $k_0 = 0.7$ that corresponds to a $\alpha_0 = -211.3764 \text{ (s}^{-1}\text{)}$. The k – mode result is very similar to **Figure 3.22**, while with α – mode turn put to be **Figure 3.23**

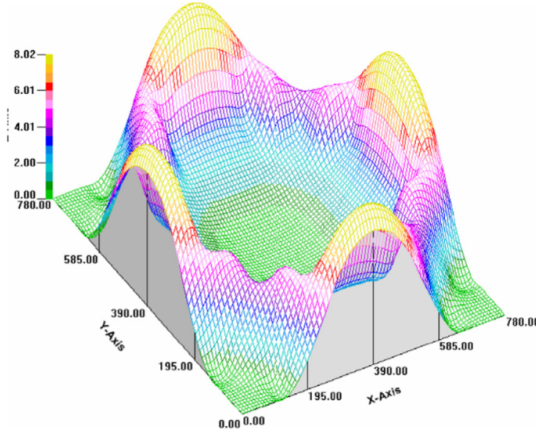
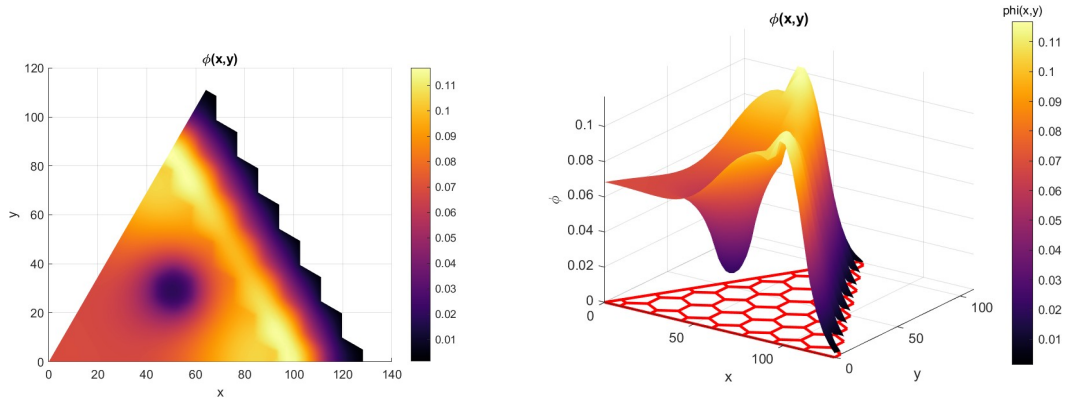


Figure 3.23: Thermal flux for both α models for a strongly sub-critical reactor with reflector in [6].

In order to verify the result in [6], the criticality problem for k has been carried out but modifying the removal term by adding to Σ_r , $\frac{\alpha}{v}$. The correctness was checked since the obtained result is the same in **Figure 3.23**. inspired by this procedure, the same calculation has been made for the system considered in this thesis work, reported in **Figure 3.24**.



(a) 2D plot of k eigenvalue formulation results for a 33G diffusion 3D model.

(b) 3D plot of k eigenvalue formulation results for a 33G diffusion 3D model.

Figure 3.24: k eigenvalue formulation total neutron flux $T_f = 673$ and $T_c = 673$ with the effective removal cross section $(\Sigma_r + \frac{\alpha}{v})$.

It is appreciable *ictu oculi* that the result is the same obtained for the α eigenvalue problem.

Let us try to understand in which circumstances such an unpleasant behaviour arises. It is well explained in [7], in which a fast sub-critical system is analysed with a *Dirac's*

delta response. It is worth to resume some of the observation of [7]. In this study the aim is to study the response of a sub-critical reflected reactor to a *pulse* through an external source of neutron (the framework of this paper is the dynamic of an ADS system). In particular the aim is to understand the evolution of the system and how it responds to an external source. There are two ways of getting rid of the influence of the source. The first one is to turn it off and deduce k_{eff} from the fluctuations at zero power. In this case, k_{eff} is not known in the real conditions of operation. The second one, which is chosen in [7], is to study the system behaviour following a source pulse. The usual method, which consists in measuring the population decay rate at long time scales (typical of delayed neutrons), is only precise for reactivities smaller than β_{eff} , which is not compatible with ADS reactivities. Moreover, it requires the knowledge of β_{eff} and a very low intrinsic source. That is why it has been chosen to deal rather with the prompt decrease following the pulse, which is today accessible to experiment. As analytic reference solution they adopted the *one group point kinetic model*:

$$\frac{dN}{dt} = \left(\nu_p \Sigma_f - (\Sigma_f + \Sigma_c + DB^2) \right) Nv \quad (3.29)$$

Where ν_p is the average number of prompt neutrons produced by fission, v is the average neutron velocity, and DB^2 is the leakage term. The cross section have been already defined for the previous models. Now, l is defined as the average time between a fission event and the previous one in the chain reaction. In the case of one group point kinetics, it is precisely the lifetime of a neutron (because the fission probability is independent of the age of neutron), given by:

$$l = \frac{1}{(\Sigma_f + \Sigma_c + DB^2)v} \quad (3.30)$$

while the k_{eff} is:

$$k_{eff} = \frac{\nu_p \Sigma_f}{(\Sigma_f + \Sigma_c + DB^2)}.$$

Combining k_{eff} definition with **Equation** (3.30) it can be seen that:

$$k_{eff} = \frac{\nu_p \Sigma_f}{(\Sigma_f + \Sigma_c + DB^2)} = \nu_p \Sigma_f v l \quad (3.31)$$

At this point is possible to define the *decrease rate* as:

$$\Omega(t) = -\frac{1}{N} \frac{dN}{dt}. \quad (3.32)$$

Using **Equation** (3.32) with **Equation** (3.29) and **Equation** (3.30), the neutron decrease rate, $\Omega(t)$, can be rewritten as:

$$\Omega(t) = -\frac{1}{N} \frac{dN}{dt} = \frac{1 - k_{eff}}{l} \equiv \Omega \quad (3.33)$$

\uparrow
 time independent

So it has been deduced that the decrease rate of neutrons inside the system according with this mathematical model should be constant, and so $N(t)$ decreases linearly. Then this conclusion has been compared with a reference decrease, simulated with a Monte Carlo code. The reference reactor used in [7] is spherical and fast system, with $k_{eff} = 0.972$ composed of a 90 cm diameter core made of 27% Pu MOX, surrounded by 20 cm thick sodium/stainless steel reflector. The simulation result of a Dirac source response is given in **Figure 3.25**.

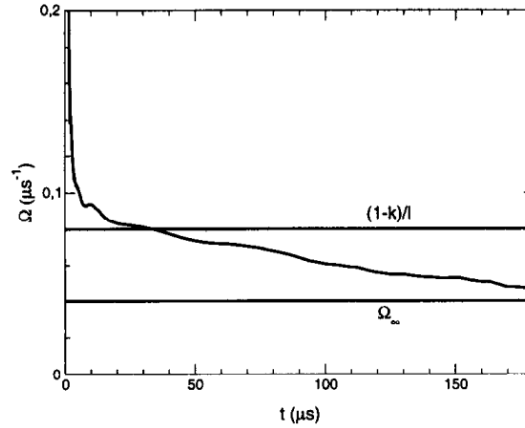


Figure 3.25: Dirac pulse system's response. Monte Carlo code result found in article [7].

The graph represents Ω , or the variation of the rate of fission reaction, which is related to N (neutron density). Neutrons are introduced into the system through the Dirac's source. As can be easily observed at $t = 0$ Ω is high, then stabilized at a value asymptotic, which is different from the expected one found in **Equation (3.33)**, called Ω_∞ . In other words, the theoretical result fails; in fact Ω_∞ can be seen as $\frac{1-k_{eff}}{l^*}$, where l^* is a *fictitious neutron lifetime* and since Ω_∞ is lower than $\frac{1-k_{eff}}{l}$, $l^* > l$. Hence the lifetime of the neutrons is bigger than the expected one. Furthermore we see that the fission rate decrease very sharply and then stabilizes at a constant value, this means that the fission reactions initially decrease very suddenly but successively more and more slowly, but at the same time we know that $l \approx const$: neutrons generated in the first seconds remain inside the system for longer time and accumulate.

The only way to account for such long times is to consider the role of the reflector. While the one group point kinetics implies an exponential distribution for intergeneration times, in an actual reactor neutrons may spend a lot of time in the reflector, where absorption cross sections are low, before coming back into the fuel. These few long-life neutrons appear to have a major impact on the kinetics of the system, in the same way as the delayed neutrons, but with an intermediate time scale. In [7] the demonstration of the role of the reflector was carried out, by considering a core with only fuel (MOX) but with same reactivity (they have considered a more enriched MOX in order to compensate the leak to reactivity). The obtained result demonstrate that if reflector

is not present, the system behaves like expected. In [7] it has been also demonstrate that even the core size plays a role on flux behavior, in particular a smaller system are more difficult to study. Is easy to understand that the presence of the reflector introduces longer time scales for one generation. How does this induce long time scales for the whole transient ? As a matter of fact, long-life neutrons constitute a very small fraction of the total number of neutrons. If all generations are present at the same time, few old neutrons of first generations will be mixed with many young neutrons of later generations and will not have a noticeable impact on the whole transient. On the contrary, if only few first generations of neutrons are present after a while, these long-life neutrons will represent a significant proportion of the population. In **Figure 3.26** is shown the effect of sub-criticality in the system considered in [7], where a Monte Carlo code was adopted.

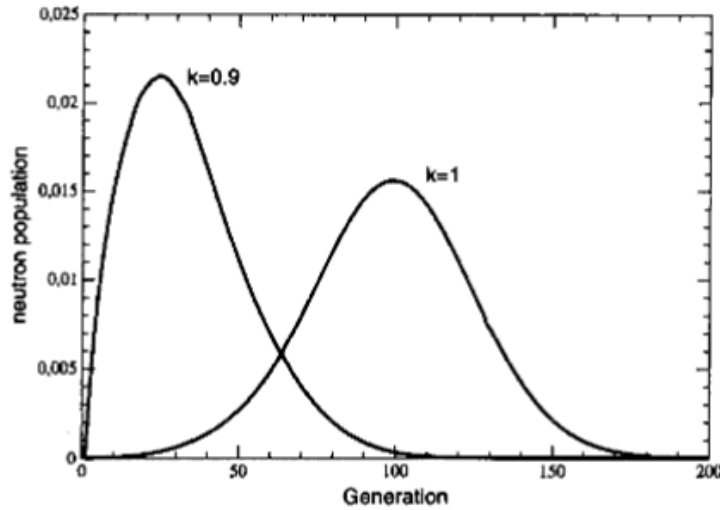


Figure 3.26: Distribution of the generations of the fissions occurring at $t = 300 \mu s$, at $k_{eff} = 1.0$ and $k_{eff} = 0.9$ in [7]. In this graph the system has been considered at time $t = 300 \mu s$, that corresponds to $100l$. In case of critical system ($k_{eff} = 1.0$) the larger amount of neutrons after $100l$ are the ones of the 100-th generation themselves; while in case of sub-criticality, the larger quote of neturons population at $100l$ is the ones of previous generations.

The greater the subcriticality, the older the neutrons present at a given time. In the same way, a growing human population will be mainly young, while a small birth rate will lead to an older population.

These considerations well explain the reason why the obtained ϕ_{α}^0 , reported in **Figure 3.16**.

References

- [1] A. F. Henry. *The application of Reactor Kinetics to the Analysis of Experiments*.
- [2] P. Ravetto. *Metodi analitici per la dinamica spaziale di sistemi non omogenei*.
- [3] Lelio Luzzi, Antonio Cammi, Valentino Di Marcello, Stefano Lorenzi, Davide Pizzocri, and Paul Van Uffelen. «Application of the TRANSURANUS code for the fuel pin design process of the ALFRED reactor». In: *Nuclear Engineering and Design* 277 (2014), pp. 173–187. ISSN: 0029-5493. DOI: <https://doi.org/10.1016/j.nucengdes.2014.06.032>. URL: <https://www.sciencedirect.com/science/article/pii/S0029549314003811>.
- [4] Nader Maleki Moghaddam, Hossein Afarideh, and Gilberto Espinosa-Paredes. «Development of a 2D-Multigroup Code (NFDE-2D) based on the neutron spatial-fractional diffusion equation». In: *Applied Mathematical Modelling* 39.13 (2015), pp. 3637–3652. ISSN: 0307-904X. DOI: <https://doi.org/10.1016/j.apm.2014.12.036>. URL: <https://www.sciencedirect.com/science/article/pii/S0307904X14007112>.
- [5] Nicolò Abrate, Sandra Dulla, Piero Ravetto, and Paolo Saracco. «On some features of the eigenvalue problem for the PN approximation of the neutron transport equation». In: *Annals of Nuclear Energy* 163 (2021), p. 108477. ISSN: 0306-4549. DOI: <https://doi.org/10.1016/j.anucene.2021.108477>. URL: <https://www.sciencedirect.com/science/article/pii/S0306454921003534>.
- [6] R.S. Modak and Anurag Gupta. «A scheme for the evaluation of dominant time-eigenvalues of a nuclear reactor». In: *Annals of Nuclear Energy* 34.3 (2007), pp. 213–221. ISSN: 0306-4549. DOI: <https://doi.org/10.1016/j.anucene.2006.12.009>. URL: <https://www.sciencedirect.com/science/article/pii/S0306454907000060>.
- [7] F. Perdu, J.M. Loiseaux, A. Billebaud, R. Brissot, D. Heuer, C. Lebrun, E. Liatard, O. Meplan, E. Merle, H. Nifenecker, and J. Vollaire. «Prompt reactivity determination in a subcritical assembly through the response to a dirac pulse». In: *Progress in Nuclear Energy* 42.1 (2003), pp. 107–120. ISSN: 0149-1970. DOI: [https://doi.org/10.1016/S0149-1970\(02\)00101-4](https://doi.org/10.1016/S0149-1970(02)00101-4). URL: <https://www.sciencedirect.com/science/article/pii/S0149197002001014>.

Chapter 4

Results

In this section the results of different LFR core configurations are discussed. To begin, it is useful to review the approach taken to address studies aimed at simulating transient phenomena using FRENETIC code.

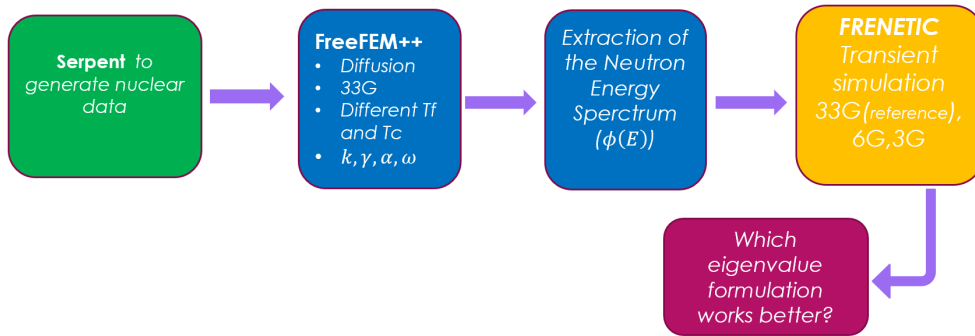


Figure 4.1: Scheme of work to simulate LFR transient analysis by using alternative weighting function (*Spectrum*) for group collapsing of nuclear data.

Consequently, based on the outlined scheme, the initial phase involves simulating the entire system using Serpent to generate the intermediate nuclear data. These cross section data are subsequently utilized as input for the FreeFEM++ solver to obtain the neutron flux distribution. From FreeFEM++ code we obtain the weighting functions which are necessary for the collapse procedure. The established method for generating the average cross sections for group g and reaction y involves computing weighted averages using the following formula:

$$\Sigma_{y,g}(\vec{r}, t) = \frac{\int_{E_g}^{E_{g+1}} dE \Sigma_y(\vec{r}, E, t) \psi(\vec{r}, E, t)}{\int_{E_g}^{E_{g+1}} dE \psi(\vec{r}, E, t)}. \quad (4.1)$$

In order to preserve reaction rates, it is common practice to utilize the total flux

$\Phi(\vec{r}, E, t)$ from a reference system configuration when dealing with the system under investigation. Even when considering time-independent cross sections, the weighting function may still vary over time, making the computation of group constants for transient calculations computationally intensive. To address this, the weighting is typically achieved by employing the flux obtained from a highly detailed transport calculation, which involves a static, k -based criticality calculation under various operating conditions. This allows for interpolation on a set of pre-calculated data to closely approximate the time-dependent conditions.

Equation (4.1) encompasses various complexities, including the selection of group boundaries $[E_1, \dots, E_G]$, the dependence on physical and operational parameters (e.g., burn-up, control rod position, thermodynamic conditions), angular effects (e.g., emission anisotropy), the determination of the weighting function $\psi(\vec{r}, E, t)$, and the choice of the weighting function model. In recent times, considerable attention has been given to optimizing the few-group structure. However, limited attention has been given to exploring alternative options for the weighting spectrum $\psi(\vec{r}, E)$. The use of the static k eigenfunction may not yield satisfactory outcomes when the system is significantly off-critical due to two main reasons:

1. The static calculation neglects the "time" capture $\frac{1}{v} \frac{\partial}{\partial t}$ and the effects of delayed neutrons.
2. The solution for the k eigenvalue may not accurately represent the energy spectrum of the physically time-dependent system.

As suggested in [1], one viable option could be utilizing the time eigenfunction $\varphi_\alpha(\vec{r}, E)$ to incorporate the system's free evolution information into the weighting procedure. This approach now carries a computational load comparable to static k calculations.

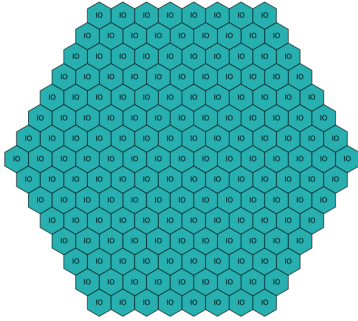
Due to the encouraging results of that work and to some gaps in the literature concerning this kind of analysis, this work focuses on assessing the advantages coming from the adoption of the different eigenfunctions associated with the transport model as weighting functions for the few-group collapsing procedure. To this aim, this paper reports some time-dependent calculations performed at first with an intermediate, reference group structure, i.e. the 33-group energy grid commonly adopted in the ECCO code [2], and then with nested 9-, 6- and 3-group structures (reported in **Table 4.1**), collapsing the data using the eigenfunctions of some of the different spectral formulations available in the literature, namely the time eigenvalue α , the collision eigenvalue γ and the multiplication eigenvalue k [3].

Table 4.1: Group boundaries in MeV adopted for the few-group calculations.

9G	$2.231 \cdot 10^0$	$4.979 \cdot 10^{-1}$	$1.111 \cdot 10^{-1}$	$2.479 \cdot 10^{-2}$	$5.531 \cdot 10^{-3}$	$2.035 \cdot 10^{-3}$	$7.485 \cdot 10^{-4}$	$5.4 \cdot 10^{-7}$
6G	$2.231 \cdot 10^0$	$4.979 \cdot 10^{-1}$		$2.479 \cdot 10^{-2}$	$5.531 \cdot 10^{-3}$		$7.485 \cdot 10^{-4}$	$5.4 \cdot 10^{-7}$
3G		$4.979 \cdot 10^{-1}$					$7.485 \cdot 10^{-4}$	

First of all some preliminary studies has been carried on with the aim of addressing the accuracy and the conformity of the developed solver on *FreeFEM++*. In fact even if, the described study of the 1 hexagon two groups-diffusion model case in **Section 2.1.2** can be seen as a verification test, it has been observed that when a more complex reactor system is considered, the error between k_{ref} and k_{FF} increase. The k_{ref} is the multiplicative eigenvalue used as reference given by FRENETIC, while k_{FF} is the result provided by FreeFEM++ code.

In **Figures 4.2** and **4.3** and ?? are reported three different system used to highlight the factors that create the discrepancies between the two results generated by the respective software.



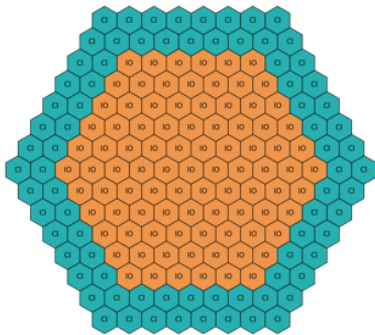
(a) Radial core illustration. Element legend: **IO**:inner fuel.

Case 3G

	2D	3D
$k_{FRENETIC}$	1.285767	0.955374
$k_{freeFEM}$	1.28559	0.954035
Δk [pcm]	17.7	134

(b) Table of 2D and 3D results for a 3 groups diffusion model.

Figure 4.2: First preliminary studied. Featuring factor: homogeneity.



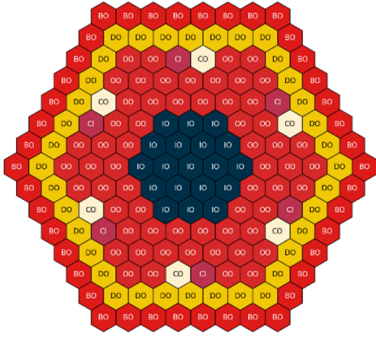
(a) Radial core illustration. Element legend: **IO**:inner fuel, **CI**: inserted control rod.

Case 3G

	2D	3D
$k_{FRENETIC}$	1.210051	0.912537
$k_{freeFEM}$	1.20694	0.908936
Δk [pcm]	311.1	360.1

(b) Table of 2D and 3D results for a 3 groups diffusion model.

Figure 4.3: Second preliminary studied. Featuring factor: heterogeneity.



(a) Radial core illustration. Element legend: **IO**:inner fuel, **OO**:outer fuel, **CI**: inserted control rod, **CO**: extracted control rod, **DO**: reflector, **BO**: barrel.

Case 33G

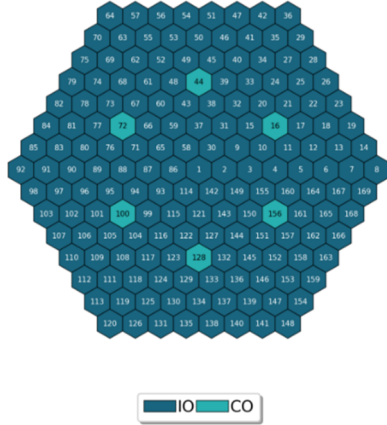
	2D	3D
$k_{FRENETIC}$	1.290001	1
$k_{freeFEM}$	1.28774	0.996224
Δk [pcm]	226.1	370.3

(b) Table of 2D and 3D results for a 33 groups diffusion model.

Figure 4.4: Third preliminary studied. Featuring factor: stronger heterogeneity and finer energy grids.

Figure 4.2a, **Figure 4.3a** and **Figure 4.4a** represent only the radial core configurations, since the systems are axially assembly-homogeneous: considering the single hexagon, the material does not change in the axial direction.

In **Figure 4.2b**, **Figure 4.3b** and **Figure 4.4b**, the $k_{FRENETIC}$ that have been used as reference value for testing the accuracy of FreeFEM++ solver's results are reported. The tabulated results consider both a 2D case - radial configuration only - and a 3D case. Looking at the three tables, it turns out that $\epsilon = \Delta k = |k_{FRENETIC} - k_{freeFEM}|$ is always lower when the axial dimension is neglected. In addition to that, also the heterogeneity of the system has a non-negligible weight on the deviation of k_{FFS} with respect to FRENETIC results; in fact, focusing on the 2D case in **Figure 4.2b** and **Figure 4.3b**, Δk increase. As concerns the 2D case in **Figure 4.4b**, Δk is lower with respect to the 2D case in **Figure 4.3b**, even if the third system is even more heterogeneous. This is due to the fact that in the third case a 33 - G grid has been used. From this evidence, it is possible to infer that refining the energy discretization, Δk decreases. The reason why, the discrepancy between the two solvers increases when 3D case is used is due to the fact that, in FreeFEM++ solver, the axial dimension is treated by introducing an axial buckling term by which it is assumed a sinusoidal profile of the neutron flux in axial direction, while in FRENETIC the actual 3D core is simulated; so it implies that the actual neutron profile in \hat{e}_z direction is not perfectly described by the buckling term and so the sinusoidal profile. Moreover, the error gets worst when a heterogeneous system is considered, since, starting from a non-perfectly represented neutron flux for each hexagon, even the interaction between neutrons of the surrounding assembly is be affected. Concerning the heterogeneity, an additional case is considered in **Figure 4.5** with the aim of better explain this phenomena.



(a) Radial core illustration. Element legend: **IO**: inner fuel, **CO**: extracted control rod

Case 1G

	CRout	CRin
$k_{FRENETIC}$	1.283957	1.099691
$k_{freeFEM}$	1.28321	1.09314
Δk [pcm]	74.7	655

(b) Table of **CRin** and **CRout** results for a 2D mono-kinetic diffusion model.

Figure 4.5: Additional preliminary studied. Featuring factor: soft heterogeneity and switching **CI** and **CO**.

In this preliminary study it is possible to appreciate the fact that when the control rods are extracted (**CO** elements), the difference k_{FF} and $k_{FRENETIC}$ is relatively small with respect to the case of inserted control rods (**CI** elements, not represented in **Figure 4.5a**). This suggests the presence of a spatial *self-shielding* phenomena. Which it involves both control rods (CRs) and fuel pellets. Practically, as one moves towards the center of the CR, the neutron flux tends to diminish. This reduction is attributed to the high absorption cross-sections prevalent in these regions, leading to a strong flux depression. Thus, the term "self-shielding" is employed to describe this phenomenon. In the **nodal method** (used by FRENETIC), the spatial resolution does not extend beyond the hexagonal level, resulting in a representation of the average neutron at the hexagon level flow. Conversely, in fine mesh methods, such as the finite element method (FF), the self-shielding effect is distinctly observed due to the resolution of the neutron flux on smaller mesh triangles. After this necessary considerations, the first set of simulated transient will be deeply described.

4.1 2D Transient analysis

The focus of this study is on the Gen-IV Lead-cooled Fast Reactor (LFR) technology, which currently undergoes extensive research and development worldwide, involving both industrial and academic sectors. The analysis considers various reactivity insertion levels, such as sub-prompt critical and super-prompt critical, as well as different few-group structures. As a case study, a scaled-down version of the ALFRED (Advanced Lead Fast Reactor European Demonstrator) core design [4] was developed. **Figure 4.6** illustrates several 2D hexagonal core configurations used in this study.

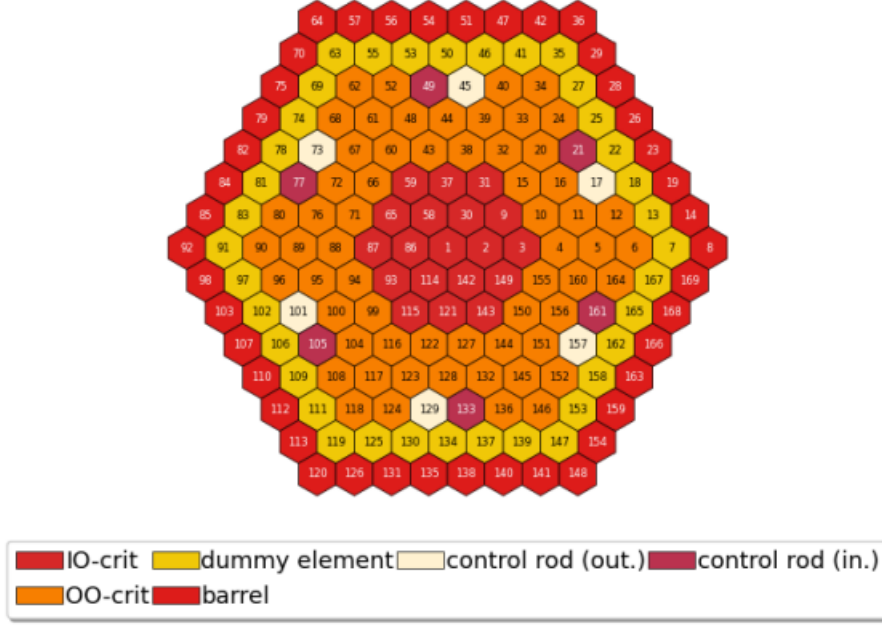


Figure 4.6: 2D core model adopted for the test calculations

The neutronic module of the multiphysics code FRENETIC, which has been developed over the past decade at Politecnico di Torino ([5, 6]), is utilized for both intermediate- and few-group transient simulations. This module, written in Fortran, incorporates a hexagonal nodal diffusion solver and various efficient methods for reactor kinetics, including the Predictor-Corrector Quasi-Static (PCQS) method [6]. All transient calculations presented in this study are conducted using this method, combined with adaptive time-step selection for solving the shape and amplitude functions. For the computation of the different spectra used in the few-group collapsing, an *ad hoc* LFR model written in the FreeFEM++ language [7] is employed. FreeFEM++ is a highly efficient finite element solver for partial differential equations. The versatility of FreeFEM++ enables the straightforward implementation of various eigenvalue problems, which would otherwise be complex and intrusive in the FRENETIC code. The following eigenvalue problems have been solved: the classical multiplication eigenvalue,

$$(\hat{L} + \hat{R})\vec{\varphi}_{k,n} = \hat{S}\vec{\varphi}_{k,n} + \frac{1}{k_n}\hat{F}\vec{\varphi}_{k,n},$$

the collision eigenvalue,

$$(\hat{L} + \hat{R})\vec{\varphi}_{\gamma,n} = \frac{1}{\gamma_n}(\hat{S} + \hat{F})\vec{\varphi}_{\gamma,n},$$

and the prompt and delayed time eigenvalue formulations, respectively,

$$\frac{\alpha_n}{\mathbf{v}}\vec{\varphi}_{\alpha,n} + (\hat{L} + \hat{R})\vec{\varphi}_{\alpha,n} = (\hat{S} + \hat{F})\vec{\varphi}_{\alpha,n},$$

$$\frac{\omega_n}{v} \vec{\varphi}_{\omega,n} + (\hat{L} + \hat{R}) \vec{\varphi}_{\omega,n} = (\hat{S} + \hat{F}_p) \vec{\varphi}_{\omega,n} + \sum_{i=1}^R \frac{\lambda_i}{\omega_n + \lambda_i} \hat{F}_{d,i} \vec{\varphi}_{\omega,n}.$$

The operators in previous equations have their conventional meanings: \hat{L} represents the leakage operator, \hat{R} denotes the removal operator, \hat{S} corresponds to the scattering operator, \hat{F} represents the total fission operator, \hat{F}_p and $\hat{F}_{d,i}$ denote the prompt and i -th delayed fission operators, respectively. The parameter n indicates the order of the flux harmonics, and in this case, we assume R to be the number of precursor families, which is set to 1. Since the first harmonic, characterized by a uniform sign over the entire domain, is the only physically relevant one, the FreeFEM++ eigenvalue solver, which acts as a wrapper to the SLEPc library [8], is specifically configured to calculate and provide this particular harmonic. In this work, all transient scenarios commence from a steady-state critical configuration. The transient is initiated at a specific time $t = \mathcal{T}^{(1)}$ by manipulating the control rods, which is simulated by replacing the control assemblies. Following a duration of time $t = \mathcal{T}^{(2)}$, the core is restored to the initial critical configuration. In FRENETIC, the group constants associated with each type of reactor assembly are updated at each time step through a straightforward linear interpolation between the data at the configuration times $\mathcal{T}^{(n)}$ and $\mathcal{T}^{(n+1)}$.

For each scenario, the following calculation approach is employed: Firstly, the reference transient simulation is conducted using the group constants collapsed onto an intermediate group structure (in this case, the ECCO 33-group grid). Subsequently, utilizing these group constants, the time, collision, and multiplication eigenvalue problems are solved for each off-critical reactor configuration. The various spectra corresponding to the configuration at $t = \mathcal{T}^{(n)}$ are then utilized as weighting functions to collapse the group constants from the intermediate to the few-group structure within the configuration time interval $t = [\mathcal{T}^{(n)}, \mathcal{T}^{(n+1)}]$. This process assumes a prior knowledge of the principal reactor configurations (e.g., control rod positions) and the associated group constants throughout the entire transient period. This assumption is typically fulfilled in most cases, often facilitated by the utilization of a pre-computed library of multi-group cross sections. In line with the approach presented in [1], the adjusted number of neutrons emitted by fission, denoted as $\bar{\nu}$, is modified to ensure that the system characterized by the different sets of few-group constants is initially critical with utmost precision. This is achieved through the employment of a correction factor $1/k_{\text{eff},x}$, where x corresponds to the eigenvalue spectrum utilized for collapsing the constants. By incorporating this correction factor, the occurrence of slight deviations from criticality due to collapsing errors is avoided, guaranteeing that all the analyzed cases commence from the same initial condition. The transient calculation is subsequently executed employing the few-group constants while maintaining the numerical settings unaltered from the reference simulation. Finally, a comparison is made between the temporal evolution of the key neutronic integral parameters computed in both cases, such as the total power $P(t)$.

4.2 Results of 2D transient analysis

This section provides a summary of the obtained results from a series of transient scenarios involving the 2D simplified version of the ALFRED reactor. These scenarios were analyzed using varying numbers of groups and different weighting spectra. The collapsing process was conducted without spatial homogenization, implying that data pertaining to the same types of regions (e.g., control assemblies) were collapsed using the flux spectrum obtained from those regions. To simplify the calculations and focus solely on the neutronic aspects, all thermal feedback effects were neglected, assuming that the core operates under cold conditions. To avoid abrupt variations in the total power of the reactor, the scenarios were initiated by a step insertion or extraction of all control rods for a very short time interval ($t=[1 \cdot 10^{-9}, 100]$ ms). Subsequently, the rods were withdrawn or inserted at a constant rate between $t=[100, 500]$ ms to restore criticality. These scenarios were designed to simulate potential reactivity insertion accidents, which represent a crucial type of safety-critical transients. Additionally, the movement of the control rods serves as the operational transient that induces the most significant spatial and energy effects on the neutron distribution, enabling an exploration of the performance of the weighting functions in a challenging yet realistic scenario. The full-developed function shape of the neutron flux for both the configuration is reported in **Figure 4.7**.

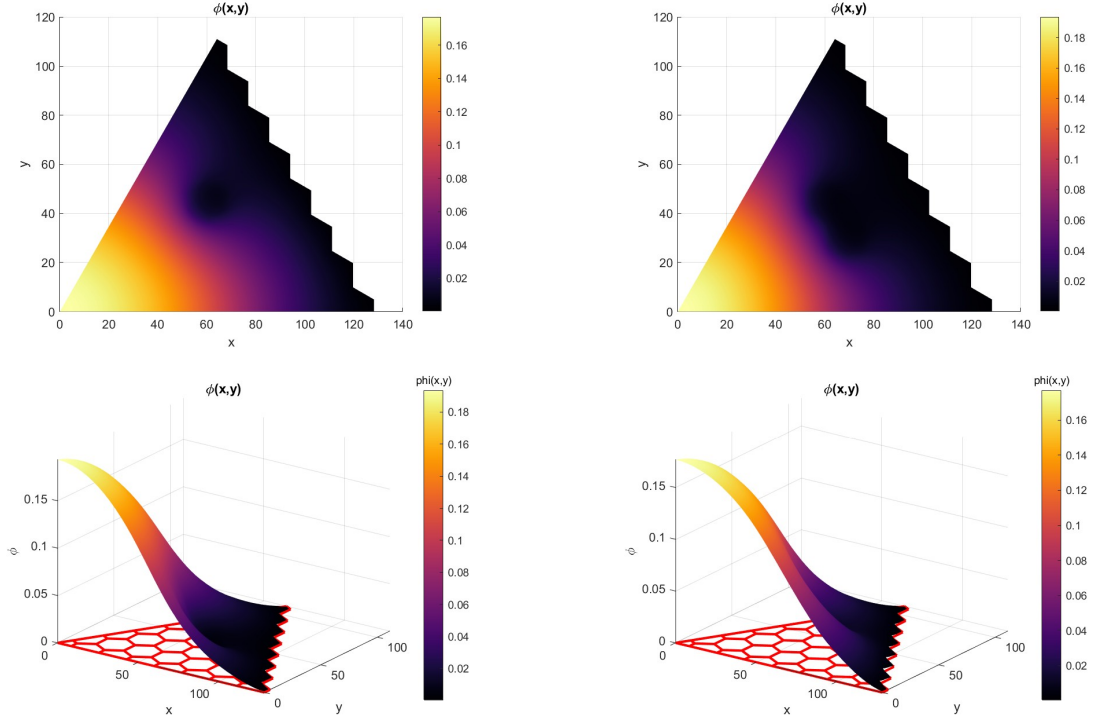


Figure 4.7: 3D plots of the neutronic profile over a sextant of the system. The three plots are of the same simulation result with different angulation. The red grid in $z = 0$ plane, is the system borders. The neutron distribution has a Gaussian-like shape. In the central region of the sextant, the flux sharply decreases, that region corresponds to the region where the *control road* is inserted.

Tables **Table 4.2** to **Table 4.3** provide a summary of the different scenarios analyzed, considering various reactivity values and few-group grids. Each case is evaluated based on the total energy deposited during the transient and the peak power of the 33-group case within the time interval $\mathcal{T}^{(1)} = 1 \cdot 10^{-9}$ to $\mathcal{T}^{(2)} = 100$ ms, which serve as references for computing relative errors compared to results obtained using different spectra. Additionally, the relative error between the time profiles of total power is also calculated as an additional measure of accuracy.

Although the three nested few-group grids exhibit a certain pattern, it is evident that the relative error does not consistently decrease when transitioning from 3 to 9 groups, except in cases where k is used as the weight. This observation deviates from the expected trend, and it can be attributed to a combination of collapsing errors and the criticality adjustment factor $1/k_{\text{eff},x}$. While preserving reaction rates does not guarantee preservation of eigenvalues, the correction factor employed to maintain criticality aligns with the spectra used for group collapsing only when $x = k$. Unfortunately, this is presently the sole method for adjusting criticality in FRENETIC, resulting in a slight bias introduced by $1/k_{\text{eff},x}$ in the collapsed system's spectrum.

Despite the expected small bias, considering the range of $k_{\text{eff},x}$ between 0.9986 and

Table 4.2: Impact of the weighting functions with some few-group grids for a negative reactivity insertion.

$\bar{\rho} = \frac{1}{\Delta t} \int_{\mathcal{T}^{(1)}}^{\mathcal{T}^{(2)}} \rho(t) dt$	group grid	weight. spectrum $\psi(E)$	% relative error		
			$E = \int P(t) dt$	P_{\min}	$\ (P_{33G} - P)/P_{33G}\ $
reference values (33-group)			1.271 [MJ]	5.017 [MW]	-
-86 pcm	3-group	k	-2.352	-0.632	9.767
		γ	0.958	0.046	4.088
		α	3.457	0.627	13.444
		ω	-4.981	-1.164	19.264
	6-group	k	0.841	0.008	3.217
		γ	2.907	0.435	11.047
		α	3.368	0.604	13.674
		ω	-0.703	-0.308	4.380
	9-group	k	0.258	0.021	1.558
		γ	1.291	0.231	5.480
		α	1.827	0.345	7.562
		ω	-1.049	-0.245	4.024
reference values (33-group)			0.810 MJ	4.596 MW	-
-240 pcm	3-group	k	-10.561	-1.833	51.364
		γ	-4.721	-0.901	23.970
		α	0.413	0.083	7.300
		ω	-9.129	-1.608	44.526
	6-group	k	-2.408	-0.517	14.496
		γ	1.008	0.039	5.604
		α	2.770	0.479	16.529
		ω	-1.634	-0.392	10.390
	9-group	k	-2.035	-0.378	11.035
		γ	-0.348	-0.106	2.591
		α	0.851	0.107	5.542
		ω	-1.399	-0.276	7.625
reference values (33-group)			1.810 MJ	3.812 MW	-
-1610 pcm	3-group	k	-12.407	-0.684	89.845
		γ	-5.284	-0.278	37.656
		α	-1.257	0.356	66.261
		ω	-1.385	0.331	62.642
	6-group	k	-5.296	-0.296	52.074
		γ	-0.095	-0.030	10.641
		α	-1.452	0.657	118.249
		ω	-1.557	0.653	116.153
	9-group	k	-4.124	-0.260	43.118
		γ	-1.528	-0.127	17.471
		α	6.855	0.454	45.053
		ω	6.646	0.455	88.636

0.9999, an examination of the tables reveals that, in most cases, particularly those

Table 4.3: Impact of the weighting functions with some few-group grids for a positive reactivity insertion ($\beta_{\text{eff}} = 330$ pcm).

$\bar{\rho} = \frac{1}{\Delta t} \int_{\mathcal{T}^{(1)}}^{\mathcal{T}^{(2)}} \rho(t) dt$	group grid	weight. spectrum $\psi(E)$	$E = \int P(t) dt$	% relative error	
				P_{max}	$\ (P_{33G} - P)/P_{33G}\ $
reference values (33-group)			4.713 MJ	7.057 MW	-
+193 pcm	3-group	k	15.371	5.267	92.440
		γ	7.868	2.691	47.476
		α	22.914	9.668	194.846
		ω	-10.866	-3.481	65.247
	6-group	k	10.849	3.679	76.194
		γ	5.619	1.902	39.224
		α	25.949	10.760	221.097
		ω	-5.835	-1.887	39.712
	9-group	k	9.191	3.084	66.385
		γ	6.614	2.208	47.136
		α	6.614	2.208	39.879
		ω	-4.808	-1.588	33.984
reference values (33-group)			19.686 MJ	12.506 MW	-
+287 pcm	3-group	k	52.655	28.592	372.772
		γ	23.324	12.028	157.499
		α	-60.062	-27.632	369.399
		ω	-53.398	-24.774	324.517
	6-group	k	41.950	22.232	357.377
		γ	17.126	8.709	127.039
		α	4.059	2.086	31.493
		ω	-25.163	-12.160	179.778
	9-group	k	36.061	18.834	357.377
		γ	23.800	12.152	181.767
		α	17.707	8.947	145.578
		ω	-25.163	-12.157	179.770
reference values (33-group)			47.488 [MJ]	2.302 [MW]	-
+331 pcm	3-group	k	66.780	12.324	349.688
		γ	21.293	4.175	117.101
		α	-237.580	-37.045	994.320
		ω	-132.475	-20.489	549.046
	6-group	k	33.519	5.914	205.941
		γ	-77.096	-12.810	355.199
		α	-175.975	-29.566	812.434
		ω	-709.027	-119.174	6489.474
	9-group	k	49.023	8.675	346.952
		γ	31.071	5.443	191.215
		α	21.952	3.784	128.830
		ω	-46.232	-7.802	244.931

with significant ρ , the k -spectrum produces relatively inaccurate results compared to

the other spectra. The performance of the prompt (α) and delayed (ω) energy spectra appears highly sensitive to ρ , with the table reporting a time-averaged value between $\mathcal{T}^{(1)}$ and $\mathcal{T}^{(2)}$. For low reactivity values ($|\rho| < 240$ pcm), the delayed spectrum, which assumes only one family of precursors, provides better results than the prompt spectrum. Conversely, as the reactivity increases, the prompt spectrum exhibits improved accuracy. This trend is particularly evident in scenarios involving super-prompt reactivity injection and aligns with observations made in [9] for a thermal, homogeneous, and infinite system. To prevent excessively large power excursions resulting from the super-prompt criticality state, the configuration times $\mathcal{T}^{(2)}$ and $\mathcal{T}^{(3)}$ are adjusted to 0.002 and 0.05 ms, respectively.

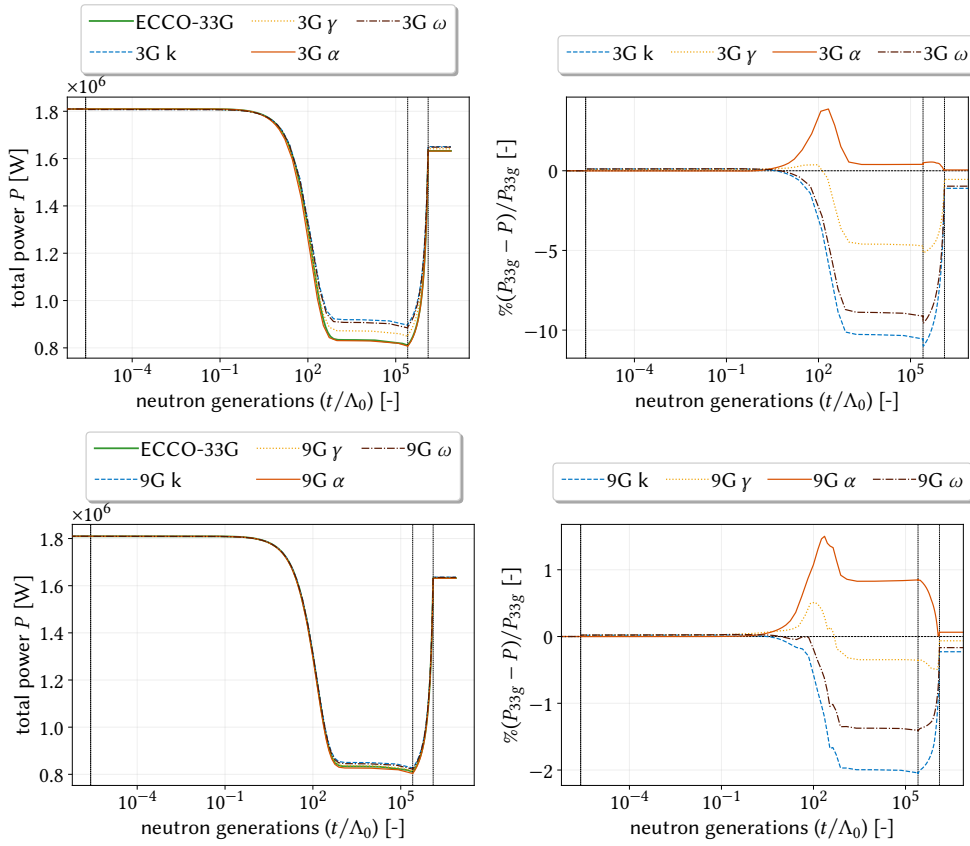


Figure 4.8: Total power evolution (left) and relative difference between the total power of the 33-group case with respect to the few-group cases (right) computed for the various eigenvalues for a negative reactivity insertion ($\bar{\rho} = -240$ pcm). The black dashed lines represent the configuration times $\mathcal{T}^{(n)}$, and $\Lambda_0 = 3.909 \cdot 10^{-4}$ ms.

Except for the slightly sub-critical case with $\bar{\rho} = -86$ pcm and the 3- and 6-group super-critical cases ($\bar{\rho} = +331$ pcm), the γ -collapsed data consistently provide a more accurate power evolution than the k case. The accuracy of the time eigenfunctions varies depending on the specific case, as shown in Figures 4.8 and 4.9. These figures display the total fission power evolution for both the reference and few-group cases (left)

and the time-dependent relative error between the reference value and the few-group values (right). The figures represent the cases of negative and super-prompt reactivity insertion for both the 3- (top) and 9-group (bottom) structures. In the sub-critical scenario, the α spectrum case is the most accurate for both the 3- and 9-group grids. It is followed by the γ and ω cases, while the k case performs the worst. One possible explanation for the superiority of the α spectrum is that the time-dependent spectrum $\psi(E, t)$ in the 33-group case is primarily dominated by prompt emissions during the initial 300 neutron generations. This suggests that using the α -collapsed data allows the few-group model to better capture the prompt jump and subsequent plateau. However, if the rod extraction occurs after a sufficiently long time, surpassing the reactor's stable period of $1/\omega_0$, the delayed effects would dominate $\psi(E, t)$, potentially altering the ranking between the two time spectra.

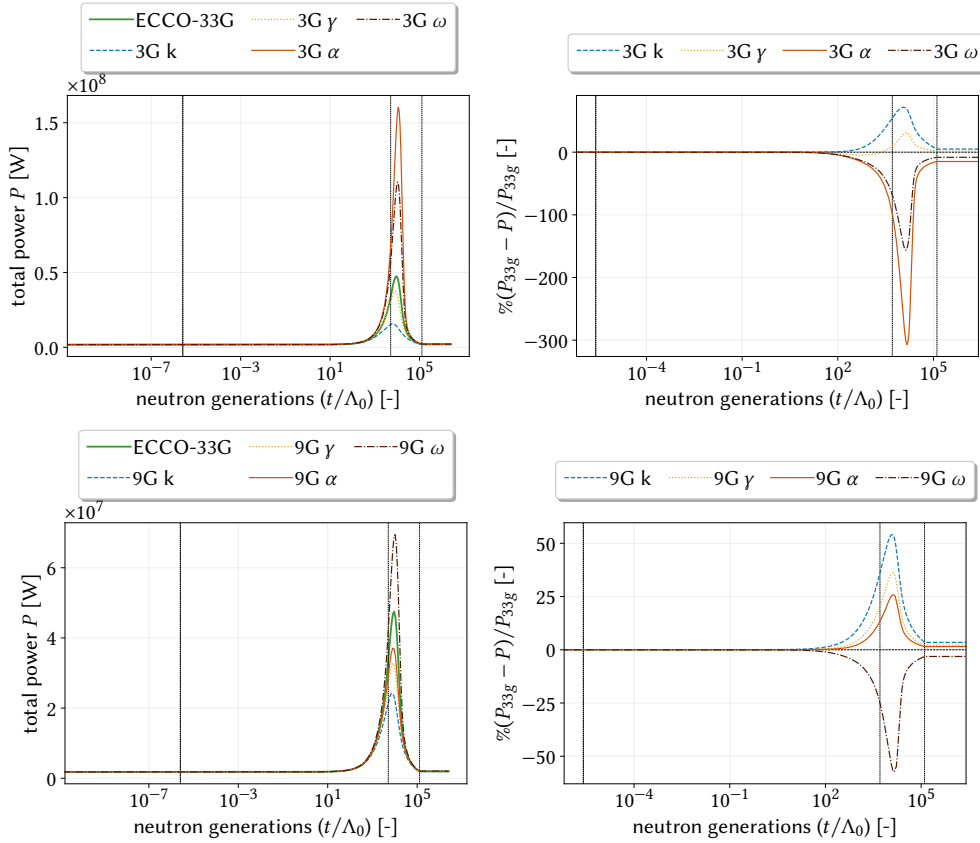


Figure 4.9: Total power evolution (left) and relative difference between the total power of the 33-group case with respect to the few-group cases (right) computed for the various eigenvalues for a super-prompt reactivity insertion ($\bar{\rho}=331$ pcm). The black dashed lines represent the configuration times $\mathcal{T}^{(n)}$, and $\Lambda_0 = 3.909 \cdot 10^{-4}$ ms.

The performance of the time spectra in the case of super-critical reactivity insertion strongly relies on the specific few-group grid used for collapsing. This indicates that there can be a discrepancy between physical expectations and the numerical effects of

the collapsing process. In both cases, the k -collapsed case consistently performs the poorest, while the γ case demonstrates favorable behavior with low sensitivity to the group structure. Calculating the fundamental eigenfunction is typically computationally expensive and highly dependent on the degree of off-criticality. As a result, the collision eigenfunction appears to offer the best compromise in terms of computational cost, as it exhibits a convergence rate similar to k while maintaining accuracy, at least for the majority of the cases presented in this study.

Chapter 5

Conclusions

This study focuses on the collapsing of group constants using different weighting spectra, specifically exploring the use of fundamental eigenfunctions associated with various eigenvalue formulations in neutron diffusion (and transport) as an alternative to the conventional choice of the k -eigenvalue spectrum.

Due to the complexity of the problem and the numerous parameters influencing group constant generation, numerical experiments were conducted using a simplified 2D version of the ALFRED core design.

The analysis revealed that predicting the performance of each weighting eigenfunction based solely on physical considerations is challenging. This is due to the occurrence of numerical error compensations in the collapsing scheme, which depend on factors such as the type of reactivity insertion, the few-group grid, the eigenfunction type, and the system energy spectrum.

Nonetheless, it can be concluded that, in most cases, the k eigenfunction tends to yield the poorest results, particularly in situations with significant reactivity. In this regard, the γ spectrum appears to be the most effective weighting option. In many cases, the prompt and delayed time eigenfunctions may offer slightly better results than γ , but their evaluation is considerably more computationally demanding. This conclusion finds support from a physical perspective, as the γ eigenvalue introduces the least distortion to the energy spectrum of the system.

To establish more general conclusions, especially regarding fast systems, further numerical experiments should be conducted in the future, with a particular focus on the thermal feedback effects in heavily off-critical systems.

References

- [1] K. Dugan, I. Zmijarevic, and R. Sanchez. «Cross-Section Homogenization for Reactivity-Induced Transient Calculations». In: *Journal of Computational and Theoretical Transport* 45.6 (2016), pp. 425–441. DOI: [10.1080/23324309.2016.1188116](https://doi.org/10.1080/23324309.2016.1188116).
- [2] G. Rimpault, D. Plisson, J. Tommasi, R. Jacqmin, and J. Rieunier. «The ERANOS code and data system for fast reactor neutronic analyses». In: *International Conference on Physics of Reactors, PHYSOR 2002, Seoul, South Korea*. 2002, pp. 1134–1143. URL: <https://hal.archives-ouvertes.fr/cea-02906396/>.
- [3] N. Abrate, S. Dulla, P. Ravetto, and P. Saracco. «On some features of the eigenvalue problem for the P_N approximation of the neutron transport equation». In: *Annals of Nuclear Energy* 163 (2021), pp. 108–477.
- [4] G. Grasso, C. Petrovich, D. Mattioli, C. Artioli, P. Sciora, D. Gugiu, G. Bandini, E. Bubelis, and K. Mikityuk. «The core design of ALFRED, a demonstrator for the European lead-cooled reactors». In: *Nuclear Engineering and Design* 278 (2014), pp. 287–301. URL: <https://www.sciencedirect.com/science/article/pii/S0029549314004361>.
- [5] R. Bonifetto. «Computational thermal-hydraulic modeling for nuclear fusion and fission applications». PhD thesis. Politecnico di Torino, 2014. URL: <https://iris.polito.it/handle/11583/2572946>.
- [6] D. Caron, S. Dulla, and P. Ravetto. «New aspects in the implementation of the quasi-static method for the solution of neutron diffusion problems in the framework of a nodal method». In: *Annals of Nuclear Energy* 87 (2016), pp. 34–48. URL: <https://doi.org/10.1016/j.anucene.2015.02.035>.
- [7] Frédéric Hecht. «New development in FreeFem++». In: *Journal of numerical mathematics* 20.3-4 (2012), pp. 251–266. URL: <https://www.degruyter.com/document/doi/10.1515/jnum-2012-0013/html>.
- [8] V. Hernandez, J. E. Roman, and V. Vidal. «SLEPc: a scalable and flexible toolkit for the solution of eigenvalue problems». In: *ACM Transactions on Mathematical Software* 31 (2005), pp. 351–362. URL: <https://doi.org/10.1145/1089014.1089019>.
- [9] K. Dugan, R. Sanchez, and I. Zmijarevic. «Cross section homogenization for transient calculations in a spatially heterogeneous geometry». In: *Annals of Nuclear Energy* 116 (2018), pp. 439–447. ISSN: 0306-4549. DOI: <https://doi.org/10.1016/j.anucene.2018.02.041>. URL: <https://www.sciencedirect.com/science/article/pii/S0306454918300951>.

Ringraziamenti

Ringrazio con sincero affetto e stima tutte le persone che hanno collaborato con me per la realizzazione di questo lavoro.

In particolare tengo a ringraziare il dottore Nicolò Abrate e la professoressa Sandra Dulla, non solo per le nozioni che mi hanno insegnato lungo questo percorso, ma anche per avermi trasmesso la passione e la professionalità con cui svolgono la loro professione: spero un domani di poter riconoscere in me le stesse qualità.

Ai miei genitori, fratelli e nonni: grazie per tutto. Ogni altra parola sarebbe superflua.

Ringrazio tutti gli amici che mi hanno regalato, durante questo lungo viaggio, leggerezza, sorrisi, ma anche il loro tempo nel momento del bisogno. Avermi al mio fianco è un dono che spero di non aver mai sprecato.

Bibliografia

- [1] M. Massone, N. Abrate, G. F. Nallo, S. Dulla, P. Ravetto e D. Valerio. «Genetic algorithm-based optimisation of the few-group structure for lead fast reactors analysis». In: *Proceedings of the ANS International Conference PHYSOR 2022*. Pittsburgh, PA: American Nuclear Society (ANS), 2022, pp. 1388–1397.
- [2] Paolo Saracco, Sandra Dulla e Piero Ravetto. «On the spectrum of the multigroup diffusion equations». In: *Progress in Nuclear Energy* 59 (ago. 2012), pp. 86–95. ISSN: 0149-1970. DOI: 10.1016/J.PNUCENE.2012.03.002.